

ÉCOLE DE TECHNOLOGIE SUPÉRIEURE
UNIVERSITÉ DU QUÉBEC

THÈSE PRÉSENTÉE À
L'ÉCOLE DE TECHNOLOGIE SUPÉRIEURE

COMME EXIGENCE PARTIELLE
À L'OBTENTION DU DOCTORAT EN GÉNIE
Ph.D.

PAR
MAROUANE TEMIMI

UTILISATION DE LA TÉLÉDÉTECTION POUR L'ESTIMATION DE LA
RÉSERVE HYDRIQUE AU BASSIN DU MACKENZIE AU NORD OUEST
CANADIEN

MONTRÉAL, LE 5 SEPTEMBRE 2006

CETTE THÈSE A ÉTÉ ÉVALUÉE PAR UN JURY COMPOSÉ DE :

M. Robert Leconte, ing., Ph.D., directeur de thèse
Département de génie de la construction à l'École de technologie supérieure

M. François Brissette, ing., Ph.D., codirecteur
Département de génie de la construction à l'École de technologie supérieure

M. Jean Sébastien Dubé, ing., Ph.D., président du jury
Département de génie de la construction à l'École de technologie supérieure

Mme. Monique Bernier, Ph.D.
Institut national de recherche scientifique, centre Eau, Terre et Environnement, INRS-ETE

M. Jean Rousselle, ing., Ph.D.
École Polytechnique de Montréal

ELLE A FAIT L'OBJET D'UNE SOUTENANCE DEVANT JURY ET PUBLIC

LE 26 JUIN 2006

À L'ÉCOLE DE TECHNOLOGIE SUPÉRIEURE

UTILISATION DE LA TÉLÉDÉTECTION POUR L'ESTIMATION DE LA RÉSERVE HYDRIQUE AU BASSIN DU MACKENZIE AU NORD-OUEST CANADIEN

Marouane Temimi

RÉSUMÉ

La présente recherche qui est appliquée au bassin du fleuve Mackenzie, vise l'estimation de l'humidité du sol en utilisant des données de télédétection captées dans le domaine des micro-ondes passives. Compte tenu de l'étendue et l'hétérogénéité du bassin du Mackenzie, un intérêt particulier a été réservé à des approches globales. Un indice d'humidité a été estimé à partir des images SSM/I, en utilisant des températures de brillance verticalement polarisées et mesurées à 19, 37 et 85 GHz. La comparaison des fractions des plans d'eau obtenues aux débits observés a montré l'existence d'une intéressante corrélation. Les micro-ondes passives sont capables de "voir" les plans d'eau et l'humidité du sol. Dans le domaine du visible, seuls les plans d'eau sont captés. Un nouvel indice d'humidité a été donc proposé en se basant sur la différence de ces sensibilités. L'indice a montré une concordance satisfaisante avec les précipitations et les températures observées.

UTILISATION DE LA TÉLÉDÉTECTION POUR L'ESTIMATION DE LA RÉSERVE HYDRIQUE AU BASSIN DU MACKENZIE AU NORD-OUEST CANADIEN

Marouane Temimi

SOMMAIRE

La présente recherche vise l'estimation de l'humidité du sol en utilisant des données de télédétection captées dans le domaine des micro-ondes passives. Cette étude a été appliquée au bassin du fleuve Mackenzie, situé dans le territoire du nord-ouest canadien. La synthèse des approches préconisées dans la littérature pour estimer l'humidité du sol en utilisant des données en micro-ondes passives a révélé deux catégories d'approches. La première catégorie regroupe des approches globales qui décrivent, à travers des indices, qualitativement l'état d'humidité d'un bassin versant. La deuxième catégorie présente plutôt des approches détaillées qui se basent sur des modèles de transfert radiatif pour estimer, quantitativement, l'humidité du sol au bassin étudié. Compte tenu de l'étendue et l'hétérogénéité du bassin du Mackenzie, objet de cette recherche, un intérêt particulier a été réservé à la première catégorie d'approche. Un indice d'humidité a été estimé à partir des images SSM/I, en utilisant des températures de brillance verticalement polarisées et mesurées à 19, 37 et 85 GHz. L'analyse de la variabilité temporelle des paramètres de l'indice appliqué a révélé l'existence d'une tendance saisonnière qui est similaire d'une saison à l'autre. Ce constat a été expliqué par l'effet du couvert végétal qui se développe au cours de la saison estivale. Il a été proposé d'utiliser des paramètres qui sont variables dans l'espace et dans le temps pour tenir compte de la variabilité spatiale et temporelle des conditions de surface. La fraction des plans d'eau par pixel a été dérivée à partir des valeurs de l'indice d'humidité. La comparaison des fractions des plans d'eau obtenues aux débits observés a montré l'existence d'une corrélation entre ces deux paramètres. Cette corrélation a été utilisée pour développer un modèle de tarage qui se base sur deux paramètres empiriques. Un déphasage a été également observé entre le maximum des débits observés et celui des fractions des plans d'eau estimées. Ce déphasage a été introduit au modèle classique de la courbe de tarage. Les paramètres de ce modèle ainsi que le terme de déphasage sont mis à jour à la réception de chaque nouvelle image SSM/I. Ainsi, le modèle a été adapté pour un suivi en temps réel de l'évolution des plans d'eau au Mackenzie. Cependant, la comparaison des fractions des plans d'eau dérivées à partir des images SSM/I à celles fournies par des images captées dans le domaine du visible a montré une différence de sensibilité entre les deux sources. En fait, les micro-ondes passives sont capables de

“voir” les plans d'eau à la surface ainsi que l'humidité du sol. Dans le domaine du visible, seuls les plans d'eau à la surface sont captés. Un nouvel indice d'humidité a été donc proposé en se basant sur la différence de ces sensibilités. L'indice a montré une concordance satisfaisante avec les précipitations et les températures observées. Cet indice reflète l'état global d'humidité dans le bassin. Pour mettre en échelle les valeurs de cet indice et estimer localement l'humidité du sol, un autre indice topographique a été proposé. Des paramètres décrivant l'état du couvert végétal ont été introduits à cet indice topographique qui prévoit l'organisation spatiale de l'humidité globale estimée précédemment. L'indice modifié a montré une corrélation intéressante avec les précipitations et les températures observées localement.

ESTIMATION OF WATER STORAGE OVER THE MACKENZIE RIVER BASIN IN NORTHWESTERN CANADA USING REMOTE SENSING DATA

Marouane Temimi

ABSTRACT

This work elaborates a method to estimate soil moisture and open water extent using remote sensing data. Specifically, Microwave data are used in this work in combination with other sources of information. This study is applied to Mackenzie River Basin as it was conducted in the framework of the MAGS project (Mackenzie GEWEX Study). The methodology developed in this work is based on the concept of the wetness index which is a surrogate of the measured soil moisture. Firstly, it was proposed to used wetness index derived from a linear combination of brightness temperatures measured by the SSM/I sensor. Beside the correlation of this index with the observed discharge at some observing points of the Mackenzie River basin, it was noticed that the empirical parameter of the index were affected by the variation in space and time of the surface conditions. The sensitivity of the wetness index was improved by considering this effect. Secondly, the potential of combination of passive microwave data and discharge observation for flood forecasting was investigated. The methodology was based on the concept of the rating curve model. The Kaman filter was used to update the parameters of the rating model at the reception of each new satellite image. The estimated water surface fractions using the discharge observations showed a reasonable concordance with those derived from visible images (NOAA-AVHRR). The publication of the AMSR-E data has enabled us to improve the spatial resolution of the passive microwave data. Thus, a new formulation of a wetness index was proposed in the third part of this work. The proposed Basin Wetness Index is based on the difference of the sensitivity of passive microwave and visible images to soil moisture. Microwave data are sensitive to the soil water content and open water extent. However, visible images can mirror only the water extent. Information about soil moisture can be derived from the difference of these sensitivities. This index was able to qualitatively describe the temporal evolution of the wetness over the Mackenzie River Basin. It is worth mentioning that vegetation distribution was considered in the formulation of the proposed index by the segregation between bare and vegetated soil soils by the mosaic approach. The BWI was finally downscaled using Digital Elevation Model data. The sensitivity of the topography attributes to the spatial distribution of soil moisture was assessed. A classical formulation of topographical index was modified in this study to take into account the difference of sensitivity of topographical attributes over bare and covered soils. The

combination of the modified topographical index and the proposed BWI enabled us to downscale the soil water content estimation and provide an estimate of soil moisture at the scale of the Digital elevation Model. Overall, the downscaling approach provided satisfactory resultants when compared to precipitation and temperature variation. Further works are needed to assess the reliability of the proposed approaches using results of distributed hydrological model outputs.

REMERCIEMENTS

Je tiens à exprimer toute ma reconnaissance à mon directeur monsieur Robert Leconte pour son encadrement et son support financier. Mes remerciements s'adressent également à mon co-directeur monsieur François Brissette pour ses judicieux conseils. Vous avez profondément marqué mes pensées. Mes vifs remerciements aux membres du jury pour leur attentive lecture de cette thèse et leurs intéressantes recommandations.

Je dédie ce travail à mes parents, Souad et Béchir pour leurs efforts pendant ce long parcours. Mes remerciements vont également à mes frères et sœurs.

Je suis particulièrement reconnaissant à ma femme Naira pour son soutien continu. Elle a su me soutenir pour la réalisation de mon diplôme d'ingénieur, ma maîtrise et mon doctorat. Merci Naira. Malgré les nuits blanches qu'elle m'a offertes, pendant la réalisation de cette thèse, je dédie avec un grand plaisir ce travail à notre bébé Lina. J'ai pris beaucoup de votre temps. Ce travail est en grande partie le vôtre.

TABLE DES MATIÈRES

	Page
SOMMAIRE	iii
ABSTRACT	v
REMERCIEMENTS	vii
TABLE DES MATIÈRES	1
LISTE DES FIGURES	4
LISTE DES ABRÉVIATIONS ET SIGLES	7
CHAPITRE 1 INTRODUCTION	8
1.1 Problématique	9
1.2 Description du bassin versant du Mackenzie	11
1.3 Objectifs de la thèse	15
1.4 Hypothèses de la recherche	16
1.5 Présentation de la thèse	17
CHAPITRE 2 UTILISATION DES MICRO-ONDES PASSIVES POUR L'ESTIMATION DE L'HUMIDITÉ DU SOL	20
2.1 Justification du choix des micro-ondes passives	20
2.2 Estimation de l'humidité du sol par les micro-ondes passives : État de connaissance	23
2.3 Les principaux facteurs affectant l'estimation de l'humidité du sol	25
2.3.1 La rugosité de surface	27
2.3.2 La végétation	29
2.3.3 Effet atmosphérique	33
2.4 Discussion	36
2.4.1 Approches globales pour l'estimation de l'humidité du sol	37
2.4.2 Utilisation du modèle de transfert radiatif pour l'estimation de l'humidité du sol	40
CHAPITRE 3 A DYNAMIC ESTIMATION OF FREE WATER SURFACE COVERAGE FROM A BASIN WETNESS INDEX OF THE MACKENZIE RIVER BASIN USING SSM/I MEASUREMENTS	43
3.1 Introduction	44
3.2 The Basin Wetness Index	47
3.3 Application	52
3.4 Conclusion	57

CHAPITRE 4 FLOOD MONITORING OVER THE MACKENZIE RIVER BASIN	
USING PASSIVE MICROWAVE DATA	64
4.1 Introduction	66
4.2 Methodology	68
4.2.1 Estimation of the water surface extent using passive microwave data	68
4.2.2 The rating curve formula.....	70
4.2.3 Use of the of Kalman filter	73
4.3 Application and Results	75
4.3.1 Study area: The Mackenzie River Basin.....	75
4.3.2 Approach reliability assessment using 1998 and 1999 data	76
4.3.3 Use of passive microwave data for discharge forecasting	79
4.4 Conclusion	81
CHAPITRE 5 FLOOD AND SOIL WETNESS MONITORING OVER THE	
MACKENZIE RIVER BASIN USING AMSR-E 37 GHZ	
BRIGHTNESS TEMPERATURE	94
5.1 Introduction	95
5.2 Methodology	97
5.2.1 Definition of the Wetness Index	99
5.2.2 The linear mixing model	102
5.2.3 Calibration of the mixing model parameters.....	105
5.2.4 Development of the Rating Curve Model	107
5.3 Results and Discussion.....	109
5.4 Conclusion	112
CHAPITRE 6 A COMBINATION OF REMOTE SENSING DATA AND	
TOPOGRAPHIC ATTRIBUTES FOR THE SPATIAL AND	
TEMPORAL CONTROL OF THE SOIL WETNESS OVER THE	
MACKENZIE RIVER BASIN	123
6.1 Introduction	124
6.2 Methodology	127
6.2.1 Area of study.....	127
6.2.2 The wetness index	128
6.2.3 Estimation of the basin wetness index, BWI, using passive microwave data	132
6.3 Results and discussion	136
6.3.1 Development of the WI maps	136
6.3.2 Estimation of the BWI	138
6.3.3 Combination of the WI and the BWI.....	140
6.4 Conclusion	144

CHAPITRE 7 ANALYSE ET DISCUSSION	155
7.1 Contribution de la thèse	155
7.2 Recommandations et travaux futurs.....	160
CONCLUSION	163
Tableau I.....	23
Tableau II	154
BIBLIOGRAPHIE	166

LISTE DES FIGURES

	Page	
Figure 1	Le bassin de drainage du fleuve Mackenzie et ses principales caractéristiques (Cohen, 1997).....	12
Figure 2	La distribution spatiale de la moyenne annuelle de précipitation dans le bassin du Mackenzie (Stewart et al., 1998).....	14
Figure 3	La moyenne mensuelle du débit à l'exutoire du Mackenzie enregistrée entre 1973-1995 (Stewart et al., 1998)	15
Figure 4	Réduction de la sensibilité à l'humidité du sol en fonction de la teneur en eau de la végétation (Jackson & Schmugge, 1991).....	31
Figure 5	La transmissivité de l'atmosphère dans le domaine des micro-ondes passives en fonction de la fréquence. (Ligne continue : atmosphère clair, ligne interrompue : 0.5 km d'épaisseur, ligne pointillée : 2 km d'épaisseur) (Schultz & Engman, 2000).	34
Figure 6	Variation de la différence entre les mesures des différentes fréquences à proximité du fleuve Mississippi (Basist et al., 1998).....	39
Figure 7	The Mackenzie River Basin.....	58
Figure 8	β_0 (figure 8a/) and β_1 (figure 8b/) variability during the summer seasons of 1999 and 1998.	59
Figure 9	Spatial distribution of the correlation coefficient of β_0 trends estimated during 1998 and 1999	60
Figure 10	Spatial variations of the FWS over the Mackenzie River Basin, during the summer season of year 2000.....	61
Figure 11	Comparison of the FWS estimates over the summer season of 1997, 1998, 1999 and 2000, in the basin outlet.	62
Figure 12	FWS estimated by constant and dynamic empirical parameters compared to the measured flow at basin outlet, during the summer of 1999.....	63
Figure 13	The Mackenzie River Basin.....	83
Figure 14	Discharge measured at the basin outlet is used as a proxy for temporal variation in WSF derived from passive microwave data	84
Figure 15	The relationship between measured flow and WSF estimated over the Mackenzie River Basin Outlet, during the summer of 1998.....	85

Figure 16	Predicted and estimated WSF compared to the Mackenzie River at Arctic Red River discharge, over the MRD, during the summer of 1998.....	86
Figure 17	Predicted and estimated WSF compared to the Mackenzie River discharge, over the MRD, during the summer of 1999.....	87
Figure 18	Predicted and estimated WSF compared to the Peace River discharge, over the PAD, during the summer of 1998	88
Figure 19	Predicted and estimated WSF compared to the Peace River discharge, over the PAD, during the summer of 1999	89
Figure 20	NOAA-AVHRR image of the PAD, August 24 th , 1999	90
Figure 21	Predicted WSF compared to those estimated from NOAA-AVHRR images, over the PAD, during the summers of 1999 and 1998.....	91
Figure 22	Predicted and observed discharge over the Slave River observing station from 1992 to 2000	92
Figure 23	Variability of the Averaged Time Lag Parameter from 1992 to 2000 over the PAD area	93
Figure 24	The Peace-Athabasca Delta, PAD.....	114
Figure 25	WSF(AMSR-E) and WSF(MODIS) temporal variability during the summer of 2003, over the PAD area.....	115
Figure 26	WSF(AMSR-E) and WSF(MODIS) temporal variability during the summer of 2002, over the PAD area.....	116
Figure 27	Flow-chart of the proposed algorithm.....	117
Figure 28	Rating Curve developed for the region of the PAD using 2002 and 2003 summer season MODIS images and discharge data	118
Figure 29	An example of flooded fraction map estimated over the PAD area on August 31, 2003	119
Figure 30	Temporal variability of the WI compared to the precipitation and temperature values observed during the summer of 2003	120
Figure 31	Temporal variability of the WI compared to the precipitation and temperature values observed during the summer of 2002	121
Figure 32	Temporal variability of the WI over the PAD compared to the measured soil moisture during the summer of 1998, 1999 and 2000.	122
Figure 33	The PAD area (Leconte et al., 2001).....	146
Figure 34	Rating Curve developed for the region of the PAD using 2002 and 2003 summer season MODIS images and discharge data	147

Figure 35	The spatial distribution of the classic WI.....	148
Figure 36	An example of variation of the vegetal cover fraction (V) over the PAD area during a summer season	149
Figure 37	Seasonal variability of the dynamic WI.....	150
Figure 38	Temporal variability of the BWI compared to the precipitation and temperature values observed during the summer of 2003	151
Figure 39	Temporal variability of the BWI compared to the precipitation and temperature values observed during the summer of 2002	152
Figure 40	Temporal variability of the WI over the PAD compared to the measured soil moisture during the summer of 1998, 1999 and 2000.	153

LISTE DES ABRÉVIATIONS ET SIGLES

MAGS	Mackenzie GEWEX Study
GEWEX	Global Energy and Water Cycle Experiment
MODIS	Moderate-resolution Imaging Spectroradiometer
AMSR	Advanced Microwave Scanning Radiometer
AMSR-E	Advanced Microwave Scanning Radiometer -EOS
SSM/I	Special Sensor Microwave/Imager
SMMR	Scanning Multichannel Microwave Radiometer
CLASS	Canadian Land Surface Scheme
NOAA	National Oceanic and Atmospheric Administration
AVHRR	Advanced Very High Resolution Radiometer
EFOV	Effective Field Of View
ISF	Indices de surface foliaire
LAI	Leaf Area Index
MRD	Mackenzie River Delta
BWI	Basin Wetness Index
PAD	Peace Athabasca Delta
WI	Wetness Index
WSF	Water Surface Fraction

CHAPITRE 1

INTRODUCTION

Au Canada, comme ailleurs, les fluctuations climatiques sont de plus en plus préoccupantes. Le suivi de la température et de la précipitation révèle des variations interannuelles importantes (Shabbar et al., 1997). Le Canada avec la plus grande réserve d'eau potable au monde se trouve très concerné par l'effet de ces variations sur ses réserves hydriques. La participation canadienne dans les recherches visant la maîtrise des facteurs régissant les phénomènes hydrologique et climatologique, se situe, entre autres, dans le cadre du projet GEWEX study (Global Energy and Water Cycle Experiment Study). Le bassin du fleuve Mackenzie, au nord-ouest canadien, fait partie des quelques bassins versants concernés par cette étude, tels que le bassin de l'Amazonie en Amérique du sud et le bassin Murray Darling en Australie. La large superficie et l'hétérogénéité de ce bassin font sa particularité. Cette thèse présente une contribution à la phase deux du projet MAGS II (Mackenzie GEWEX Study II) qui est une composante du projet GEWEX.

La modélisation des processus hydrologiques et climatologiques dans le bassin a montré l'importance d'une estimation journalière de l'humidité du sol (Soulis et al., 2000). La maîtrise de ce facteur est indispensable pour le suivi et la prévision aussi bien à court qu'à long terme des conditions météorologiques. L'intégration de cette donnée dans des modèles d'hydrologie et de météorologie améliorera également la compréhension des processus d'échange d'énergie entre le bassin et son environnement. Ce sont ces besoins qui ont défini les objectifs ultimes du présent projet de recherche.

1.1 Problématique

Deux raisons principales suggèrent, en général, l'estimation de l'humidité du sol. La première raison découle du rôle important joué par ce paramètre au niveau de l'échange d'énergie avec l'atmosphère. En effet, ce paramètre affecte considérablement l'énergie à la surface du sol ainsi que le flux des radiations émis par ce dernier. Ce sont ces radiations et cette énergie disponible à la surface qui contrôlent en réalité le flux d'évapotranspiration à la surface du sol. Ce dernier paramètre qui s'avère bien connecté à l'humidité du sol influence le bilan hydrique et les conditions climatiques dans les petits et grands bassins. Quelques centimètres seulement au niveau de la couche superficielle du sol contribuent à l'évapotranspiration. Dans la même optique, l'humidité du sol peut être utilisée pour l'initialisation des logiciels hydrologiques et climatologiques.

La deuxième raison qui suggère la nécessité d'estimer l'humidité du sol est la calibration et la validation des modèles hydrologiques et climatologiques. Généralement, la calibration et la validation des modèles hydrologiques se basent sur la comparaison des valeurs simulées et comparées des débits et des niveaux d'eau. L'humidité du sol peut être utilisée également comme une source d'information supplémentaire pour ces étapes incontournables à une utilisation judicieuse de ces logiciels.

Au cours de la première phase du projet MAGS, l'humidité du sol qui alimente les modèles hydrologiques a été fournie par des schémas de surface, communément appelés de première génération. Les schémas de surface modélisent la transformation pluie-débit par un transfert des eaux de surfaces et des eaux souterraines d'une cellule à l'autre. Les cellules sont des fractions du bassin simulé qui ont généralement une géométrie régulière (carré ou triangle) et qui correspondent à des pixels dans les images satellites.

En faisant appel à ces schémas, les modèles hydrologiques se sont avérés incapables de reproduire les débits observés au cours de certaines périodes de l'année (Soulis et al., 2000). Afin de surmonter cette difficulté, l'amélioration des schémas de surface par la mise en œuvre d'une deuxième et nouvelle génération a été nécessaire.

Le schéma de surface canadien, CLASS (Canadian Land Surface Scheme), a été développé par Environnement Canada (Verseghy, 2000). Ce schéma de surface est au cœur du programme canadien visant le développement d'une deuxième génération de schémas de surface. L'objectif de ce programme est de combiner CLASS au modèle hydrologique WATFLOOD qui a été développé par l'université de Waterloo (Rouse, 2000), dans le but d'améliorer la représentation de l'humidité du sol et de mieux estimer le débit du ruissellement.

Le résultat du rattachement de CLASS à WATFOOLD est un module combiné, communément appelé WATFLOOD/CLASS ou WATCLASS. L'apport de cette combinaison réside dans la considération de la distribution verticale de l'eau dans le sol simultanément avec le transfert entre cellules de l'humidité du sol. Le bassin du Mackenzie objet de la présente recherche a été sélectionné pour tester le produit de ce couplage.

Le couplage WATFLOOD/CLASS a montré une sous-estimation de l'humidité du sol. La sous-estimation de l'humidité est d'autant plus importante que la profondeur est grande (Soulis et al., 2000). Le modèle a présenté également une sous-estimation de l'évaporation cumulative. Une meilleure estimation de débit a toutefois été obtenue par le modèle WATCLASS au cours de l'épisode humide. Cependant, pendant le temps sec le modèle WATCLASS surestime le débit. Ainsi, par rapport à la première version

(WATFLOOD), le modèle couplé, sous-estime l'humidité dans le sol et l'évaporation afin de compenser la différence entre les débits mesuré et simulé.

Ces résultats permettent néanmoins d'apprécier l'apport de la combinaison de deux modules WATFLOOD et CLASS. Cependant, cet apport reste toujours difficile à valider à cause de l'absence d'une source externe d'information. L'intérêt sera donc de développer une approche permettant d'estimer la distribution spatiale et temporelle de l'humidité du sol. Cette nouvelle source de données devra être compatible avec WATCLASS afin de pouvoir valider ses résultats. La disponibilité de cette information supplémentaire sera un pas de plus vers la validation des résultats du couplage WATCLASS et l'appréciation de ses performances. L'hétérogénéité et la grande superficie du Mackenzie, objet de cette étude, motivent le choix d'opter pour la télédétection comme source d'information à explorer.

1.2 Description du bassin versant du Mackenzie

Le fleuve Mackenzie, un parmi les plus grands fleuves au monde, draine un bassin d'une superficie totale de 1.8 million de km², approximativement 20% de la superficie du Canada (Figure 1). Le bassin du Mackenzie se compose de six sous-bassins hydrographiques. Il comprend également trois lacs parmi les plus grands au monde, à savoir, le lac de l'Athabasca, le lac des Esclaves et le lac de l'Ourse. Le delta de l'Athabasca qui s'étale sur une superficie approximative de 4 000 km², à l'extrême ouest du lac, est l'un des plus grands deltas intérieurs au monde.

La végétation au bassin du fleuve Mackenzie est très variable. Elle est plus dense (boréale) au sud du bassin et moins dense (toundra) au nord. Le relief du bassin est également très variable. Les montagnes occupent les limites ouest du bassin. Les régions

centrales, à l'est, sont généralement planes. Le débit à l'exutoire du fleuve, qui s'écoule du sud vers le nord, avec une moyenne annuelle de 9 100 m³/s, est le deuxième au pays de point de vue importance après celui du fleuve Saint-Laurent. Le régime d'écoulement dans le fleuve et les rivières dans le bassin est souvent perturbé pendant la fonte printanière à cause de la formation d'embâcles. Ceci augmente les niveaux d'eau et accentue le risque d'inondation dans le bassin. Cependant, cette importante ressource hydrique est sujette à des fluctuations considérables générées par la variation des conditions climatiques (Shabbar et al., 1997). Ces fluctuations sont expliquées dans les paragraphes subséquents.



Figure 1 Le bassin de drainage du fleuve Mackenzie et ses principales caractéristiques (Cohen, 1997)

L'effet de la variation des conditions climatiques se reflète sur trois paramètres principaux, à savoir, la température, la précipitation et le débit à l'exutoire. En premier lieu, la température saisonnière moyenne dans le bassin varie de -30°C pendant l'hiver jusqu'à +15°C pendant l'été. Au cours de certains jours particuliers de l'année cette température peut atteindre -50°C en hiver et +30°C en été présentant ainsi un gradient considérable de 80°C. Cependant, c'est la variation interannuelle de la température qui semble être la plus dramatique pour le bassin. En effet, le Mackenzie présente actuellement un des plus grands taux de réchauffement dans le monde atteignant pendant la saison froide une valeur de 2°C par 10 ans. La non-linéarité de cette augmentation complique encore plus la situation (Stewart et al., 1998).

Par ailleurs, la moyenne annuelle de la précipitation dans le bassin du Mackenzie a été estimée de 400 mm/an avec des quantités plus importantes habituellement pendant l'été. Le suivi de l'évolution au cours des années de la précipitation dans le bassin laisse voir également une variation interannuelle. La distribution spatiale de l'intensité moyenne de précipitation, obtenue à partir de l'étude de Stewart et al. (1998) est illustrée par la figure 2 et montre des intensités plus élevées dans la région sud-ouest du bassin, avec une moyenne qui peut atteindre 1 000 mm/an. Dans les régions centrales, la précipitation annuelle moyenne est considérablement réduite par les montagnes se trouvant tout au long de la limite ouest du bassin. Ces montagnes, s'élevant de 2 à 3 km d'altitude, jouent le rôle d'obstacles au déplacement de l'humidité provenant de l'océan Pacifique.

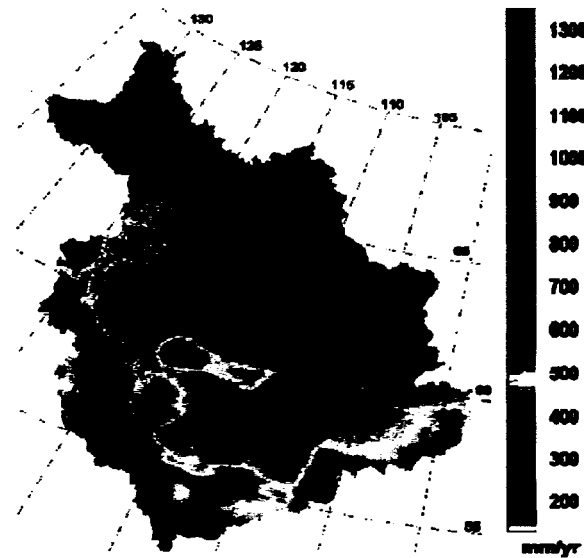


Figure 2 La distribution spatiale de la moyenne annuelle de précipitation dans le bassin du Mackenzie (Stewart et al., 1998).

Le débit à l'exutoire du bassin est également sujet à des fluctuations interannuelles considérables. La figure 3 suivante illustre l'évolution du débit à l'exutoire du fleuve Mackenzie. Selon cette figure, le maximum qui excède régulièrement 20 000 m³/s a été souvent observé durant le mois du juin. Pour certaines années, comme 1988 et 1979, les débits maximaux ont été enregistrés avec un retard approximatif de 3 à 4 semaines par rapport au 23 années de mesures de 1973 à 1995. Au cours de l'hiver, le débit est considérablement réduit et peut être aussi faible que 2 000 m³/s. Les fluctuations interannuelles qui affectent le débit à l'exutoire du fleuve Mackenzie sont par conséquent très significatives, à l'instar des bassins versants situés en région dominée par un climat nordique.

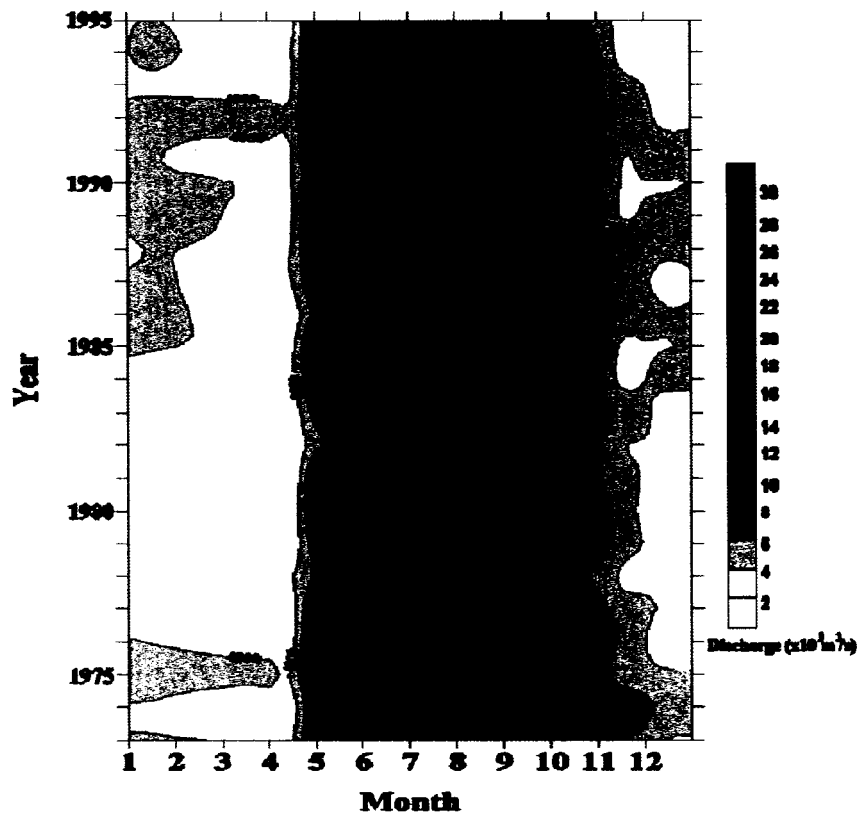


Figure 3 La moyenne mensuelle du débit à l'exutoire du Mackenzie enregistrée entre 1973-1995 (Stewart et al., 1998)

1.3 Objectifs de la thèse

L'objectif du présent travail est le développement d'une approche pour le suivi de l'évolution de la réserve hydrique dans le bassin du Mackenzie en utilisant des images satellites captées dans le domaine des micro-ondes passives. Les cartes d'humidité du sol dérivées des images captées en micro-ondes passives reflètent la présence de l'eau libre dans la couche superficielle du sol (quelques centimètres de profondeur) et des plans d'eau existants à sa surface (Basist et al., 2001; Fily et al., 2003).

L'atteinte de l'objectif de cette recherche nécessite une maîtrise de la variabilité temporelle et spatiale de l'humidité du sol à l'échelle du bassin. Les cartes d'humidité qui seront développées pourraient servir, entre autres, à la validation des résultats de WATCLASS. Toutefois, le produit final de ce travail devrait être facilement transposable et adaptable pour pouvoir l'utiliser éventuellement dans d'autres études.

L'atteinte de l'objectif ultime de ce travail nécessite la réalisation de deux objectifs secondaires principaux. Le premier objectif consistera à développer un indice d'humidité du Mackenzie visant une description qualitative de l'évolution spatiale et temporelle de la réserve hydrique dans le bassin. Cet indice devrait refléter l'état de la réserve hydrique dans le Mackenzie. Le deuxième objectif de ce travail visera la considération de l'hétérogénéité du bassin et l'évolution dans le temps des conditions à sa surface dans l'algorithme de calcul de l'indice d'humidité. L'hétérogénéité et la large étendue qui caractérisent le Mackenzie imposent une considération de la variabilité spatiale et temporelle des paramètres à la surface de son sol, tels que, la végétation, la texture du sol et le relief. Un intérêt plus particulier sera réservé à cet aspect dans ce travail. Le principe de l'ajustement dynamique des paramètres de surface sera considéré dans les algorithmes développés.

1.4 Hypothèses de la recherche

L'hypothèse de base de ce travail est la dominance de l'effet de l'humidité de sol et des plans d'eau tels que les lacs et les rivières dans le signal capté en micro-ondes passives. Il a été supposé également que la sensibilité des micro-ondes passives à l'humidité du sol dépend de l'hétérogénéité des pixels visés par le satellite. Ceci signifie que la considération de l'hétérogénéité est susceptible d'améliorer l'estimation de l'humidité du sol. Ce travail portera, entre autres, sur la vérification de cette deuxième hypothèse et

le filtrage du bruit qui pourrait être introduit par le couvert végétal et/ou la rugosité de la surface.

La troisième hypothèse porte sur la variabilité spatiale et temporelle des paramètres caractérisant l'état de la végétation et la rugosité de surface dans la région du Mackenzie. La prise en compte de la variabilité dans l'espace est exigée par l'hétérogénéité et la diversité des modes d'occupation du sol dans le bassin. La variabilité dans le temps est par ailleurs suggérée par l'évolution rapide au cours de la saison d'été du couvert végétal et des conditions à la surface. Il a été supposé dans cette recherche que cette variabilité temporelle est périodique et qu'elle respecte la même tendance d'une saison à l'autre.

L'analyse de cette variabilité spatio-temporelle est donc essentielle pour une meilleure estimation de la réserve hydrique dans le Mackenzie. Un des objectifs de ce travail sera de valider cette hypothèse et d'adapter le principe de l'ajustement dynamique des paramètres pour estimer le contenu en eau du sol par un modèle alimenté par des paramètres variables dans l'espace et dans le temps.

1.5 Présentation de la thèse

Tout d'abord, il est important de dégager la particularité de ce sujet de thèse qui a été réalisé au sein d'une école de génie, l'école de technologie supérieure (ÉTS). Cette recherche a commencé en janvier 2002. Afin de respecter les exigences de l'école, dix-huit crédits de cours, dans les domaines de la télédétection et des systèmes d'information géographique, ont été suivis à l'université McGill et à l'université de Montréal. Ces cours ont été succédés par un examen prédoctoral à l'été 2003. Compte tenu de

l'importance des publications dans le processus du transfert technologique, la formule de la thèse par articles a été choisie.

Le premier chapitre de cette thèse est une introduction qui présente la problématique du sujet de recherche, ses objectifs et ses hypothèses. Le deuxième chapitre présente une synthèse bibliographique assez exhaustive des travaux de recherche qui ont traité la problématique de l'utilisation des micro-ondes passives pour l'estimation de l'humidité du sol. Ce deuxième chapitre discute aussi l'effet des facteurs, tels que la végétation, la rugosité de surface et l'atmosphère sur les micro-ondes passives. À la fin de ce chapitre, une synthèse des approches préconisées pour l'estimation de l'humidité de sol a été présentée.

Quatre articles ont été soumis dans le cadre de la présente thèse. Ces articles font l'objet des chapitres 3, 4, 5 et 6. Ces articles ont été soumis, en anglais, respectivement au Journal canadien de télédétection, Remote Sensing of Environment, Journal of Hydrology et IEEE-Transactions.

Le troisième chapitre applique une approche pour l'estimation de l'humidité du sol à l'échelle du Mackenzie. Ce chapitre définit également un indice qui reflète l'étendue des plans d'eau dans le bassin. Dans ce chapitre, la variabilité des paramètres de l'indice a été analysée. Une corrélation a été notée entre l'indice d'humidité estimé et les débits observés. Cette corrélation a été exploitée au chapitre quatre pour le développement d'un modèle de tarage qui se base sur deux paramètres empiriques. Ce modèle présente un potentiel intéressant pour le suivi de l'évolution des plans d'eau, en temps réel en utilisant les débits observés à l'amont ou à l'aval du site étudié. Le deuxième article qui a fait l'objet du chapitre quatre a été déjà publié dans le journal Remote Sensing of Environment (Temimi et al., 2005). Dans ce deuxième article, les estimations de la

fraction des plans d'eau dérivées des micro-ondes passives ont été comparées à celles estimées à partir des images captées dans le domaine du visible. Une différence de sensibilité a été notée entre les deux sources. En fait, les micro-ondes passives surestiment les fractions des plans d'eau car elles sont sensibles à l'eau retenue à la surface ainsi que l'eau libre stockée dans le sol. En se basant sur ce constat, un indice d'humidité a été développé au troisième article qui a fait l'objet du chapitre 5. L'indice d'humidité développé reflète l'état d'humidité global dans le bassin étudié. La mise en échelle de ses valeurs est donc nécessaire pour obtenir des estimations locales de l'humidité du sol. Cet objectif a été poursuivi au quatrième article qui a été présenté au chapitre 6. Dans ce chapitre, un indice topographique classique a été modifié en introduisant un paramètre décrivant la densité de végétation par pixel. Cet indice présente le potentiel d'humidité de chaque pixel. Autrement dit, cet indice distribue spatialement le contenu en eau qui a été estimé globalement dans le chapitre 5. Ainsi, l'approche proposée au chapitre 6 vient comme une suite logique des chapitres précédents. Le produit final au terme de ce chapitre est une estimation locale de l'humidité du sol en se basant sur des approches qui tiennent compte de la variabilité temporelle des conditions de surface.

Ces quatre chapitres sont succédés d'un septième chapitre de synthèse qui résume les résultats des articles et présente des recommandations pour les recherches futures. Finalement, le dernier chapitre a été réservé pour la conclusion générale de cette recherche. Nous espérons avoir répondu avec cette recherche aux objectifs arrêtés.

CHAPITRE 2

UTILISATION DES MICRO-ONDES PASSIVES POUR L'ESTIMATION DE L'HUMIDITÉ DU SOL

2.1 Justification du choix des micro-ondes passives

La sensibilité des micro-ondes à l'humidité du sol a été prouvée par plusieurs études (Jackson & Le Vine, 1996; Mattikalli et al., 1998; Njoku & Kong, 1977; Schmugge, 1998). Dans ce domaine du spectre, deux techniques existent, à savoir, les micro-ondes passives et les micro-ondes actives.

Les émissions naturelles de la surface du sol sont mesurées, en micro-ondes passives, à l'aide d'un radiomètre et sont exprimées en températures de brillance. Les micro-ondes actives sont produites par un radar pour mesurer le coefficient de rétrodiffusion qui est également fortement affecté par l'humidité du sol. Comparativement aux mesures en micro-ondes passives, la couverture spatiale des radars est limitée. Par contre, leur résolution spatiale est beaucoup plus fine. Compte tenu de la large étendue du bassin du Mackenzie, l'utilisation des micro-ondes passives s'avère comme un choix indispensable.

Du et Ulaby (2000) ont ressorti les avantages et les inconvénients de chacune de ces deux techniques. La sensitivité à l'humidité du sol présente le point commun de ces deux techniques. La végétation, la rugosité de surface et l'atmosphère affectent les mesures réalisées à la fois en micro-ondes passives et actives.

Les micro-ondes passives présentent cinq avantages principaux (Jackson, 1993).

- 1- La contribution de l'atmosphère est faible, voire nulle, dans les longueurs d'ondes de l'ordre de quelques centimètres.
- 2- Le couvert végétal est semi transparent.
- 3- L'émissivité du sol dépend de sa constante diélectrique qui est reliée à l'humidité dans le sol.
- 4- Les mesures en micro-ondes passives sont indépendantes des radiations solaires. Les mesures dans ce domaine sont donc possibles pendant le jour et la nuit.
- 5- Une large couverture spatiale et une fréquence élevée d'acquisition dans le temps.

Selon l'étude de Njoku et Entekhabi (1996), les deux capteurs à plate-forme satellitaire, les plus appropriés dans le domaine des micro-ondes passives, pour l'estimation de l'humidité du sol, sont le SMMR (Scanning Multichannel Microwave Radiometer) (Gloersen & Barath, 1977) et le SSM/I (Special Sensor Microwave/Imager) (Hollinger et al., 1990). Ces deux capteurs fonctionnent respectivement dans les domaines du spectre électromagnétique de 6.6-37 GHz et 19.3-85.5 GHz. Cependant, l'effet de l'atmosphère et la végétation, dans ces domaines du spectre, est plus significatif. L'interprétation des données ne doit se faire donc que par une considération de cet effet.

Par ailleurs, ces deux capteurs présentent deux avantages opérationnels majeurs. Le premier avantage réside dans leur multi-polarisation et leur multi-fréquence. La diversité des canaux facilite le filtrage des effets relatifs à la végétation et à la rugosité de surface. Le deuxième avantage de ces deux capteurs correspond à la constance de leur angle d'incidence. En fait, les images sont prises sous le même angle d'incidence (51° pour SSM/I), indépendamment de la position du satellite sur son orbite. Ainsi, les corrections angulaires ne sont pas nécessaires pour les images acquises.

Cependant, ces deux capteurs présentent, pour certaines études, une limitation au niveau de leur faible résolution spatiale (27-150 Km pour SMMR et 15-70 km pour SSM/I). Le flux des émissions du sol est relativement faible dans le domaine des micro-ondes passives. Les dimensions des antennes des capteurs passifs, limitées par des contraintes techniques, exigent que le flux soit émis par une surface suffisamment grande pour qu'il soit capté. Cela limite en conséquence, la résolution spatiale de ces capteurs.

Récemment le nouveau capteur AMSR-E a été lancé (Njoku et al., 2003). L'avantage principal de ce capteur réside dans sa capacité de fournir des températures de brillance mesurées à 6,9 et 10,7 GHz. Ces fréquences présentent une meilleure sensibilité à l'humidité du sol à cause de la moindre sensibilité à la présence de végétation qui masque en partie les émissions en provenance du sol. En outre, ce capteur a amélioré la résolution spatiale des mesures effectuées à des fréquences supérieures à 19 GHz. Cependant, la résolution spatiale de ces mesures demeure faible, notamment à 6,9 et 10,7 GHz. La comparaison des estimations de l'humidité du sol à partir de ces mesures est donc difficile. Le tableau suivant résume les caractéristiques principales des différents capteurs.

Tableau I

Caractéristiques principales des capteurs micro-ondes passives (Njoku & Li, 1999)

Paramètres	SMMR	SSM/I	AMSR-E
Fréquences (GHz)	6.6, 10.7, 18, 21 et 37	19.3, 22.3, 37 et 85.5	6.9, 10.7, 18.7, 23.8, 36.5 et 89
Période de fonctionnement	1978-1987	1987-Opérationnel	2002
Résolution (km)			
Pour 6 GHz	95x48	N/A	43x75
Pour 37 GHz	18x27	28x37	8x14

2.2 Estimation de l'humidité du sol par les micro-ondes passives : état de connaissance

Généralement, l'extraction de l'humidité du sol à partir des mesures des micro-ondes passives émises par la surface du sol ne doit se faire que suite à la correction de l'effet de certains facteurs, notamment la rugosité de surface et la végétation. Suite à ces corrections, les mesures devraient représenter exclusivement les émissions du sol et isoler ainsi l'effet de la constante diélectrique dû à la présence de l'eau. Les mesures corrigées servent donc à l'extraction de l'humidité du sol.

Plusieurs études ont recommandé la bande L (1.4 GHz / 21 cm) pour l'estimation de l'humidité du sol (Burke et al., 2002; Jackson & Le Vine, 1996; Jackson et al., 1995; Liou & England, 1998; Njoku & Entekhabi, 1996). L'avantage principal de cette bande est la minimisation de l'effet de végétation et de la rugosité de surface. Ceci augmente sa sensibilité à l'existence de l'eau dans le sol. Cette bande présente également une profondeur de pénétration de l'ordre de quelques centimètres, suffisante pour refléter le contenu en eau de la couche superficielle du sol. Aucun capteur satellitaire n'est équipé de cette fréquence jusqu'à date. Les algorithmes développés, utilisant la bande L (1.4 GHz / 21 cm), ont été validés par des mesures prises par des capteurs à plate-forme aéroportée.

En absence des mesures prises dans la bande L (1.4 GHz / 21 cm) à partir d'un capteur satellitaire, d'autres approches ont été développées utilisant des températures de brillance en provenance des capteurs satellitaires tel que SMMR et SMM/I. Les algorithmes développés ont été adaptés aux fréquences utilisées. La sensibilité des capteurs à la présence d'eau dans le sol varie avec la fréquence. La différence entre les approches réside notamment dans la considération du couvert végétal. Cet effet du couvert végétal est essentiellement tributaire de la teneur en eau de la végétation. En effet, pour des fréquences élevées (> 18 GHz) comme celles du SSM/I, la diffusion du signal électromagnétique dans le couvert végétal n'est plus négligeable (Choudhury et al., 1990). La prise en compte de cet effet est indispensable. Cependant, dans le cas des fréquences moins élevées (< 18 GHz), la modélisation du phénomène de transfert radiatif peut être simplifiée en négligeant l'effet de la diffusion de la végétation sous des conditions de faible densité du couvert végétal.

Cependant, la correction de l'effet de la rugosité a été recommandée pour toutes les bandes utilisées (Njoku & Entekhabi, 1996). Le filtrage de l'effet de la surface rugueuse ramène la réflectivité à celle d'une surface lisse exprimée par les formules de Fresnel

(Ulaby et al., 1982). Cette réflectivité dépend de la constante diélectrique de la surface et de l'angle local d'incidence.

Par ailleurs, pour des longueurs d'ondes inférieures à 2 cm, correspondant à des fréquences supérieures à 15 GHz, l'effet atmosphérique devient remarquable (Choudhury, 1991; Schultz & Engman, 2000). Pour des mesures prises avec SSM/I (19 GHz, 1,5 cm) ces perturbations atmosphériques sont significatives. L'atmosphère contribue par deux effets, soit un effet additif, dû à la température du globe et un effet multiplicatif relié à la réduction par la transmissivité des couches atmosphériques, en présence des molécules d'eau et d'oxygène.

De cette dernière discussion, il ressort que trois corrections sont nécessaires avant l'inversion du modèle de transfert radiatif, à savoir les corrections atmosphériques, les corrections de l'effet du couvert végétal et les corrections de la rugosité de surface. Toutefois, une ou plusieurs de ces perturbations peut être négligée dépendamment de la fréquence utilisée. Cela conduit à la simplification du modèle de transfert radiatif. Dans le paragraphe suivant, les principaux modèles préconisés pour la correction de l'effet des différents facteurs seront exposés.

2.3 Les principaux facteurs affectant l'estimation de l'humidité du sol

Pour un sol nu avec une surface lisse la température de brillance, T_b , s'exprime en fonction de l'émissivité et la température de la surface selon la relation suivante :

$$T_b = \varepsilon T \quad (2.1)$$

ε : Émissivité

T : Température de Surface ($^{\circ}$ K)

La réflectivité d'une surface est reliée à l'émissivité par la formule suivante :

$$\epsilon = 1 - r_0 \quad (2.2)$$

r_0 est la réflectivité de Fresnel.

r_{0v} est la réflectivité de Fresnel en polarisation verticale.

r_{0h} est la réflectivité de Fresnel en polarisation horizontale.

$$r_{0v} = \left| \frac{e_r \cos \theta - \sqrt{e_r - \sin^2 \theta}}{e_r \cos \theta + \sqrt{e_r - \sin^2 \theta}} \right|^2 \quad (2.3.a)$$

$$r_{0h} = \left| \frac{\cos \theta - \sqrt{e_r - \sin^2 \theta}}{\cos \theta + \sqrt{e_r - \sin^2 \theta}} \right|^2 \quad (2.3.b)$$

Où :

e_r est la constante diélectrique du sol

θ est l'angle d'incidence relative à la normale à la surface.

La réflectivité de surface est fortement tributaire de la constance diélectrique (Njoku & Entekhabi, 1996). Donc, l'émissivité du sol et sa température de brillance dépendent de la constante diélectrique du sol. Les émissions naturelles du sol sont perturbées par la rugosité de surface, le couvert végétal et l'atmosphère.

Dans le cadre de la présente étude, l'importance des conditions à la surface (rugosité et végétation) et la localisation du bassin du Mackenzie au nord-ouest canadien suggèrent

de considérer exclusivement la période estivale. Pendant l'hiver, le sol dans le Mackenzie est généralement couvert de neige et/ou gelé. L'effet de la neige dépend notamment de son équivalent en eau. Sous ces conditions, la physique de la propagation des micro-ondes passives diffère considérablement de celle des sols humides. En fait, dans les deux cas, les molécules d'eau sont reliées par une liaison supplémentaire qui empêche leur rotation et la forte atténuation du rayonnement électromagnétique. Ainsi, l'extraction de l'humidité du sol serait fortement compromise par la présence du manteau nival et de la glace.

2.3.1 La rugosité de surface

L'émission des radiations à partir des surfaces rugueuses respecte également la relation (2.2). Cependant, la réflectivité (r_0) dans cette relation doit tenir compte du phénomène de la diffusion du rayonnement au niveau de la surface. Ainsi, une écriture semi-empirique de la réflectivité a été proposée par Wang et Choudhury (1981) :

$$r_p = [Qr_{0q} + (1-Q)r_{0p}] \exp(-h') \quad (2.4)$$

Où :

r_{0p} et r_{0q} sont respectivement les réflectivités qui auraient mesuré la surface si elle était lisse, aux polarisations p et q.

h' et Q sont deux paramètres du modèle qui varient selon la fréquence et le type du sol. Leur détermination se fait expérimentalement. Pour des valeurs nulles de ces paramètres, on obtient la réflectivité d'une surface lisse. Lorsque les caractéristiques de la rugosité de surface sont inconnues, Jackson (Jackson, 1993) a recommandé, pour une fréquence de 1,4 GHz, une valeur nulle de Q et une valeur variant entre 0 et 0,3 pour h' .

Lakshmi (1996) a calculé la réflectivité de la surface rugueuse par une relation proposée par Choudhury et al. (1979). Cette relation est une simplification de la relation précédente proposée par Wang et Choudhury (1981). Elle s'écrit comme suit :

$$r_p = r_{op} \exp(-h) \quad (2.5)$$

Les valeurs de h varient entre 0 pour une surface lisse et 0,5 pour une surface rugueuse.

Mo et Schmugge (1987) ont proposé une formule semi-empirique, qui tient compte de l'effet de l'angle d'incidence sur l'estimation de la réflectivité du sol. Cette expression s'écrit comme suit :

$$r_p(\theta) = r_{op}(\theta) \exp(-G) \quad (2.6)$$

Où θ est l'angle d'incidence,

G est une fonction logarithmique qui fait intervenir les caractéristiques de la géométrie de la surface ainsi que la longueur d'onde.

Généralement, la rugosité de surface baisse la réflectivité, augmente donc l'émissivité et la valeur de la température de brillance (T_b). Ce facteur réduit également l'écart entre les deux polarisations verticale et horizontale de la T_b . Bien que l'effet de la rugosité de surface ne soit pas prépondérant dans les mesures de T_b , sa correction reste toujours indispensable pour une meilleure estimation de l'humidité dans le sol (Ulaby et al., 1986).

Par ailleurs, le sol réduit par son volume et ses cavités la valeur T_b . Le taux de réduction de T_b dépend de la longueur d'onde. Ce phénomène est notamment présent dans le domaine des courtes longueurs d'ondes, de l'ordre de quelques millimètres. Cependant,

la réduction par l'effet du volume du sol est généralement négligée dans les mesures de T_b car elle est compensée par la microrugosité de la surface même si cette dernière est considérée lisse.

2.3.2 La végétation

Le couvert végétal a été souvent considéré comme une couche homogène qui enveloppe la surface du sol. Ainsi, l'origine des radiations sera donc un milieu à deux couches, celle du sol, dont la surface est considérée généralement rugueuse, et celle de la végétation. La modélisation de la transmission des radiations de la surface du sol jusqu'à la surface limite supérieure du couvert végétal dépend de la fréquence. Généralement, l'effet du couvert végétal est minimisé à des fréquences inférieures à 3 Ghz (Njoku & Li, 1999). Cependant, pour des fréquences supérieures à la bande X, soit 10 Ghz, la contribution du couvert végétal domine et la caractérisation de son feuillage, ses branches, ses tiges doit être prise en compte dans la formulation du modèle de transfert radiatif (Njoku et al., 2003). Pour les fréquences 6 et 10 Ghz comme celles du capteur AMSR ou de l'ancien SMMR, l'effet de la végétation est présent mais il n'est pas dominant.

Njoku et Entekhabi (1996) ont proposé la relation suivante pour calculer la température de brillance au niveau de la couche supérieure du couvert végétal :

$$T_{bp} = \varepsilon_p T_e \exp(-\tau) + (1 - w) T_c [1 - \exp(-\tau)] [1 + r_p \exp(-\tau)] \quad (2.7)$$

Pour des fréquences moins élevées (< 3 GHz) le terme "w" qui représente la diffusion dans le milieu végétal devient négligeable. Dans ce cas, la T_b s'écrit selon la formule suivante :

$$T_{bp} = \varepsilon_p T_e \exp(-\tau) + T_c [1 - \exp(-\tau)] [1 + r_p \exp(-\tau)] \quad (2.8)$$

Où :

T_c est la température de la végétation,

T_e est la température effective du sol,

ε_p et r_p sont respectivement l'émissivité et la réflectivité de la surface du sol, à la polarisation p,

τ est l'opacité du couvert végétal. C'est le paramètre clé dans la considération du couvert végétal. Sa valeur dépend du type de la végétation, de sa teneur en eau ainsi que de la longueur d'onde. Parmi les facteurs affectant l'opacité de la végétation, la teneur en eau (W) semble être la plus importante, car elle agit directement sur l'émissivité du milieu et par la suite sur T_b .

Jackson et Schmugge (Jackson & Schmugge, 1991) ont noté une proportionnalité entre la teneur en eau de la végétation et son opacité. Ils ont proposé ainsi la relation suivante pour estimer τ :

$$\tau = b W \quad (2.9)$$

Le coefficient de proportionnalité, b, varie peu avec le type de la végétation notamment pour les basses fréquences. A titre indicatif, pour une fréquence de 1,4 GHz et une teneur en eau variant entre 0,5 et 6 Kg.m⁻², une valeur de b égale à 0,12 devrait être concluante (Jackson & Schmugge, 1991).

La sensibilité de la T_b à l'humidité du sol diminue exponentiellement avec l'augmentation de la teneur en eau de la végétation (Figure 4). D'où la nécessité

également de corriger l'effet du couvert végétal pour avoir des estimations assez exactes de l'humidité du sol.

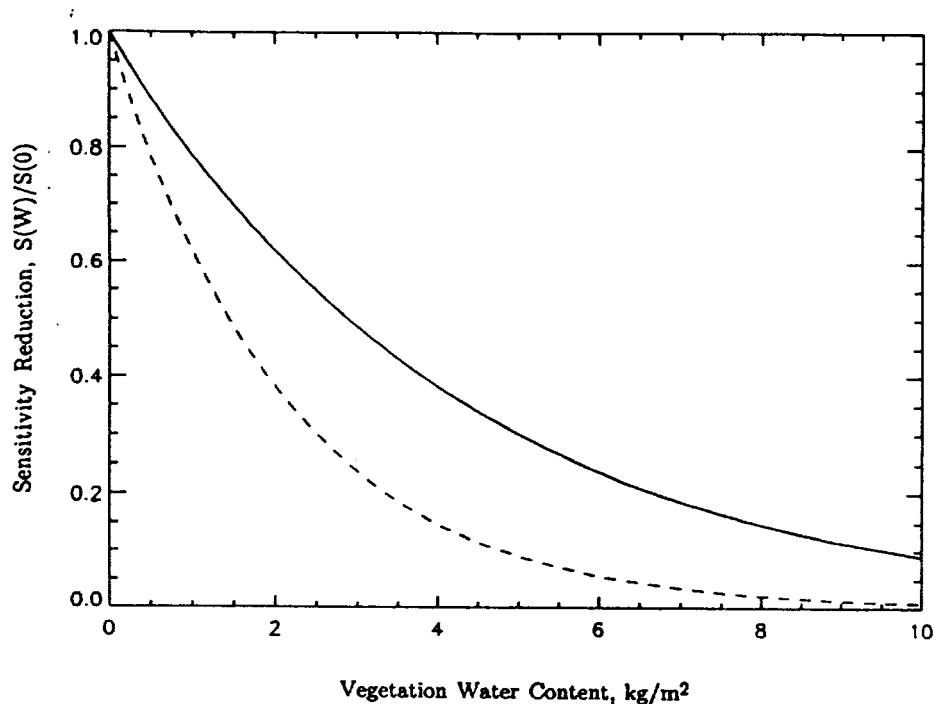


Figure 4 Réduction de la sensibilité à l'humidité du sol en fonction de la teneur en eau de la végétation (Jackson & Schmugge, 1991)

Pour des fréquences supérieures à 18 GHz, telles que celles de SSM/I, Choudhury et al. (Choudhury et al., 1990) ont proposé une approche plus complexe qui tient compte de la diffusion du rayonnement électromagnétique dans le milieu végétal. Selon cette étude, le couvert végétal contribue à l'atténuation du rayonnement par trois composantes : le feuillage, les branches et les tiges. La réflectivité de chacune de ces composantes a été estimée séparément. La réflectivité effective de l'ensemble sol-végétation a été formulée selon la relation linéaire simplifiée suivante :

$$A = R(\mu_0) \exp(-2\alpha) + A_c(1 - \exp(-2\alpha)) \quad (2.10)$$

Où :

- A_c : Réflectivité du couvert végétal

$$A_c = \frac{1 - (E(\mu_0)/K(\mu_0))^{\frac{1}{2}}}{1 + (E(\mu_0)/K(\mu_0))^{\frac{1}{2}}}$$

E et K sont deux fonctions qui dépendent des caractéristiques du couvert végétal.

- $R(\mu_0)$: Réflectivité de la surface du sol, en fonction de $\mu_0 = \cos \theta$, avec $\theta=54^0 7'$. Pour le SSM/I, l'angle d'incidence est de $51^0 3'$. Choudhury et al. (Choudhury et al., 1990) considèrent que la différence entre les deux angles est faible et qu'elle n'affecte pas les simulations réalisées par les données SSM/I.
- "α" est un paramètre caractérisant la diffusion et l'absorption du signal dans la végétation. Pour estimer sa valeur, Choudhury et al. (Choudhury et al., 1990) proposent des relations complexes faisant appel à des données en relation avec l'orientation du feuillage, la profondeur du couvert végétal, les caractéristiques des branches, des tiges constituant le milieu végétal. Ce paramètre dépend implicitement du contenu en eau de chacune des composantes du milieu à savoir les feuilles, les branches et les tiges. Pour un sol nu, ce paramètre "α" est nul. Il tend vers l'infini pour un couvert végétal dense. Le coefficient "α" s'écrit selon la relation suivante :

$$\alpha = (3E(\mu_0)K(\mu_0))^{\frac{1}{2}} \quad (2.11)$$

Il ressort donc que la réflectivité effective du milieu sol-végétation est tributaire essentiellement de deux paramètres reliés au couvert végétal soit "α" et A_c . Les expressions de ces deux paramètres sont toutefois complexes et exigent une

connaissance précise des caractéristiques du milieu végétal, ce qui dans le cas du bassin Mackenzie, est impossible à obtenir vu la taille et les difficultés d'accès à ce bassin

2.3.3 Effet atmosphérique

Dans le domaine des micro-ondes passives, la transmissivité de l'atmosphère est inférieure à 1 pour des fréquences supérieures à 15 GHz. L'effet de l'atmosphère est d'autant plus important que la fréquence est élevée (figure 5). Les fréquences captées par le SSM/I sont donc particulièrement concernées par la correction de l'effet de l'atmosphère. Dans cette optique, Choudhury et al. (1991) ont estimé l'épaisseur optique de l'atmosphère par une relation linéaire qui s'écrit en fonction de la vapeur d'eau précipitable dans l'air :

$$\text{Pour 19 GHz : } \tau = 0.011 + 0.0026 V \quad (2.12 \text{ a})$$

$$\text{Pour 37 GHz : } \tau = 0.037 + 0.0021 V \quad (2.13 \text{ b})$$

τ : épaisseur optique

V : volume d'eau précipitable dans l'atmosphère.

L'ordonnée à l'origine de cette équation représente l'absorption de l'oxygène alors que sa pente est plutôt reliée à l'absorption par la vapeur d'eau.

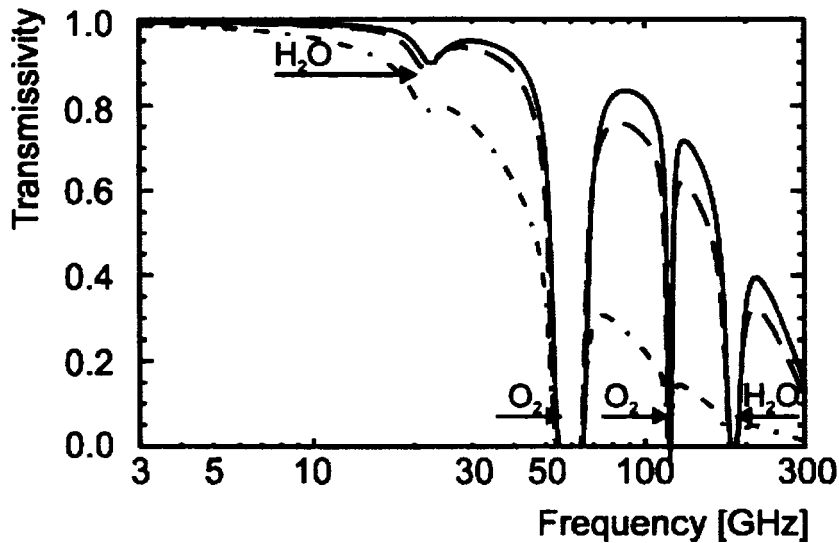


Figure 5 La transmissivité de l’atmosphère dans le domaine des micro-ondes passives en fonction de la fréquence. (Ligne continue : atmosphère clair, ligne interrompue : 0.5 km d’épaisseur, ligne pointillée : 2 km d’épaisseur) (Schultz & Engman, 2000).

Selon la même étude de Choudhury et al. (1991), la transmissivité de l’atmosphère s’écrit en fonction de son épaisseur optique et de l’angle d’incidence ($\mu = \cos \theta$), comme suit :

$$t_a = \exp(-\tau/\mu) \quad (2.14)$$

L’auteur a noté également que la contribution de l’atmosphère en terme de températures de brillance ascendantes (Upward : T_u) et descendantes (Downward : T_d) est quasiment la même. Les deux flux sont comparables. Par conséquence, l’égalité suivante peut s’écrire comme suit :

$$T_{sky} = T_d = T_u = T_e \cdot (1 - t_a) \quad (2.15)$$

Avec T_e la température effective de l'atmosphère. Choudhury et al. (1991) a estimé T_e en fonction de la température de l'air et de la vapeur d'eau dans l'atmosphère pour deux fréquences différentes :

$$\text{Pour 19 GHz : } T_e = T_a - (8+0.06V) \quad (2.16 \text{ a})$$

$$\text{Pour 37 GHz : } T_e = T_a - (18-0.12V) \quad (2.16 \text{ b})$$

À la surface du milieu sol-végétation, la température de brillance T_b s'écrit comme une combinaison linéaire de la température du milieu T_0 qui peut être approchée par la température de l'air, T_{sky} et la réflectivité effective du milieu, sol-végétation. L'expression de T_b s'écrit donc comme suit :

$$T_b = A \cdot T_{sky} + (1-A) \cdot T_0 \quad (2.17)$$

L'atmosphère contribue au signal capté par le satellite par deux effets. Un premier effet multiplicatif exprimé par sa transmissivité " t_a " causé par la présence de la vapeur d'eau et de l'oxygène dans l'atmosphère. Le deuxième effet est additif. Il correspond aux radiations atmosphériques entrant au capteur qui ont été approximées par " T_{sky} " (Lakshmi & Wood, 1997).

Ainsi, la température de brillance " T_B " mesurée au niveau du capteur s'écrit comme suit :

$$T_B = t_a \cdot T_b + T_{sky} \quad (2.18)$$

Il importe toutefois de noter que l'effet additif de l'atmosphère “ T_{sky} ” peut être éliminé par une différence de polarisation qui s'écrit comme suit :

$$\Delta T = T_{BV} - T_{BH} = t_a \cdot (T_{bv} - T_{bh}) \quad (2.19)$$

2.4 Discussion

Les approches préconisées pour l'estimation de l'humidité du sol par l'utilisation des mesures de micro-ondes passives peuvent être classées en deux catégories principales. La première catégorie comporte des approches globales se basant généralement sur le concept de l'indice d'humidité du bassin ou sur des régressions simple entre l'humidité du sol et la température de brillance (Basist et al., 1998; Fily et al., 2003; Paloscia et al., 2001; Tanaka et al., 2000). Les effets introduits par la rugosité, la végétation et l'atmosphère sont généralement négligées dans cette catégorie.

La deuxième catégorie fait appel plutôt à des modèles de transfert radiatif (Bindlish et al., 2003; Jackson et al., 2002; Lakshmi, 1996; Njoku & Li, 1999). Certaines études dans cette catégorie visent exclusivement la détermination de l'humidité du sol (Basist et al., 1998; Lakshmi & Wood, 1997). D'autres études dans la même catégorie optent pour la détermination d'autres variables telles que la température de surface et/ou la profondeur optique du couvert végétal (Njoku et al., 2003). Dans les deux cas, l'obtention des ces paramètres se réalise par une inversion du modèle de transfert radiatif en minimisant par un processus itératif l'écart entre les températures de brillance simulées et observées. Dans le cas des fréquences élevées là où l'effet de l'atmosphère et de la végétation devient non négligeable, Lakshmi (Lakshmi, 1996) a proposé de minimiser l'écart entre les indices de polarisation observés et simulés. Ainsi, il a pu éliminer l'effet de ces perturbations dans le processus d'optimisation.

Wigneron et al. (2003) ont publié une synthèse assez exhaustive des différentes approches recommandées pour l'estimation de l'humidité du sol par des mesures de micro-ondes passives. Un intérêt plus particulier a été donné dans leur recherche aux études utilisant des fréquences des capteurs SMMR, AMSR, AMSR-E ou la bande L. Ces fréquences sont inférieures à celles du capteur SSM/I.

2.4.1 Approches globales pour l'estimation de l'humidité du sol

En raison de la dominance de l'effet de l'atmosphère et de la végétation dans le cas des fréquences élevées, certains auteurs ont opté pour des approches globales. Dans cette perspective, Paloscia et al. (Paloscia et al., 2001) ont proposé une approche simplifiée recommandée pour des bassins de larges étendues et utilisant des données en provenance du capteur SMMR ou SSM/I. L'approche se base sur une relation linéaire entre l'indice de polarisation PI et l'humidité de sol. Le PI s'écrit comme suit :

$$\text{PI} = (\text{Tbv} - \text{Tbh}) / 0.5 * (\text{Tbv} + \text{Tbh}) \quad (2.20)$$

Paloscia et al. (2001) ont noté que les coefficients de la relation linéaire entre le PI et l'humidité de sol dépendent de la végétation et particulièrement le "Leaf Area Index" LAI comme indice de surface foliaire. L'algorithme proposé débute donc par une estimation de LAI. Cette estimation recommande donc la relation linéaire appropriée pour la densité de végétation considérée. Finalement, le PI sera calculé et l'équation linéaire inversée pour la détermination de l'humidité de sol. La précision de l'algorithme est d'autant plus faible que la végétation est dense.

L'approche de Tanaka et al. (2000) est basée sur le principe de l'augmentation de la différence entre les émissivités du sol et du plan d'eau avec l'augmentation de la fréquence. Des mesures du capteur SSM/I, à 19 et 37 GHz, ont été utilisées pour le suivi des inondations de 1998, en Chine. L'estimation de la fraction du plan d'eau a été calculée par le ratio des différences des températures de brillance captées en 19 et 37 GHz.

Fily et al. (2003) ont établi une méthodologie pour l'estimation de la fraction du plan d'eau. Des images SSM/I ont été utilisées également pour la mise en application de l'approche. Contrairement à l'étude de Tanaka et al. (2000) qui ont utilisé des différences de fréquences en gardant la même polarisation, Fily et al. (2003) ont employé la différence entre les polarisations H et V à la même fréquence pour estimer la température de surface et déduire l'émissivité du sol. La fraction des plans d'eau dans la scène observée a été calculée à partir de l'émissivité estimée par le ratio suivant :

$$FWS = (ep - edray) / (ew - edray) \quad (2.21)$$

FWS : "Fraction of Water Surface"

ep : émissivité du pixel.

edray : émissivité du sol sec

ew : émissivité de l'eau

Le FWS est tributaire des effets des plans d'eau et de l'humidité dans les couches supérieures du sol (quelques centimètres). C'est la réponse des plans d'eau qui domine dans l'estimation de FWS. L'isolement de l'un ou l'autre des effets est impossible par l'utilisation des micro-ondes passives seulement. L'utilisation d'autres sources de

données telles que les images radar ou des images dans le visible semble être indispensable pour l'estimation des plans d'eau et le suivi de leur évolution.

Dans la même perspective, Basist et al. (Basist et al., 1998) ont utilisé la différence entre des températures de brillance captées à des fréquences différentes pour développer un indice d'humidité de sol. Cette différence est illustrée par la figure 6, pour des mesures prises à proximité du fleuve Mississippi.

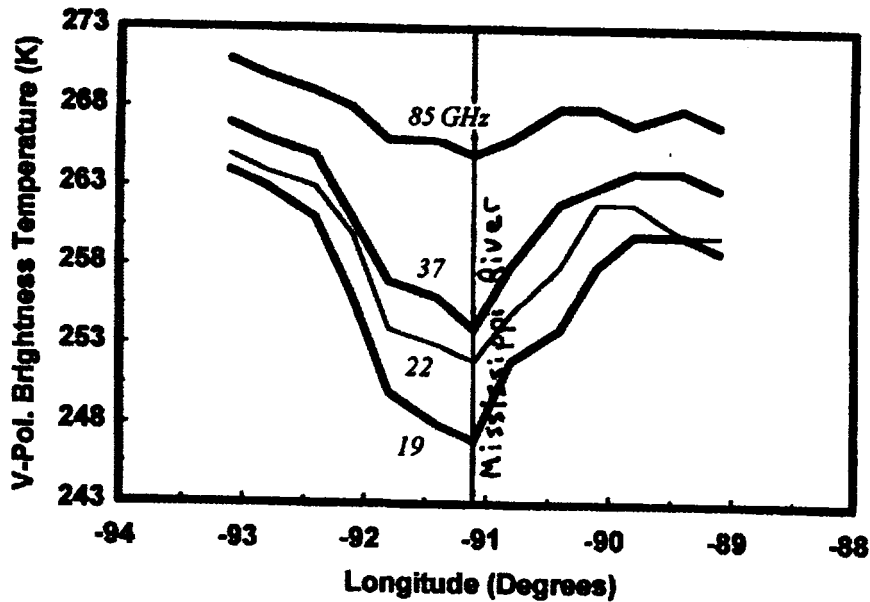


Figure 6 Variation de la différence entre les mesures des différentes fréquences à proximité du fleuve Mississippi (Basist et al., 1998)

En effet, la réduction de l'émissivité du sol engendrée par la présence de l'eau dans ses couches superficielles a été exprimée, dans cette étude par une relation qui regroupe les émissivités mesurées à des fréquences différentes. Cette relation s'écrit comme suit :

$$\Delta\epsilon = \beta_0[\epsilon(v_1) - \epsilon(v_2)] + \beta_1[\epsilon(v_3) - \epsilon(v_2)] \quad (2.22)$$

où : β_0, β_1 des paramètres empiriques et $\varepsilon(v_i)$ émissivité à la fréquence i

Cette différence a été associée à une différence des températures de brillance mesurées (Figure 6). Le BWI indique qualitativement l'évolution de l'état de la réserve hydrique dans le bassin du Mackenzie. Le FWS, similaire à celui qui a été présenté dans l'étude de Fily et al. (Fily et al., 2003), a été développé à partir de BWI. Les indices BWI et le FWS ont été exprimés par les relations suivantes :

$$\text{BWI} = \beta_0 [T_b(v_1) - T_b(v_2)] + \beta_1 [T_b(v_3) - T_b(v_2)] \quad (2.23)$$

$$\text{FWS} = (1 - T_b/T_s)/0,33 \quad (2.24)$$

T_b : Température de brillance à 19 GHz

T_s : Température de surface corrigée

0,33 : l'écart entre l'émissivité d'une surface sèche et humide

2.4.2 Utilisation du modèle de transfert radiatif pour l'estimation de l'humidité du sol

L'utilisation des fréquences élevées impose une considération de l'effet de l'atmosphère et du couvert végétal qui contribue par ses différentes composantes, feuillage, branches et tiges. Le modèle proposé par Choudhury et al. (1990) a été recommandé pour ces fréquences élevées.

Lakshmi (1996) s'est basé principalement sur l'approche de Choudhury et al. (1990) pour la caractérisation du couvert végétal et la modélisation de la diffusion du rayon électromagnétique dans le milieu végétal. Il a également fait appel à un modèle

hydrologique pour simuler l'humidité dans la couche superficielle du sol. Le logiciel utilisé par Lakshmi (1996) est similaire à WATCLASS (Verseghy, 2000). L'approche recommandée par les deux auteurs (Choudhury et al., 1990; Lakshmi, 1996) s'avère exigeante en terme d'informations caractérisant le couvert végétal. Son application dans le cas du Mackenzie nécessite donc une connaissance exacte des caractéristiques du couvert végétal.

Par ailleurs, le modèle proposée par Njoku et al. (2003) simplifie la modélisation de l'effet de la végétation. Le modèle a été validé par des mesures SMMR afin de pouvoir l'utiliser avec les données du nouveau capteur AMSR-E. L'apport principal de l'approche suggérée par Njoku et al (2003) réside dans l'estimation d'un vecteur d'inconnu par un processus itératif visant la minimisation de l'écart entre les températures de brillances simulées par le modèle de transfert radiatif et celles observées par le capteur. Njoku et al. (2003) ont utilisé trois fréquences, chacune avec deux polarisations, générant ainsi un vecteur de six variables d'entrée. Dans une autre étude, Bindlish et al. (2003) ont également utilisé la même méthodologie itérative pour estimer un vecteur de trois inconnues à savoir, l'humidité du sol, la température de surface et l'épaisseur optique de la végétation. Bindlish et al.. (2003) ont utilisé une seule fréquence (10,65 GHz) avec deux polarisations en créant un vecteur d'entrée composée par T_{bh} , T_{bv} et le ratio T_{bh}/T_{bv} . Dans les deux études de (Bindlish et al., 2003; Njoku et al., 2003) la méthode des moindres carrés itératives a été utilisée pour minimiser l'écart entre les variables d'entrée et les résultats des simulations.

La limitation principale de ces deux dernières études réside dans la constance des paramètres du modèle de transfert radiatif. Les paramètres de végétation et de la rugosité mis en jeu dans ces études sont constants et ne varient pas avec l'évolution des conditions à la surface. L'approche de Njoku et al. (Njoku et al., 2003) a été testée sur un site homogène (le désert). Le changement de l'état de la végétation au cours de la

saison estivale recommande fortement l'ajustement des paramètres du modèle. Par ailleurs Njoku et al. (2003) ont noté que l'approche a été validée par des paramètres météorologiques. Ils ont recommandé pour une meilleure évaluation de ses performances l'utilisation d'un modèle hydrologique sol-atmosphère similaire à WATCLASS, capable de fournir des estimations indépendantes de l'humidité du sol.

Par ailleurs, il ressort donc que les approches globales sont plus appropriées pour répondre aux objectifs de cette étude, compte tenu de l'étendue et l'hétérogénéité du bassin étudié. La complexité du modèle de transfert radiatif tel qu'il a été proposé par Choudhury et al. (1990) motive encore plus la préconisation de ces approches globales. De plus, la constance des paramètres du modèle de transfert radiatif s'avère comme une deuxième carence de cette approche. Ceci définit donc les objectifs des chapitres subséquents qui portent sur l'application des approches globales pour l'estimation de l'humidité du sol.

CHAPITRE 3

A DYNAMIC ESTIMATION OF FREE WATER SURFACE COVERAGE FROM A BASIN WETNESS INDEX OF THE MACKENZIE RIVER BASIN USING SSM/I MEASUREMENTS

Abstract

This work elaborates a method to obtain dynamic estimates of Free Water Surface coverage in the Mackenzie River Basin in Northwest Canada. The method used in this study is based on the Basin Wetness Index (BWI), which is computed using the brightness temperature remotely sensed by SSM/I in the 19, 37 and 85 GHz channels. In its basic formulation, the BWI uses two empirical parameters. These parameters are constant in time, but they may vary in space depending on the surface type. Hence, a preliminary classification exercise is necessary to apply the BWI. The temporal evolution of the vegetation state and the basin heterogeneity suggest that these parameters could vary, in both time and space. An alternative approach is therefore proposed that allows for a reassessment of the empirical constants at the reception of each new image. This approach allows the preliminary classification step to be eliminated. The variability of the parameters over time will account for the evolution of the vegetation cover and improve the BWI sensitivity to the surface wetness. The index was computed for each pixel, 625 km^2 , on a daily basis for the summer seasons from 1997 to 2000, over the entire surface of the Mackenzie River Basin ($1.8 \times 10^6 \text{ km}^2$), which comprises roughly 20% of Canada. Based on the BWI estimates, the Free Water Surface coverage, FWS, was computed. The reliability of this approach is assessed by analyzing the agreement of the FWS variability with the fluctuations of the climatological and hydrological conditions.

Résumé

Ce travail vise l'estimation dynamique de la fraction en eau libre au bassin du Mackenzie, au nord-ouest canadien. La méthodologie préconisée est basée sur le concept de l'indice d'humidité du bassin (BWI). Cet indice se calcule par une combinaison linéaire des températures de brillance mesurées par le capteur SSM/I aux fréquences 19, 37 et 85 GHz. L'expression du BWI fait appel à deux paramètres empiriques. Ces paramètres sont constants dans le temps mais ils peuvent varier dans l'espace dépendamment du type du sol. Cependant, l'évolution temporelle du couvert végétal et l'hétérogénéité du bassin étudié font que ces paramètres soient variables dans l'espace et dans le temps. Ainsi, une nouvelle approche a été proposée permettant l'estimation des paramètres empiriques de l'indice à la réception de chaque nouvelle image. Cette approche permet de surmonter l'étape préliminaire de classification. D'autre part, la variabilité des paramètres dans le temps a été générée par le développement du couvert végétal et le changement des conditions à la surface. Cette variabilité a amélioré la sensibilité du BWI à l'humidité de surface. L'indice a été estimé, pour chaque pixel, 625 km², sur une base journalière et ce pour tout le bassin du Mackenzie (1.8 million km²) qui comprend environ 20% de la superficie totale du Canada. En se basant sur les valeurs du BWI, la fraction d'eau libre à la surface (FWS) a été calculée. La fiabilité de l'approche a été évaluée en analysant la concordance entre la variabilité du FWS avec les fluctuations des conditions climatologiques et hydrologiques.

3.1 Introduction

This work is part of the Mackenzie Global Energy and Water cycle Experiment (GEWEX) Study, or MAGS. MAGS is the Canadian contribution to the GEWEX international program. The main objective of the MAGS project is to understand the

hydrological and climatological processes occurring within the Mackenzie River Basin, (MRB), in northwestern Canada. Soil moisture is a crucial parameter in both hydrologic and climatologic studies. In-situ measurements of soil moisture are not significantly representative at the basin scale especially over large basins. The potential for the use of passive microwaves for soil moisture retrieval was demonstrated in several studies e.g. (Jackson & Le Vine, 1996; Njoku & Entekhabi, 1996; Schmugge, 1998; Ulaby et al., 1986). The high dielectric constant of water decreases soil emissivity and affects its surface brightness temperature. Wetter soils therefore have lower brightness temperatures than dryer soil surfaces.

The L band (1.4 GHz) has been strongly recommended to retrieve soil moisture, since it minimizes atmospheric effects and maximizes the penetration depth (Jackson, 1993; Njoku & Entekhabi, 1996; Ulaby et al., 1986). The signal sensed at the L band frequency is emitted by the soil layer few centimeters below the surface. This depth could, under certain conditions, reveal the amount of water storage in the root zone. However, there are no passive satellite sensors operating at this frequency. Thus, other approaches have been developed to retrieve soil moisture using brightness temperature measured by other sensors such as SMMR (Gloersen & Barath, 1977) and SSM/I (Hollinger et al., 1990).

Passive microwave approaches to determine soil wetness generally fall into one of the following categories. In the first category, inversion of a radiative transfer model is generally applied to estimate soil moisture. In some studies, inverting the radiative transfer model leads to simultaneous retrieval of soil moisture and parameters such as surface temperature and vegetation water content. (Bindlish et al., 2003; Lakshmi & Wood, 1997; Njoku et al., 2003). The formulation of the radiative transfer model depends on the microwave frequencies used. How vegetation parameters are handled

accounts for the most important differences between radiative transfer model formulations.

In the second category, simplistic approaches have been developed based on the wetness index concept, or on statistical correlations between brightness temperature and other climatological and hydrological variables and/or some surface features (Basist et al., 1998; Basist et al., 2001; Paloscia et al., 2001; Prigent, 1997; Tanaka et al., 2000). In these cases, the effects of surface roughness and atmospheric contribution are generally neglected.

In the case of high microwave frequencies (>19GHz), atmospheric and vegetation effects are important. It is more complicated to accurately take into account the contribution of these effects, particularly vegetation scattering. Due to this difficulty, simplistic approaches are more attractive when using high frequencies. Paloscia et al. (2001) proposed an approach to estimate soil moisture over large watersheds based on the use of a linear relationship between soil moisture and a polarization index estimated from vertical and horizontal polarized brightness temperature measurements. In their study, the linear relationship coefficients were dependent on the Leaf Area Index value. Tanaka et al. (2000) have used the variability of the differences between soil surface and water emissivities to calculate the fraction of flooded area on a pixel per pixel basis. Tanaka et al. (2000) used brightness temperature sensed at 19 and 37 GHz. Recently, Fily et al. (2003) recommended a different approach using SSM/I images. Their approach is based on the difference between horizontal and vertical brightness temperature polarizations at the same frequency. Using this concept, they estimated surface temperature and soil emissivity. Basist et al. (1998) have an approach based on the correlation between the decrease of emissivity and the brightness temperature differences. The gradual change in space of the land emissivity depends on the frequency and the amount of water on the surface. They defined a Basin Wetness Index,

BWI, which is sensitive to liquid water on the surface within the satellite field of view (FOV). However, SSM/I frequencies used to develop the BWI do not usually penetrate more than a few millimeters into the soil. Therefore, surface emissivities are strongly influenced by flooded areas.

In this work, a particular interest has been given to the wetness index proposed by Basist et al (1998). This index was selected because of its simplicity and the availability of data allowing its application, namely brightness temperature remotely sensed by SSM/I in three different channels, 19, 37 and 85 GHz, and surface temperature provided by the Global Environmental Multiscale (GEM) model (Côté et al., 1998). Furthermore, this index allows the calculation of the Free Water Surface coverage (FWS), which is a potential indicator of water storage within the upper soil layer. This approach was applied to the Mackenzie River Basin. The mean annual runoff at the basin outlet is about 9100 m³/s. Accurate estimates of basin wetness are necessary to close the water balance and retrieve interannual variability, both of which are essential to better understand the hydrologic cycle of the Mackenzie River Basin.

3.2 The Basin Wetness Index

The Basin Wetness Index (BWI) suggested by (Basist et al., 1998) is based on the correlation between the emissivity decrease and the presence of water at or near the soil surface which affects the brightness temperature differences measured at 19, 37 and 85 GHz. The moisture in the soil reduces its emissivity and affects the differences between emissivities estimated at different frequencies. The emissivity reduction can be computed as:

$$\Delta\epsilon = \beta_0[\epsilon(v_1) - \epsilon(v_2)] + \beta_1[\epsilon(v_3) - \epsilon(v_2)] \quad (1)$$

where β_0 and β_1 are two empirical parameters (to be discussed later).

This relationship between emissivity reduction and emissivity differences could be expressed by a linear combination of brightness temperature differences that defines the Basin Wetness Index (BWI). Thus, the BWI is written as:

$$\text{BWI} = \beta_0[T_b(v_2) - T_b(v_1)] + \beta_1[T_b(v_3) - T_b(v_2)] \quad (2)$$

where $T_b(v_1)$, $T_b(v_2)$ and $T_b(v_3)$ are brightness temperatures remotely sensed by the SSM/I at 19, 37 and 85 GHz, respectively. These brightness temperatures correspond to the vertically polarized channels in order to minimize the emissivity variation due to wet surfaces. β_0 and β_1 are two empirical parameters that account for the non-linear decrease of the emissivity with moisture at high frequencies. In addition, these parameters account for the mismatching FOV's which vary from 60 km at 19 GHz to 15 km at 85 GHz (Basist et al., 2001; Tanaka et al., 2003a). Refer to Basist et al (1998) for a complete description of the procedure to calculate the BWI.

Wetness reduces the emissivity and therefore the sensed brightness temperature. To accurately estimate the surface temperature, the wetness effect should be taken into account by adding the BWI to the brightness temperature. The BWI can therefore be considered as a compensation for the vertically polarized brightness temperature reduction at 19 GHz due to soil wetness (Basist et al., 1998). The surface temperature can be estimated by the following relation:

$$T_s = \frac{1}{\varepsilon_0}(T_{b(19\nu)} + \text{BWI}) \quad (3)$$

where ϵ_0 is the dry land emissivity assumed to be equal to 0.95 and approximately frequency independent. However, Fily et al (2003) used the value of 0.97. According to their study, this difference could result in a 3% relative difference in the final FWS estimate.

A Free Water Surface coverage (FWS) parameter has been defined in several studies (Choudhury, 1991; Fily et al., 2003; Prigent, 1997; Tanaka et al., 2000). It is the fraction of surface within a pixel covered by water. Generally, the FWS is estimated by an emissivity difference ratio:

$$FWS = \frac{(e_{drysurface} - e_{soil})}{(e_{drysurface} - e_{wetsurface})} \quad (4)$$

In the Basist et al (1998) study, this parameter is written as :

$$FWS = \frac{1 - \frac{T_{b(19V)}}{\frac{1}{\epsilon_0}(T_{b(19V)} + BWI)}}{0.33} \quad (5)$$

where T_{b19V} is the vertical polarization brightness temperature at 19 GHz. The value of 0.33 is the average (empirically determined) difference between wet and dry soil surface emissivities.

Soil emissivity in equation 4 is estimated in equation 5 by the ratio of the brightness temperature measured at 19 GHz, vertically polarized, divided by the estimated surface temperature with the wetness correction. Thus, the FWS is related to the BWI. Both are linked to the amount of liquid water at or near the surface within the satellite FOV. In addition, both are sensitive to water intercepted by vegetation and flooded or wet open

areas between plants. Their sensitivity to water on the ground depends on the state of vegetation. A dense vegetation cover should attenuate the underlying soil signal and reduce the index sensitivity, especially at high microwave frequencies. Temporal evolution of vegetation cover is critical for the determination of BWI and FWS. The dynamic effect should be filtered out in order to increase the BWI sensitivity to the water at the soil surface. Despite the dominance of the surface water effect, free water at the soil surface also contributes to the radiating signal. However, it is impossible to separate the combined responses exclusively by the use of passive microwaves (Fily et al., 2003). Other sources of data should be used to achieve this objective.

Empirical parameters β_0 and β_1 of the BWI formula should minimize the difference between the linear combination of brightness temperature (equation 2) and the difference between surface temperature and brightness temperature at 19 GHz, vertically polarized, divided by ϵ_0 .

These parameters should extract the maximum correlation. The relationship between the surface temperature and the vertically polarized brightness temperature at 19 GHz, divided by ϵ_0 , and the linear combination of brightness temperature differences are affected by the variation of the amount of water at the soil surface and by the vegetation cover. The accuracy of the empirical parameters is important to improve the BWI estimates.

According to Basist et al (1998), these empirical parameters are constant for both space and time. Williams et al (2000) have proposed calibrating them based on surface types. Hence, a preliminary classification exercise was required in their study to identify surface types. Six different surface types were identified. The accuracy of the results was

shown to vary from one surface type to another. In order to improve the reliability of the approach more surface types need to be defined (Williams et al., 2000).

The temporal evolution of the vegetation and surface conditions should have an effect on the emission process and consequently on the relationship between the BWI and the brightness temperature differences. Therefore, temporal variations of soil emissivity can be subdivided into two components: 1) fluctuations around a fitted curve caused by rapid variations of the atmospheric contribution and of the surface temperature, and 2) a trend that depends for the most part on the slow variation of the vegetation. The vegetation growth during the summer season decreases the portion of soil surface “seen” by a microwave sensor and affects the soil emissivity. However, brightness temperatures are highly affected by the presence of moisture near the soil surface. As a result, the BWI sensitivity to soil moisture should vary during the summer season. Therefore, the relationship between the emissivity reduction, due to wetness, and the brightness temperature differences which define the BWI, needs to be readjusted over time. It is essential to take into account the evolution of the vegetation cover in order to improve the index sensitivity to wet surfaces.

In order to overcome the classification step and account for the temporal evolution of the vegetation cover, it is suggested to dynamically update the parameters of the BWI at the reception of each new image and on a pixel per pixel basis. Hence, a mobile window was programmed to scan the image. It is expected that this dynamic readjustment will improve the BWI sensitivity to the liquid water on the soil surface. Also, empirical parameters should present a similar variability during summer seasons due to the repeatability of the vegetation development cycle.

The window width was fixed at 5 pixels. Considering the SSM/I image resolution, the total width of the window is 125 km. This width was chosen to satisfy two criteria: 1) to include a reasonable number of pixels to compute the empirical parameters from a simple regression formulation, and 2) a limited width to retain a homogenous area for the determination of parameters. The estimated empirical parameters could vary with the size of the mobile window. Despite this variation, it is expected that they will maintain the same trend. Considering that it is the trend of the parameters that will be used to estimate BWI and FWS, the size of the mobile window does not seem to be crucial, as long as it satisfies the two conditions mentioned above. At the reception of each new image, the empirical parameters are estimated for the central pixel of the mobile window, allowing the temporal variation of these parameters to be assessed. The first step of the applied algorithm will aim to verify the similarity of the assumed parameter trends. Secondly, an average trend will be determined for each pixel. Finally, simulations will be carried out using the average trend. In order to better appreciate the results of the proposed approach, a comparison between the FWS's determined using constant empirical parameters and the FWS's determined using variable empirical parameters will be made.

3.3 Application

The methodology proposed in this work was applied to the Mackenzie River Basin (MRB) (Figure 7). The basin is divided into six major sub-basins. Northward, the vegetation in the Mackenzie Basin varies from the prairies, through the boreal forests, to the tundra zone in the most northerly part of the basin. In the western part of the basin the mountains rise to 2-3 km, and the north and central eastern sites are roughly the lowest parts of the basin (Rouse, 2000; Stewart et al., 1998). The Mackenzie Basin contains some of the largest freshwater lakes in the world: Great Bear Lake, Great Slave Lake and Athabasca Lake. These lakes were included in the BWI estimate although the

methodology could not be applied accurately on extended water surfaces since the emissivity is so reduced over these surfaces that the atmospheric contribution becomes significant (Williams et al., 2000).

SSM/I data were extracted from the National Snow and Ice Data Center (NSIDC) database. The resolution of the SSM/I imported images is 25 km for 19 and 37 GHz and 12.5 km for 85 GHz, which are mapped in polar azimuthal equal-area grids (ascending mode). A mask, in which the sub-basins were identified, was applied to the SSM/I images. Air temperatures were computed by the Global Environmental Multiscale (GEM) model, a meteorological forecast model developed by the Canadian Meteorological Centre (Côté et al., 1998). This model produces forecasts for all of North America. Daily estimations of surface temperatures are needed to apply the methodology proposed in this work. Regardless of the GEM forecast performance, which is beyond the objective of this work, the model results were considered to be measurements since they provide a daily coverage of the entire MRB. Air temperatures were used in this work as an approximation for soil temperatures.

First, brightness temperatures and air temperatures measured during the summers of 1998 and 1999 were used to estimate the empirical parameters of the BWI, daily and on a pixel per pixel basis. The resulting curves were filtered to extract temporal trends of the parameters during the summer season. The fitted curves were than averaged. As a second step, variable parameters from the fitted averaged curves were used to compute the BWI and therefore the FWS for other years. By using the average trend of the empirical parameters it was also possible to carry out simulations for the years used for the calibration step, 1998 and 1999.

Figure 8 illustrates the variability of the empirical parameters during the summer seasons of 1998 and 1999. Simulations were carried out over one pixel in the basin's delta (Long. = 134.13 W; Lat.= 69.01). The MRB delta is a flat open area in the northerly part of the basin. First of all, the figure shows that the empirical parameters are not time invariant. The variability of the parameters and the repeatability of this variability over time seem to be principally caused by the evolution of the vegetation cover. Fluctuations around the fitted curve are a combination of the changing atmospheric conditions, surface state evolution and the heterogeneity effect, which all affect the determination of empirical parameters using the moving window. Secondly, figures 8a and 8b show that fitted curves estimated for the years 1998 and 1999 are very similar. In fact, on a pixel per pixel basis the correlation coefficient of the parameter β_0 (figure 9) between the two years' trends is higher than 0.7 over most of the MRB, except for the mountainous area in the west. A topography effect that has not been considered in this research is probably responsible for the observed lack of correlation. Furthermore, it was noticed that β_0 values are generally higher than β_1 values (figure 8), since the emissivity depression is greatest at low frequencies. Hence, more weight is given to the [Tb37 - Tb19] difference. Moreover, this difference is less affected by the vegetation cover than the [Tb85 – Tb37] difference and therefore is more sensitive to free water bodies at the soil surface.

An average trend was generated for each pixel based on the fitted curves derived for each summer season. The trends were then used along with equations 3 and 5 to estimate the BWI and FWS from SSM/I data for the summer seasons 1997, 1998, 1999 and 2000. Instead of using constant parameters in the BWI formula, β_1 and β_0 trends were used. The variability of these parameters reflects the evolution of the vegetation cover and surface conditions (Williams et al., 2000).

Based on the simulation results, a similar temporal and spatial variability was observed for both the BWI and the FWS. It should be noted that both indices reflect the amount of water on the surface of the watershed, but they differ in terms of units employed, as the BWI is expressed in Kelvin units, while the FWS is expressed as the percentage of area covered with water. For practical reasons of presentation, only the FWS simulation results will be presented in this work.

Figure 10 is an example of average monthly FWS estimates computed using SSM/I data measured during the summer season of 2000. FWS values vary between 0 (dry land) and 100 (water). This figure clearly indicates the spatial variability of the water surface area over the basin. The FWS increases progressively from the southern to the northern part of the basin. The largest lakes, i.e. Great Bear, Great Slave and Athabasca are gradually covered by water as the snowmelt progresses. Some water bodies have begun to thaw south of Lake Athabasca and in the eastern part of the MRB, between the largest lakes. The southwest region of the basin has the highest average annual precipitation (Stewart et al., 1998). Therefore, it is generally the wettest part of the basin. However, there is some uncertainty because of the presence of relatively dense vegetation cover and a topography effect that is not considered in our study. Also, the area between Great Bear Lake and Great Slave Lake has higher FWS values compared to other parts of the basin. It is interesting to note that except for the basin delta, this area is roughly the lowest part in the Mackenzie. The spatial distribution of the FWS parameter agrees well with the basin topography.

The variation of the FWS over the basin's outlet is presented in Figure 11. The FWS values were computed for the summer seasons of the years 1997, 1998, 1999 and 2000. FWS values computed for the 1998 summer season, are higher than those for other years. It is worth mentioning that the EL NIÑO phenomenon was observed during that year (Rouse, 2000). Temperatures over the basin for 1998 were above normal.

Moreover, the summer season of 1998 was the 8th wettest summer on record (Kochtubajda et al., 2000). The unusually high temperatures during the spring season extended the free-ice period and caused the melting of larger quantities of snow and ice. These observations explained the higher values of FWS, especially at the beginning of summer 1998. In addition, in August 1998 the basin was considered a source of moisture as evaporation exceeded precipitation by nearly 17 mm/month, compared to (Precipitation - Evaporation) values of 6.92 and 9.33 mm/month for August 1997 and 1999, respectively, which were normal years (Proctor et al., 2000). For this reason, the slope of the FWS decrease at the end of the summer of 1998 was much steeper compared to other years.

The FWS indicates the fraction of water surface within a pixel. Its temporal evolution can be related to climate variations, and thus can potentially be related to climate variability. As seen in figure 11, the FWS curve displays a similar trend, first characterized by a sustained increase at the beginning of the spring season as the melting snow extends the water surface. This is followed by a flattening of the curves during the months of June and July as precipitation and snowmelt are compensated by evaporation and discharge. Finally, a decrease of the FWS is noticed as snowmelt is no longer contributing to the hydrologic cycle and evaporation plus runoff exceeds precipitation.

Figure 12 presents the variation of estimated FWS, using constant empirical parameters, over the Mackenzie River outlet. In order to achieve this simulation, the mean values of each variable parameter, β_0 and β_1 , were used. We assume that the basin's delta area over which the simulation was carried out is homogenous. According to this figure, the FWS variability in this case is different than what was described above. The FWS parameter reaches its maximum just at the beginning of the spring. In summer, it maintains almost the same value, before a decrease at the end of the summer season, but not for FWS estimated using constant empirical parameters. The agreement between the FWS curve

and the outlet hydrograph improves when using variable empirical parameters (Figure 12). The use of the empirical parameters trend instead of two constant values enables the effect of changing surface conditions to be filtered out. Hence, the BWI and FWS are more sensitive to moisture conditions over the soil surface. Furthermore, the proposed approach was applied without a preliminary classification step. It was possible to account for the basin heterogeneity by the use of empirical parameter trends calculated for each pixel of the basin. Hence, both spatial and temporal variations were considered by the proposed approach.

3.4 Conclusion

The aim of this work was to provide a dynamic estimation of the free water surface (FWS) coverage over the Mackenzie River Basin. Simulations were carried out over the period of the summers of 1997, 1998, 1999 and 2000. The method used relates the BWI to brightness temperature measurements, similar to the approach proposed by Basist et al (1998). To apply this methodology, SSM/I images taken at 19, 37 and 85 GHz were used as well as temperature data. The basin heterogeneity and the temporal change of the surface conditions indicate that variable empirical parameters should be used to determine the BWI. The proposed methodology accounts for the evolution of the vegetation cover over time and overcome the classification step. This parameter readjustment maximizes the correlation between the wetness index and the amount of water in the soil. Based on the BWI values, the FWS was computed. The results are encouraging, as the FWS is sensitive to hydrological and climatological variations.

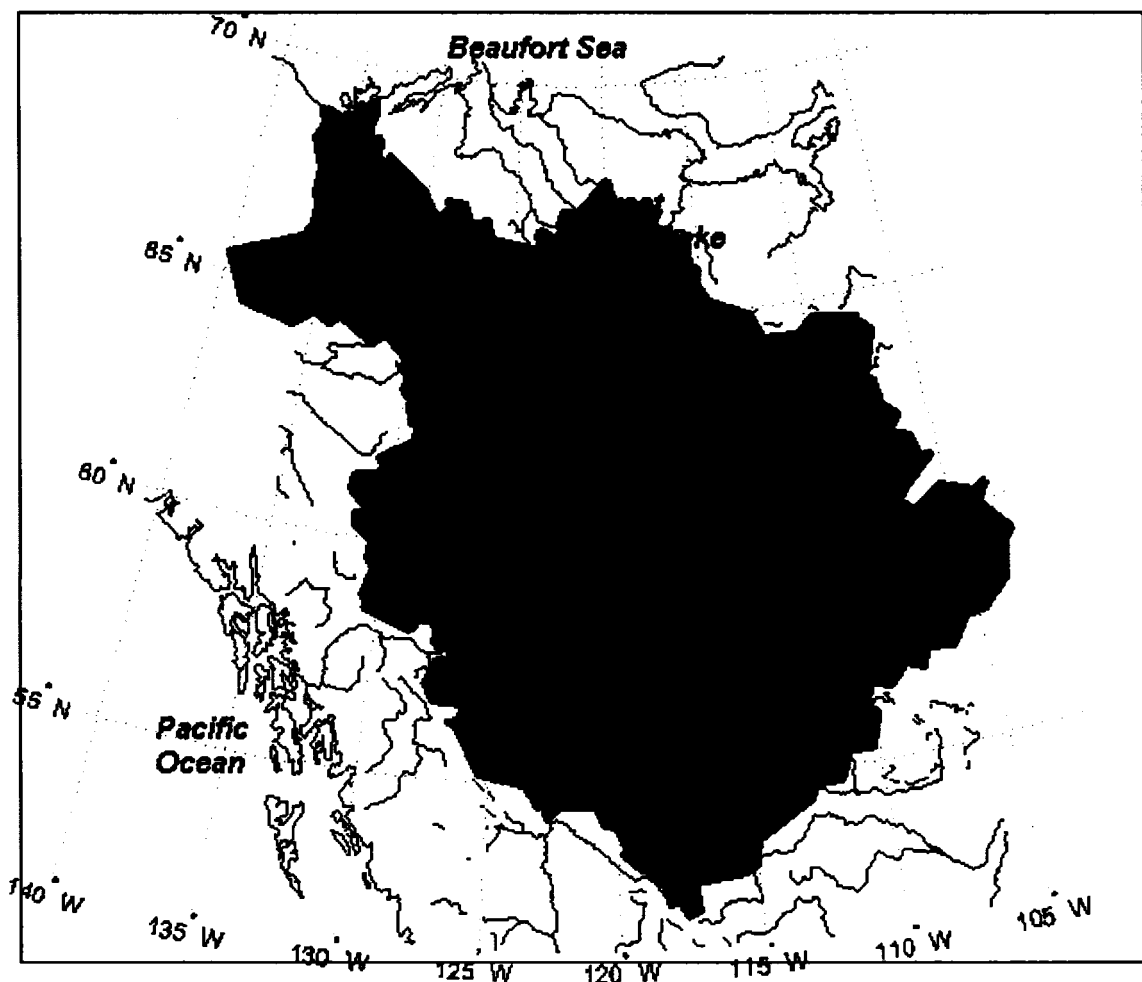
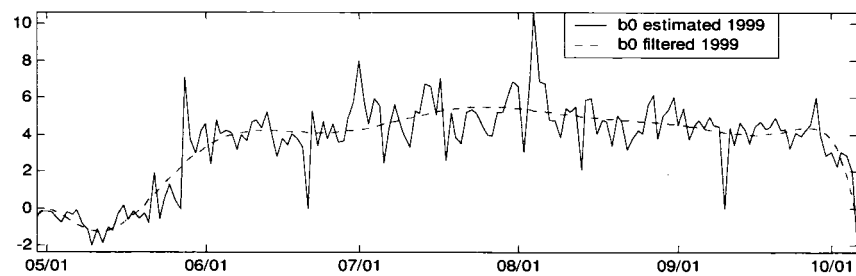
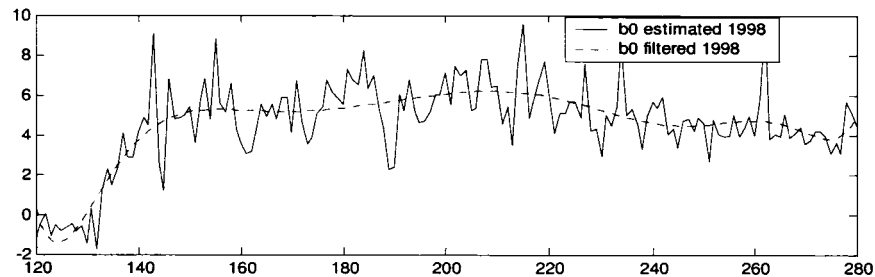


Figure 7 The Mackenzie River Basin

2a/



2b/

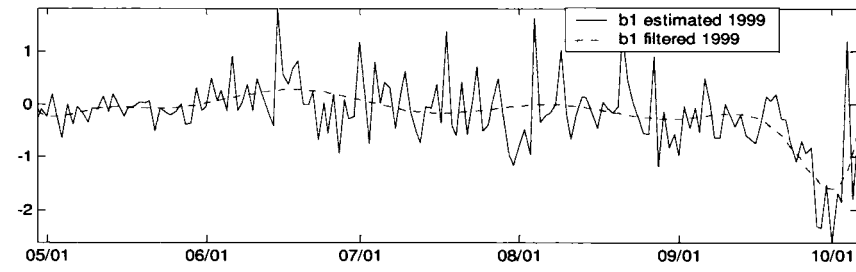
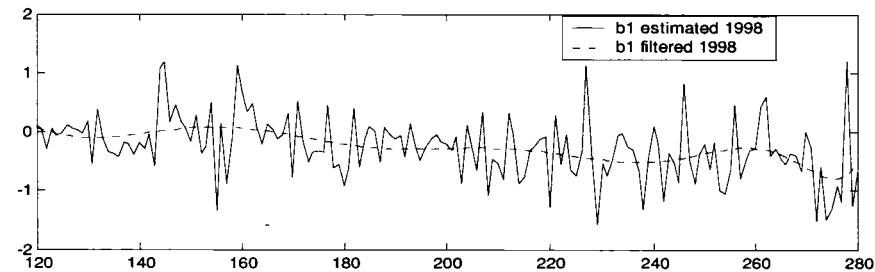


Figure 8 β_0 (figure 8a/) and β_1 (figure 8b/) variability during the summer seasons of 1999 and 1998.

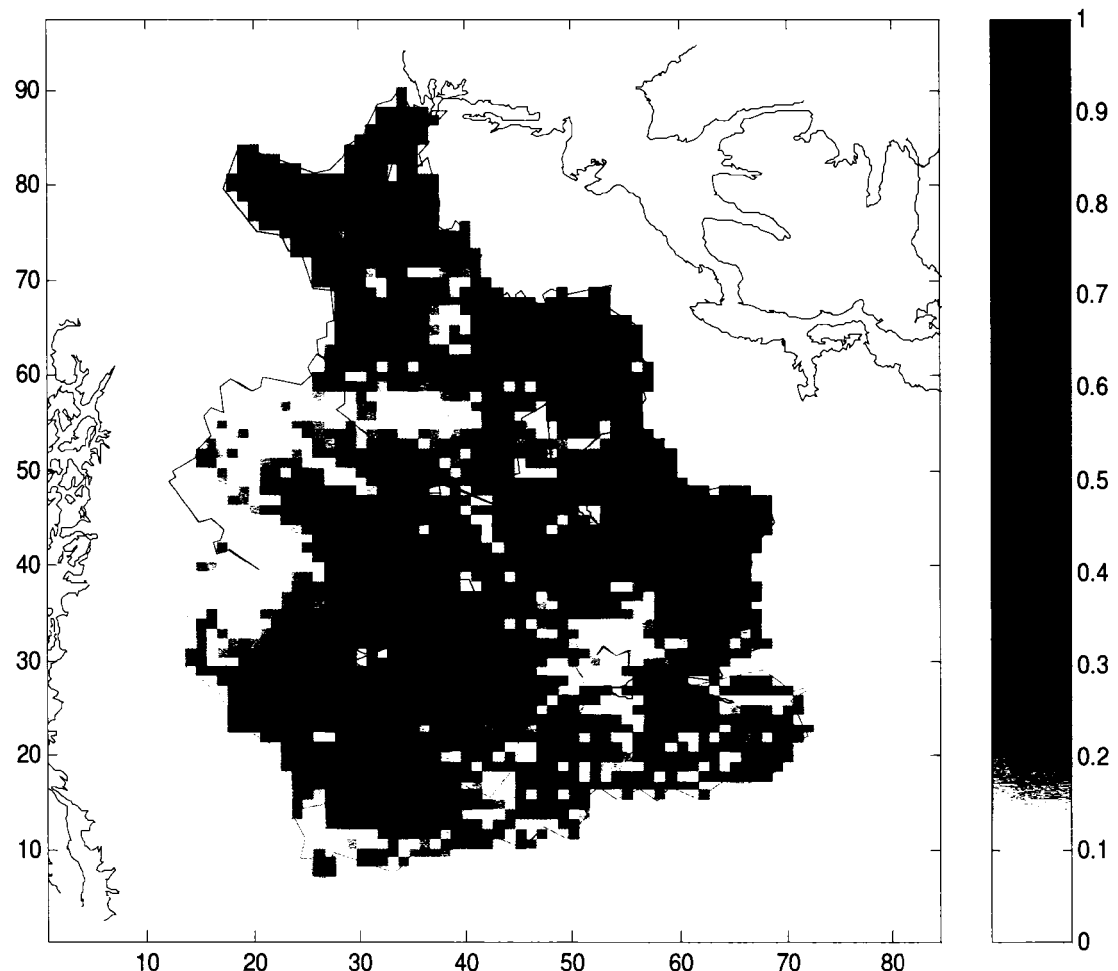


Figure 9 Spatial distribution of the correlation coefficient of β_0 trends estimated during 1998 and 1999

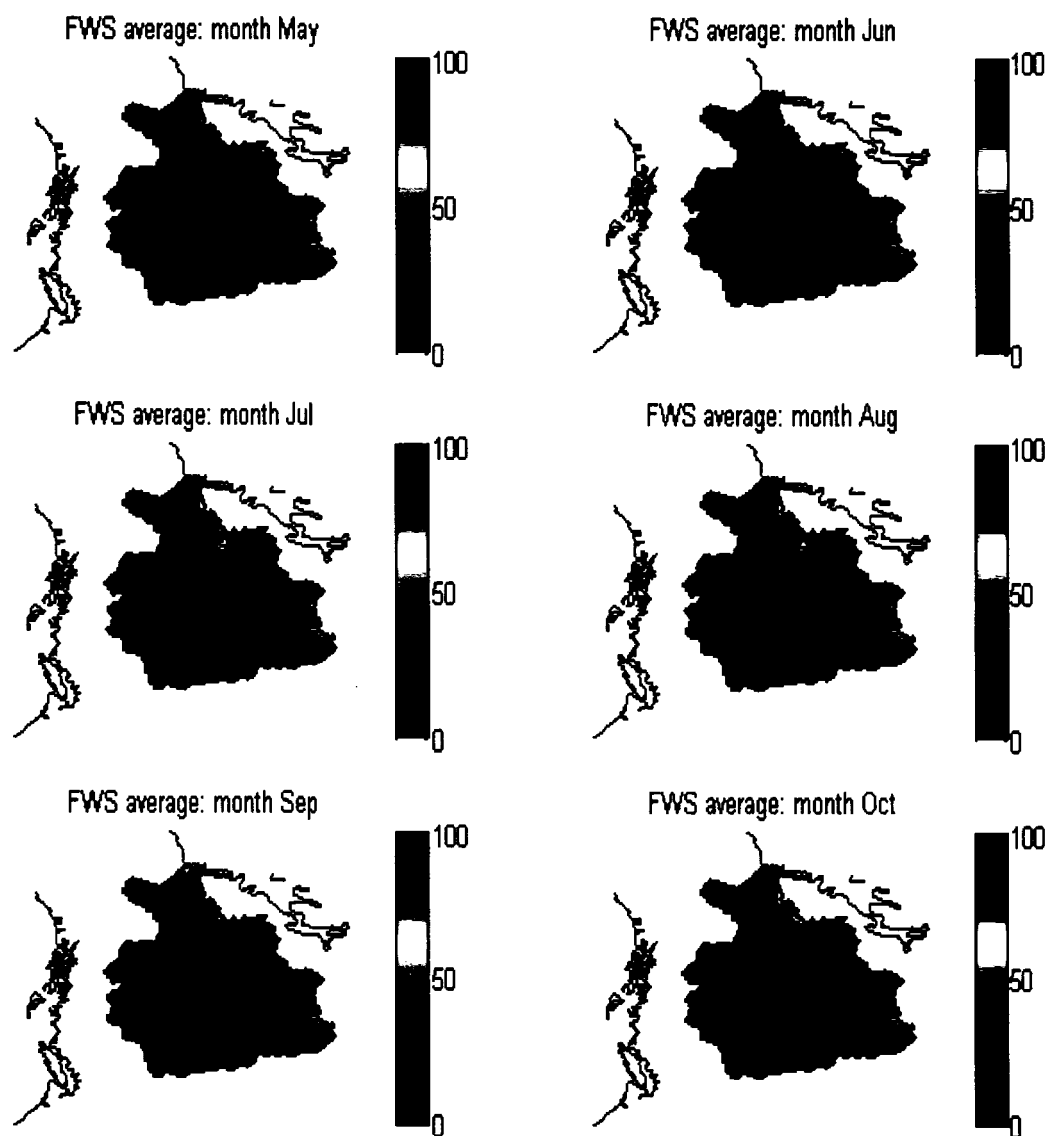


Figure 10 Spatial variations of the FWS over the Mackenzie River Basin, during the summer season of year 2000

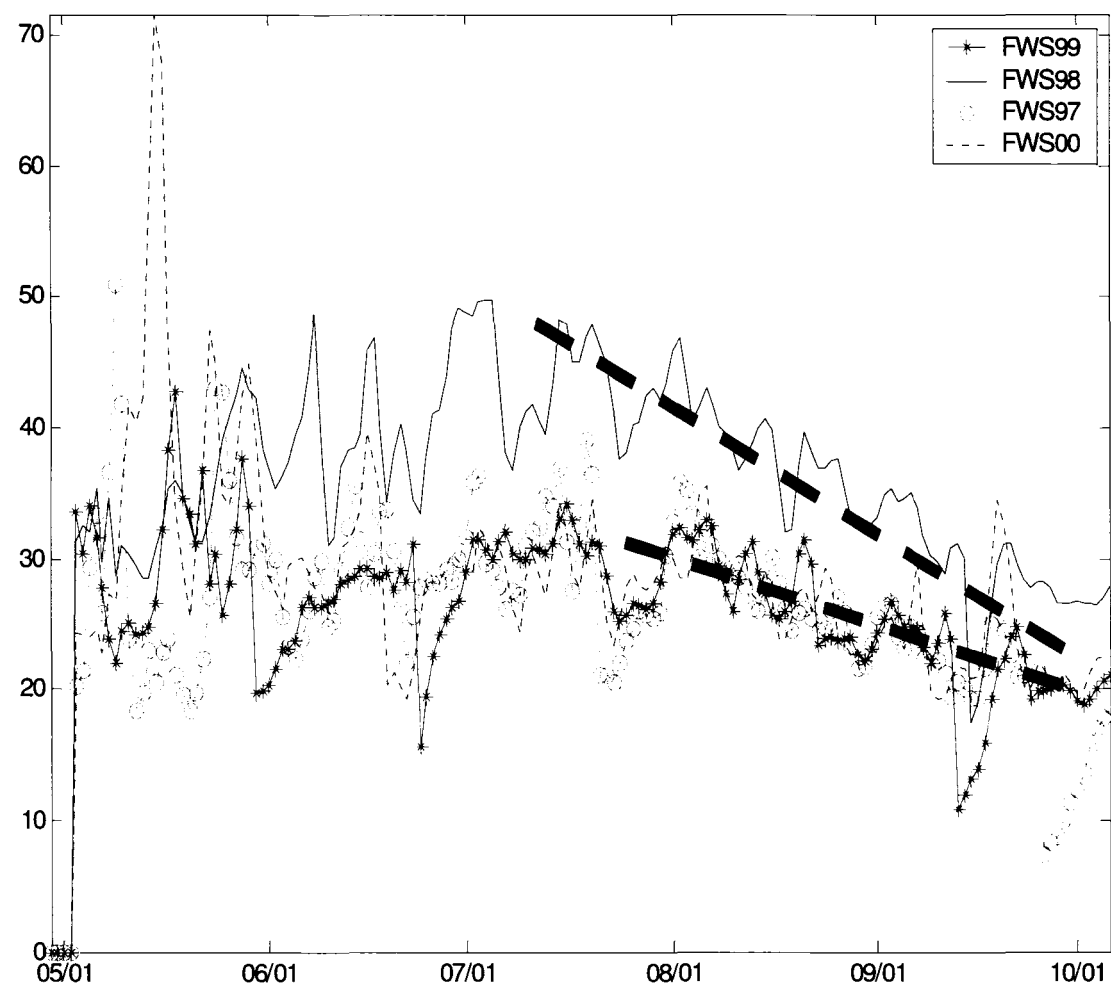


Figure 11 Comparison of the FWS estimates over the summer season of 1997, 1998, 1999 and 2000, in the basin outlet.

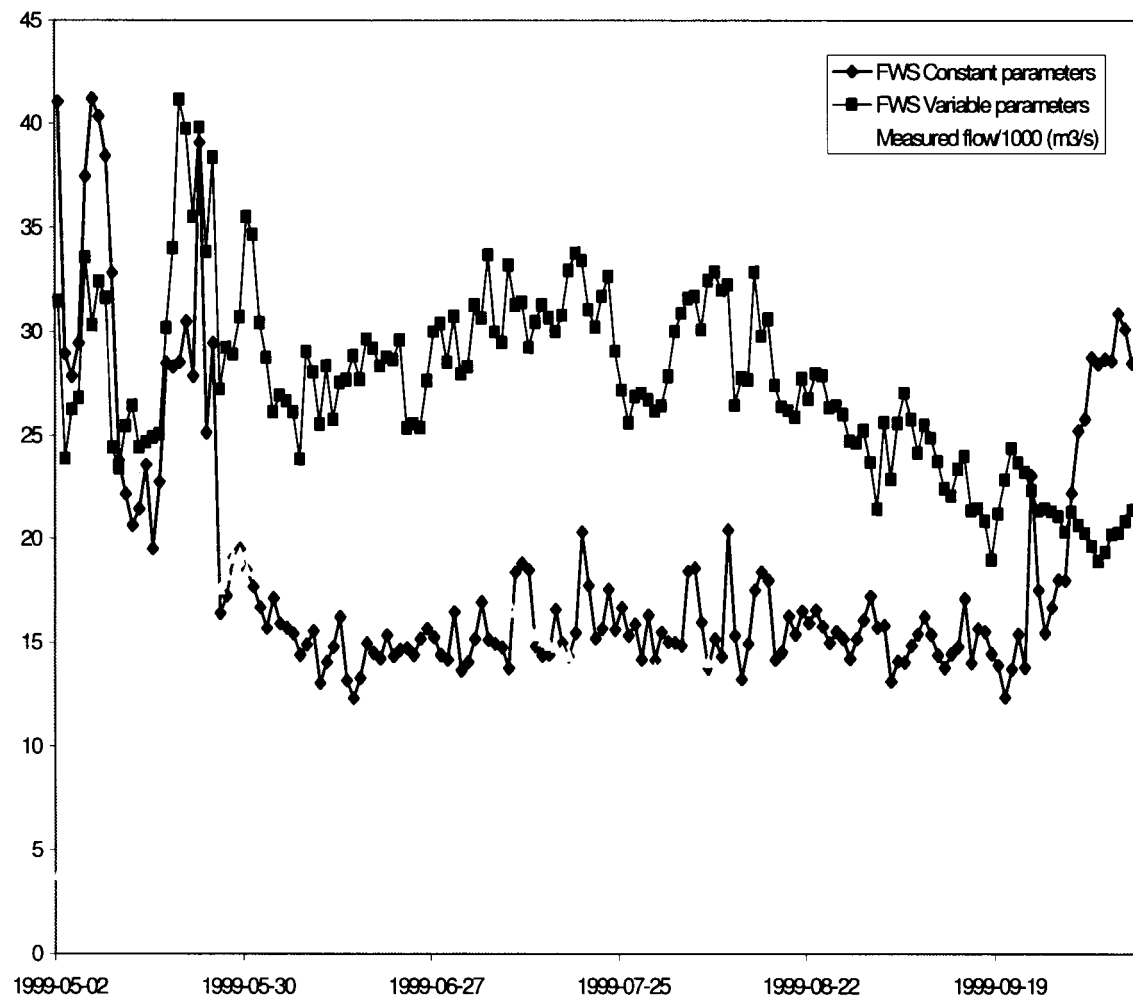


Figure 12 FWS estimated by constant and dynamic empirical parameters compared to the measured flow at basin outlet, during the summer of 1999.

CHAPITRE 4

FLOOD MONITORING OVER THE MACKENZIE RIVER BASIN USING PASSIVE MICROWAVE DATA

Abstract

Flooding over the Mackenzie River Basin, which is situated in northwestern Canada, is a complex and rapid process. This process is mainly controlled by the occurrence of ice jams. Flood forecasting is of very important in mitigating social and economic damage. This study investigates the potential of a rating curve model for flood forecasting. The proposed approach is based on the use of discharge observations and a Water Surface Fraction derived from SSM/I passive microwave images. The rating curve model is based on an existing correlation between flooded areas and measured discharge. However, a time lag can be observed between these two variables. Thus, the rating curve model has been modified by the introduction of a lag term that could vary depending on the flooding intensity and the features of the basin. Hence, the lag term is computed dynamically using a cross-correlation function between the flooded area and the discharge vectors. The rating curve model is based on two empirical parameters that depend on the site features, which vary in both space and time. To overcome this dependency, the rating curve model was linked to a Kalman filter in order to dynamically estimate the empirical parameters according to the forecasting errors encountered at each time step. With the Kalman filter, the dynamic rating curve model continuously readjusts its parameters to satisfy the non-stationary behaviour of hydrological processes. The model is thus sufficiently flexible and adapted to various conditions. Simulations were carried out over the Mackenzie River Basin (1.8 million km²) during the summers of 1998 and 1999. NOAA-AVHRR images were used to validate the forecast WSF values. The predicted flooded areas agree well with those derived from the NOAA-AVHRR images. Further simulations were carried out from

1992 to 2000 using the rating curve model to predict discharge at an upstream location. Even though an interannual variability of the water surface fractions was observed over the PAD area, the modified model was sufficiently flexible to be readjusted and to reproduce satisfactory results. This implies that a combination of passive microwave data and discharge observations presents an interesting potential in flood prediction.

4.1 Introduction

This work is part of the Mackenzie GEWEX Study, MAGS. MAGS is the Canadian contribution to the GEWEX international program. The main objective of the MAGS project is to provide an understanding of the hydrological and climatological processes occurring within the Mackenzie River Basin (MRB), in northwestern Canada. The estimation of the Water Surface Fraction (WSF) over a basin is of great importance for modeling hydrological and climatological processes. WSF is a useful indicator of water storage fluctuations and a crucial parameter in flood monitoring as it indicates the variation of flooded areas in both space and time. However, hydrological processes can vary rapidly. Moreover, ice jamming significantly controls the occurrence of flooding in northern climates. To predict the evolution of these processes, a real-time forecasting of the WSF is needed. Remote sensing presents an interesting potential for flood prediction.

Usually, the WSF is estimated using a combination of one or multiple frequencies at different polarizations. Fily et al. (2003) proposed an approach to estimate WSF based on the ratio $(e_{\text{soil}} - e_{\text{dry soil}}) / (e_{\text{wet soil}} - e_{\text{dry soil}})$, where e_{soil} , $e_{\text{dry soil}}$, $e_{\text{wet soil}}$ are the emissivities of the observed, dry and wet soils, respectively. The emissivity, in the work of Fily et al. (2003), was estimated from a relationship established between 19 and 37 GHz brightness temperatures vertically and horizontally polarized, provided by SSM/I sensor. Tanaka et al. (2003b) tested two different methods. The first was based on the use of the SSM/I 37 GHz channel as a single frequency. The 37 GHz horizontally polarized channel was considered optimal as it has a smaller effective field of view (EFOV) and a horizontal polarization that presents a greater contrast between water and dry soil. The second method was based on the use of a polarization difference at the 37 GHz frequency level, also using SSM/I data. Both of these methods showed a good agreement with WSF derived from NOAA-AVHRR data. SSM/I data were used also by

Jin (1999) to compute a flooding index (FI), defined as the difference between vertically polarized brightness temperatures measured at 37 and 85 GHz frequencies, respectively. The FI was compared to predetermined threshold F_0 indicating flood detection.

A Basin Wetness Index (BWI) was suggested by (Basist et al., 1998). The BWI is based on the correlation between the emissivity decrease and the presence of water at or near the soil surface, which affects the brightness temperature differences measured at 19, 37 and 85 GHz. The moisture in the soil reduces its emissivity and affects the differences between emissivities estimated at different frequencies. In this work, a particular interest has been given to the wetness index proposed by Basist et al (1998). This index was selected because of its simplicity and the availability of data allowing its application. Furthermore, this index allows the calculation of the WSF, which is a potential indicator of water storage within the upper soil layer.

This work aims to provide a real-time forecast of the WSF over the Mackenzie River Basin, which is situated in northwestern Canada (Figure 13), using passive microwave data. The method is based on a rating curve relating discharge measurements to water extent derived from microwave data. In addition a Kalman filter has been used to update the empirical parameters of the rating curve model. Section 4.2 of this article will discuss firstly the potential of passive microwave to estimate WSF over large watersheds and secondly the use of the Kalman filter to take into account the temporal variability of the empirical parameters of the rating curve model. Finally, the results of the application of the proposed method will be presented in section 4.3.

4.2 Methodology

4.2.1 Estimation of the water surface extent using passive microwave data

Basist et al (1998) proposed an approach based on the correlation between the decrease of emissivity and the brightness temperature differences. The gradual change in space of the land emissivity depends on the frequency and the amount of water at and/or near the surface. They defined a Basin Wetness Index (BWI), which is sensitive to liquid water within the satellite field of view (FOV). This index was estimated by a linear combination of brightness temperatures remotely sensed by SSM/I in the 19, 37 and 85 GHz vertically polarized frequencies. Thus, the BWI and WSF derived from this index are written as:

$$BWI = \beta_0 [T_b(v_2) - T_b(v_1)] + \beta_1 [T_b(v_3) - T_b(v_2)] \quad (4.1)$$

$$WSF = \frac{1 - \frac{T_{b(19V)}}{\frac{1}{\varepsilon_0} (T_{b(19V)} + BWI)}}{0.33} \quad (4.2)$$

where $T_b(v_1)$, $T_b(v_2)$ and $T_b(v_3)$ are brightness temperatures remotely sensed by the SSM/I at 19, 37 and 85 GHz, respectively. β_0 and β_1 are two empirical parameters that account for the non-linear decrease of the emissivity with moisture at high frequencies. In addition, these parameters account for the mismatching FOVs, which vary from 60 km at 19 GHz to 15 km at 85 GHz (Basist et al., 2001; Tanaka et al., 2003a). This index allows the calculation of the WSF (Equation 2.b), which is a potential indicator of water storage within the upper soil layer. Refer to Basist et al. (1998) for a complete description of the procedure to calculate the BWI.

According to Basist et al (1998), empirical parameters, β_0 and β_1 , are constant for both space and time. Williams et al (2000) have proposed calibrating them based on surface types. Hence, a preliminary classification exercise was required in their study to identify surface types. Several surface types need to be defined in order to improve the reliability of the approach (Williams et al., 2000).

The temporal evolution of the vegetation and surface conditions should have an effect on the emission process and consequently on the relationship between the BWI and the brightness temperature differences. The vegetation growth during the summer season decreases the portion of soil surface “seen” by a microwave sensor and affects the soil emissivity. However, brightness temperatures are highly affected by the presence of moisture near the soil surface. As a result, the BWI sensitivity to soil moisture should vary during the summer season. Therefore, the relationship between the emissivity reduction, due to wetness, and the brightness temperature differences which define the BWI, needs to be readjusted over time. It is essential to take into account the evolution of the vegetation cover in order to improve the index sensitivity to wet surfaces.

In order to overcome the classification step and account for the temporal evolution of the vegetation cover, it is suggested to dynamically update the parameters of the BWI at the reception of each new image and on a pixel per pixel basis. Hence, a mobile window was programmed to scan the image. The window width was fixed at 5 pixels. Considering the SSM/I image resolution, the total width of the window is 125 km. Considering that it is the trend of the parameters that will be used to estimate BWI and FWS, the size of the mobile window does not seem to be crucial. At the reception of each new image, the empirical parameters are estimated for the central pixel of the mobile window, allowing the temporal variation of these parameters to be assessed. The results obtained will be used in this study as an estimation of the WSF. It is expected

that this dynamic readjustment will improve the BWI, and therefore the WSF sensitivity to the liquid water on the soil surface.

SSM/I data, used in this study, were extracted from the National Snow and Ice Data Center (NSIDC) database (Armstrong et al., 1994). The resolution of the SSM/I imported images (ascending mode) is 25 km for 19 and 37 GHz, and 12.5 km for 85 GHz, which are mapped in polar Azimuthal Equal-Area grids. The 19, 37 and 85 GHz vertically polarized frequency channels of the SSM/I sensor were used to estimate the WSF by a linear combination of these frequencies.

4.2.2 The rating curve formula

Several studies have proven that there is a strong correlation between hydrological parameters, discharge or stage, and flooded areas (Frazier et al., 2003; Mosley, 1983; Smith et al., 1996; Vorosmarty et al., 1996). Smith et al. (1995) used the measurements of flooded areas derived from ERS-1 SAR images to estimate the discharge of a glacial river in British Columbia. Their approach was based on a rating curve model written as:

$$W = a Q^b \quad (4.3)$$

where W is the effective width which is defined as the total water surface area divided by the length of the main drainage channel. Q is the measured discharge and “ a ” and “ b ” are two empirical parameters. Despite its simplicity and interesting potential, particularly over large watersheds, the main problem of using this simple empirical relationship in flood forecasting is its dependency on surface type conditions. The empirical parameters vary significantly from one site to another. Moreover, the temporal evolution of the surface conditions in the basin suggests that these parameters may well

vary with time. It is interesting to analyze the potential of this model for water surface extent prediction using passive microwave data and discharge measurements. The problem of spatial and temporal constancy of the classic power law model parameters will be particularly examined.

The relationship between flooded areas and discharge in northern climates depends largely on the occurrence of ice jams in the main channel of rivers. Moreover, the presence of vegetation and semi-active zones that join the hydrological network only during flooding can also control the relationship between discharge and water body extent. Generally, the flooded area increases with increasing discharge (Figure 14). This relationship leads to a rating curve model relating the flooded area to the discharge, written as:

$$\text{WSF}(t) = a \cdot Q^b(t) \quad (4.4)$$

where WSF is the Water Surface Fraction, Q is the measured discharge, and a and b are two empirical parameters. Generally, these empirical parameters are determined by a linearization of Equation 4.4. The power law model (Equation 4.4) was selected because of its simplicity and the availability of the parameters required for its implementation. The easy availability of the parameters represents a great advantage for estimating the water body extent. The relationship between the flow and the WSF is expected to vary with time. Figure 15 shows the relationship between the measured flow and the estimated WSF over the Mackenzie River Basin outlet, during the summer of 1998. This figure shows that there are two sets of data, one for the flooding phase, and a second set for the recession phase. These different data sets will affect the estimation accuracy of the parameters of the rating curve model. Thus, the estimation of the parameters should account for the changing relationship between the flow and the WSF.

The rating curve relation under its classical equation implies a systematic synchronism between the inundation and discharge curves. However, a lag time is generally observed between the flow peak and maximum water surface area over large watersheds (Sippel et al., 1998). Furthermore, the river stage can increase while the flooded area decreases (Kruus et al., 1981). These phenomena were also observed in the Mackenzie River Basin. Consequently, the assumption of a systematic synchronism is therefore not realistic. In order to account for the occurrence of a time lag, an additional term was introduced into the rating curve formula. Thus, the model is now written as:

$$WSF(t) = a \cdot Q^b (t + d.\Delta t) \quad (4.5)$$

where "d. Δt " is a time lag between the discharge and the flooded area. Many factors are likely to generate a time lag between flows and the flooded area: 1) the flow measurement location in the basin; 2) the river morphology; 3) ice jamming, and 4) vegetation density in the flooded area. Furthermore, three situations can be encountered: the lag parameter can be positive if the peak flow occurs after the peak flooded area; it is equal to zero if the two maxima coincide, and finally, if the discharge peak precedes the maximum flooded extent, the time lag will be negative. The model is thus sufficiently flexible and adaptable to those conditions.

Theoretically, the time lag term will maximize the value of the cross-correlation function between the discharge and flooded area curves. This lag depends on the site morphology, and can vary even over the same site during the summer particularly if the site experiences multiple flood events. Hence, a window is programmed to follow data acquisition, extract the last ten values of the discharge and flooded area, and estimate the lag term using the cross-correlation function.

The dependency on the river morphology is the main weakness of the classic rating curve approach. This model, and therefore its empirical parameters, cannot be easily extrapolated from one site to another, even in the case of braided rivers. Moreover, the occurrence of ice jams can affect the relationship between the observed discharge and the estimated WSF, thus suggesting an update of the empirical parameters of the rating curve, which were considered as constant according to the classical formula of the model. Hence, the variability of the empirical parameters of the model presents temporal and spatial components. To overcome these weaknesses, the rating curve model can be related to a Kalman filter in order to dynamically identify its empirical parameters according to the forecasting errors compared at each time step. Using the Kalman filter, the dynamic rating curve model will continuously readjust its parameters to satisfy the non-stationary behavior of the hydrological phenomenon.

The parameter constancy and the systematic synchronism between the flooded area and the discharge are two weaknesses that inhibit the use of the rating curve model for flood forecasting. By introducing a lag term and relating the classical model formula to the Kalman filter, it is expected that these weaknesses should be overcome. With this dynamic formula, it is expected that the model will present an interesting potential for flood forecasting over large basins, where spatial conditions can vary largely from one site to another. It will also eliminate the classical calibration approach that leads to the estimation of two constant values of the empirical parameters. These parameters will vary with time and space in order to produce, at near real time, the highest correlation between the flooded area and the discharge expressed by the rating curve model.

4.2.3 Use of the Kalman filter

The use of the Kalman filter is based on the application of the logarithm to the modified rating curve formula. A linear relationship can be written as:

$$\text{Log} (\text{WSF}(t)) = \log(a) + b \log (Q(t+d\Delta t)) \quad (4.6)$$

$$\text{or} \quad Y = A X + B \quad (4.7)$$

where: $Y = \text{Log} (\text{WSF}(t))$

$$X = \log (Q(t+d\Delta t))$$

A and B are two model parameters

According to the linear relationship, the rating curve model can be written as a matrix product:

$$Y_t = H_t \cdot A_t \quad (4.8)$$

where $Y_t = Y$

$$A_t = \begin{bmatrix} A \\ B \end{bmatrix}$$

$$H_t = \begin{bmatrix} X & 1 \end{bmatrix}$$

The Kalman filter can therefore be applied to the rating curve model by considering the modeling and observation noises. The state and observation equations will be written as:

$$A_{t+1} = \Phi_t A_t + W_t \quad (4.9)$$

$$Y_t = H_t A_t + V_t \quad (4.10)$$

Upon reception of a satellite image (i.e. SSM/I), a WSF is calculated, followed by a readjustment of the parameters of the rating curve model by the Kalman filter. The cross-correlation function evaluates the lag time between the two vectors of observation. Hence, the WSF value will be predicted using updated parameters and an estimated time lag. It is expected that the combination of these two procedures will improve the flood prediction potential of the rating curve model.

4.3 Application and Results

4.3.1 Study area: The Mackenzie River Basin

The methodology proposed in this work was applied to the Mackenzie River Basin (MRB) (Figure 13). Going from south to north, the vegetation zones in the Mackenzie Basin vary from prairies to boreal forests to tundra, in the northerly part of the basin. In the western part of the basin, mountains rise up to 3 km, and the lowest zones lie in the northern and central-eastern parts of the basin (Rouse, 2000; Stewart et al., 1998). The Mackenzie Basin contains some of the largest freshwater lakes in the world: Great Bear Lake, Great Slave Lake and Athabasca Lake. These lakes play an important role in water cycle monitoring in the Mackenzie River Basin. Freshwater lakes and distributary channels cover up to 50% of the total Mackenzie Delta area (Burn, 1995).

The water cycle in the MRB is largely affected by the spring snow melt period, during which ice thawing is its major source of freshwater. Similarly, in the Basin's lakes and rivers, the water level rises to its highest level during this period. Consequently, river discharge becomes very significant and many lakes flooded. Note that flooding over the Mackenzie River Basin is largely affected by ice jamming. Marsh and Hey (1989) stated that 33% of lakes in the Mackenzie Delta can be considered as high-closure lakes. In this case, ice jamming dominates flooding. Thus, these lakes are mainly flooded during the spring melt period, when ice jamming occurs. Over the Peace-Athabasca Delta, Toyra et al. (2002) observed several wetland basins surrounding the delta. The central part of the delta is mainly composed of large and shallow lakes which are connected to Lake Athabasca by several channels. Generally, these wetland basins are not connected to the main channel. However, following the ice break-up, a portions of these basins flood rapidly (Leconte et al., 2001). Hence, flooding in two major deltas of the Mackenzie River Basin, namely, the Mackenzie River delta and the Peace-Athabasca Delta,

depends largely on the spring snow melt period. Furthermore, flooding frequencies in these areas are highly related to their morphology as most of these wetland basins are disconnected, and only join the main river during the spring melt period as a result of ice jams. Therefore, during the spring melt period, these flooded areas include either basins covered by shallow water or wetlands with highly moist soils.

4.3.2 Approach reliability assessment using 1998 and 1999 data

WSF values over the Mackenzie River Basin were estimated during the summers of 1998 and 1999 on a pixel-per-pixel basis. These estimations were used in this application to carry out offline simulations, and were considered as “true” values to which the predicted WSF were compared. From the daily generated WSF maps, the Peace Athabasca Delta (PAD) and the Mackenzie River delta (MRD) were selected as control sections in order to assess the reliability of the proposed approach (Figure 13). The PAD and the MRD have areas of about 4000 and 12000 km², respectively. The estimated WSF was averaged over each control section in order to apply the proposed methodology. The estimated WSF can be affected by atmospheric conditions, especially during wet seasons (Kerr & Njoku, 1993). However, the flooding effect will dominate the WSF variability as simulations were carried out over two deltas with a high flood potential. The existence of a significant correlation between flooded areas and discharges over these areas is the most important reason for choosing these two deltas for the application of the methodology. Furthermore, the flat topography of these selected deltas reduces the contribution to the satellite signal of high-closure lakes that do not join the main river stem, even during the spring melt period. Moreover, previous studies (Sippel et al., 1992; Vorosmarty et al., 1996) recommended an analysis of the correlation between discharge and floodplain extent within the main stem. The main river stems were included in the selected portions in this study.

River runoff data were provided by two observation sites, the first being at the Arctic Red River ($67^{\circ}27' N$, $133^{\circ}44' W$), which corresponds to an outflow of almost 95% of the MRB (MacKay et al., 2003), and the second at the Peace River ($59^{\circ}6' N$, $112^{\circ}25' W$), for the MRD and PAD, respectively. The location of these stations is very important with respect to the time lag between discharge and flow measurements. Generally, the observation sites over the Mackenzie Basin allow accurate measurements of river runoff. However, the accuracy is sometimes reduced, especially during the ice-cover and spring melt periods (Stewart et al., 1998). In spite of the ice jam effect which occurs during the spring melt period, discharge measurements provided by these stations are reasonably accurate for the purposes of this study.

It is interesting to note that according to the proposed approach, the calibration step of the rating curve model is not needed as the rating curve parameters are adjusted upon the reception of each new WSF value. Therefore, the entire 1998 and 1999 data set was used to carry out the simulations. With two zones and two summer seasons, four flooding events were used to assess the reliability of the approach. Figures 16, 17, 18 and 19 illustrate the results obtained with the approach.

Results show a good agreement between the estimated and predicted WSF. For all four flooding events, the rating curve model was able to satisfactorily simulate the trend of the estimated WSF. All analyzed events show an increasing WSF during the spring melt period as ice thawing and precipitations contribute to extend the WSF over the Mackenzie River Basin. This is followed by a flattening of the curves during the months of June and July, as precipitation and snowmelt are compensated by evaporation and discharge. However, some flooding events can be observed during the summer seasons, with a lower magnitude as compared to those of the spring melt period (Marsh & Hey, 1989). Finally, a decrease of the WSF is noticed as the snowmelt no longer contributes to the hydrological cycle and evaporation plus runoff exceeds precipitation.

Furthermore, the predicted WSF for 1998 were higher than those for 1999, over the same area. It is interesting to note that 1998 was 8th wettest year observed in the Mackenzie River Basin (Kochtubajda et al., 2000). The EL Nino phenomenon was observed during this year (Rouse, 2000).

Moreover, a perfect synchronism between the estimated and predicted WSF can be obtained as a result of the introduction of the time lag. Although the predicted WSFs are generated from the discharge data, which does not necessarily coincide with the estimated water surface extent, the dynamic rating curve model was nonetheless able to eliminate this lag and synchronize the estimated and predicted WSF. The time lag parameter is estimated on a daily basis using the ten last discharge and WSF observations. The absolute values of the obtained time lag vary between 0 and 7 days in the PAD case study. It was expected that this parameter would be of no more than a few days due to the small size of the PAD area (4000 km^2) and the close location of the flow observation station over the Slave River to the PAD area.

In order to assess the reliability of the proposed approach, WSF maps were generated using NOAA-AVHRR images taken over the Mackenzie River Basin during the summers of 1998 and 1999. Three channels (channel 1: $0.58\text{-}0.68 \mu$, channel 2: $0.72\text{-}1.10 \mu$ and channel 3: $3.55\text{-}3.93 \mu$) were classified in order to identify the WSF extent. The Peace Athabasca Delta site was selected for the validation process. Figure 20 constitutes an example of the NOAA images taken over the selected site. Available NOAA-AVHRR images were examined, and those that were cloud-free were retained for analysis. WSFs were derived from NOAA-AVHRR and SSM/I data covering the same region, which is little larger than that used previously with SSM/I data in order to improve the classification performance. The results of the comparison are shown in Figure 21. A satisfactory agreement can be observed between the WSF estimated from NOAA-AVHRR images and those predicted by the modified rating curve model. Both

of them follow the general trend described above for the WSF evolution over the Mackenzie River Basin. However, an abrupt decrease was observed during the 1998 summer season. WSF seemed to be underestimated during this period of the year.

Although, the reliability of this approach has been tested over two delta sites, its applicability over the entire Mackenzie River Basin should be assessed in further studies, which will be our goal in future works. On the other hand, considering that only the spring and summer periods were examined in this study, it was assumed that the contribution of ice thawing to inundation is larger than that of precipitation during this period in the MRB (Marsh & Hey, 1989). This implies a larger correlation between discharge and flooded areas, which improves the potential of the proposed approach in sub-artic regions.

4.3.3 Use of passive microwave data for discharge forecasting

The existing correlation between discharge and WSF can be used also to predict discharge values particularly in case of positive time lag when the peak flow occurs after the peak flooded area. In this particular case the discharge can be written as:

$$Q = a \cdot WSF^b (t + d \cdot \Delta t) \quad (4.11)$$

The proposed algorithm can, therefore, be applied to predict discharge values in an upstream location. The empirical parameters and the time lag term are dynamically readjusted as it was previously discussed. The availability of discharge observations and passive microwave data has enabled us to extend simulations beyond the two years, 1998 and 1999. The flow observed over the Slave River, which is located at $59^{\circ}52' N$, $111^{\circ}35' W$ (Figure 13), was used in combination with SSM/I measurements over the

PAD from 1992 to 2000. Only summer periods were considered in carrying out simulations. WSF values were used to predict the flow over the Slave River Site because of the upstream location of the discharge observing station.

A predefined regression relationship between flooded areas and discharges is not needed in this case to extend the record of the flooded area as the use of the Kalman filter allows the readjustment of the rating parameters dynamically. Figure 22 shows the simulation results. The predicted and observed discharge values were averaged on a weekly basis. A satisfactory agreement was observed between the predicted and observed discharge. Moreover, this figure demonstrates an apparent interannual variability of the discharge over Slave River observing station. From 1992 to 2000, the PAD area drained by the Slave River was fluctuating between wet and dry years. The 1995/1996 water year seems to be the beginning of a wetting phase of the delta, which ended during the summer of 1998, which coincides with an EL Nino phenomenon, with an abnormally high temperatures. Leconte et al. (2001) stated that 1996 seems to be one of the wettest years on record. On the other hand, an abnormally low discharge was observed during the 1994/95 water year (Strong et al., 2002) which corroborates the predicted discharge.

These simulations show again that the time lag parameter varies in absolute value between 0 and 7 days, when WSF is estimated over the PAD and discharge is observed over the Slave River. However, this parameter does not show a significant interannual variability as its annual average (Figure 23) varies slightly, at approximately two days. An average surface flow speed of 0.6 m/s (Louie et al., 2002) and a time lag value of 2.5 days lead to a runoff distance of 130 km that is compatible with the actual drainage distance between the discharge observation station over the Slave River and the PAD area, which is about 100 km.

It is worth mentioning that the dynamic readjustment of the parameters of the model offers a satisfactory flexibility to the model and enables its use either for flood or flow forecasting, as was tested previously (Smith et al., 1996). In these two cases, the Kalman filter dynamically readjusts the model parameters upon the reception of each new satellite image. The daily availability of the passive microwave data is very important for the application of the proposed approach.

4.4 Conclusion

In northern climates, ice jamming complicates the flooding process, causing it to evolve rapidly, and causing considerable economic and social damage. Hence, flood forecasting over this area is of great importance. This aim of this work is to provide a real-time forecasting of the water surface extent over two control sites selected from the Mackenzie River Basin using discharge observations. The proposed methodology is based on the rating curve model, which was modified, by having a lag term introduced into its classical formulation. This lag term is responsible for a lag time observed between the WSF and discharge peaks. The modified rating curve model was coupled with the Kalman filter to update the empirical parameters of the model upon the reception of each new SSM/I image. The modified model is flexible and adapted to variable morphological features. Furthermore, the proposed approach makes it possible to overcome the site dependency of the rating curve model. The reliability of the approach was tested over the Peace Athabasca Delta, PAD and the Mackenzie River Delta, MRD. The WSF, estimated using NOAA-AVHRR images, were compared to those predicted over the PAD control site using SSM/I passive microwave data. The WSF from NOAA-AVHRR images fit the predicted values reasonably well. Satisfactory results were also obtained from the summers of 1992 to 2000 despite an interannual variability of both discharge and flooded areas. This implies that a combination of

passive microwave data and discharge data presents an interesting potential in flood and discharge prediction.

Acknowledgments

We would like to thank Normand Bussières of Environment Canada for providing NOAA-AVHHR images and Dr. Venkat Lakshmi of the University of South Carolina for valuable comments. The constructive criticisms from anonymous referee are also gratefully acknowledged. This work has been supported by the Mackenzie GEWEX (Global Energy and Water Cycle Experiment) Study (MAGS) and Natural Sciences and Engineering Research Council of Canada, NSREC.

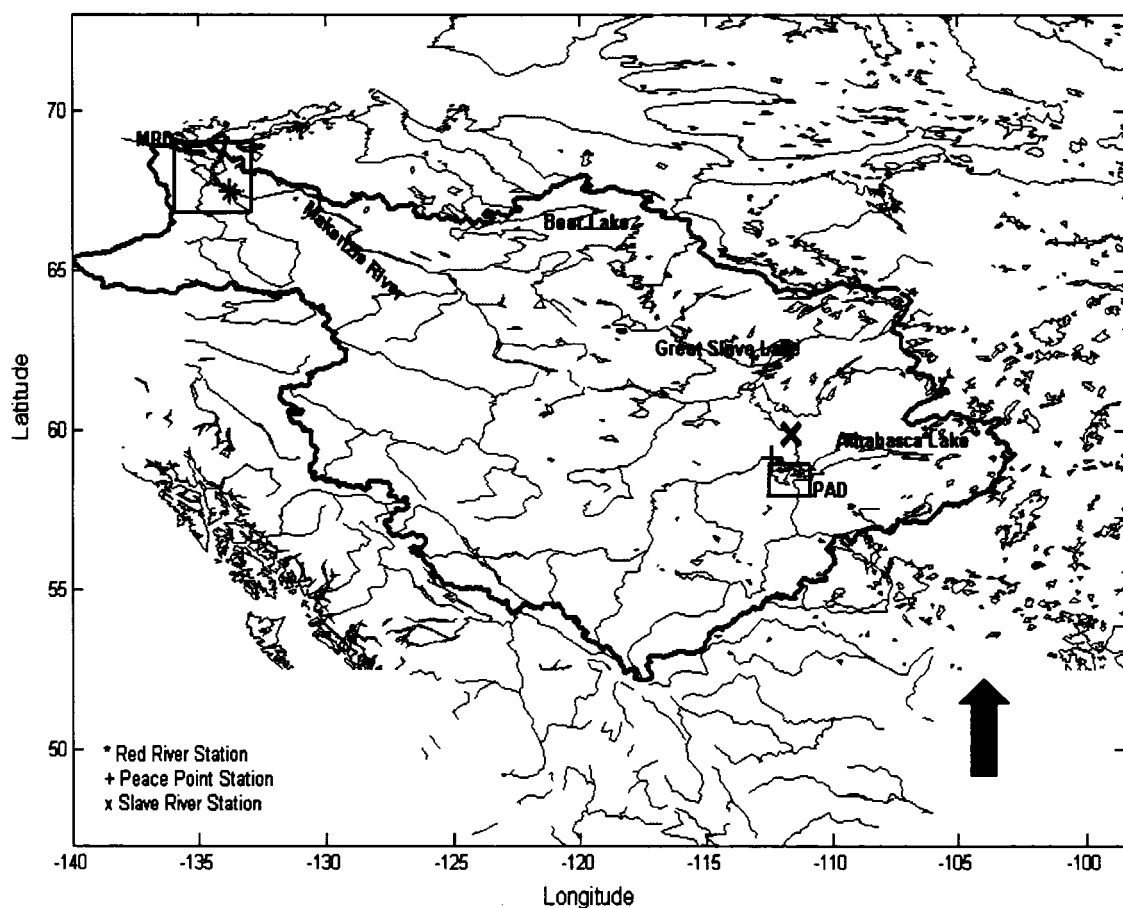


Figure 13 The Mackenzie River Basin

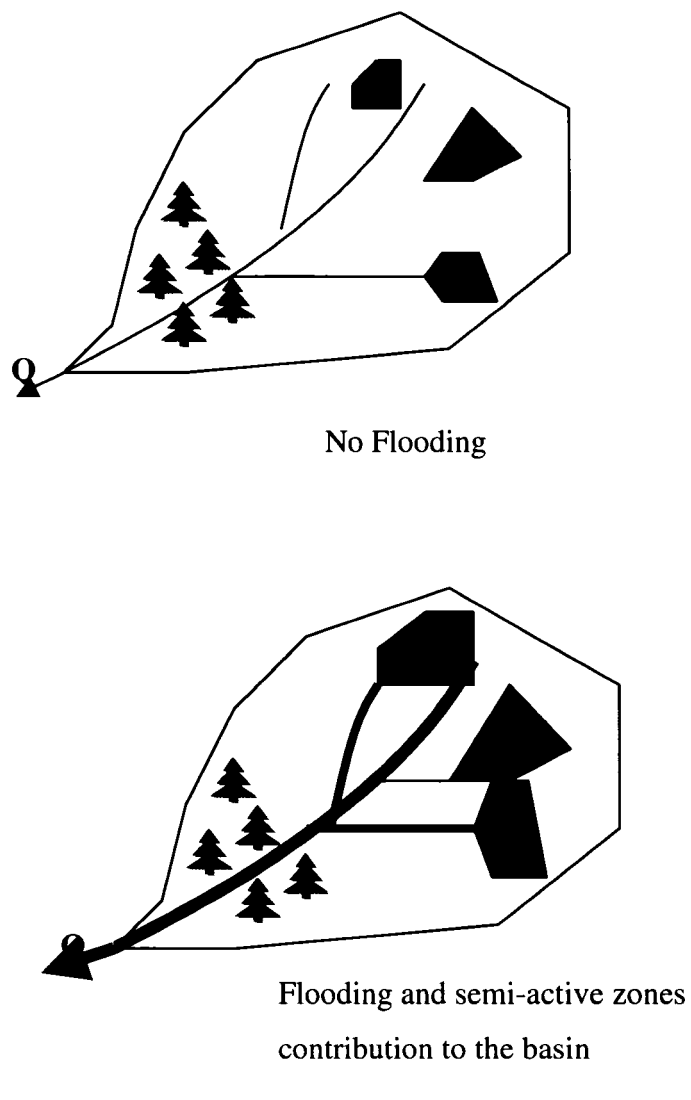


Figure 14 Discharge measured at the basin outlet is used as a proxy for temporal variation in WSF derived from passive microwave data

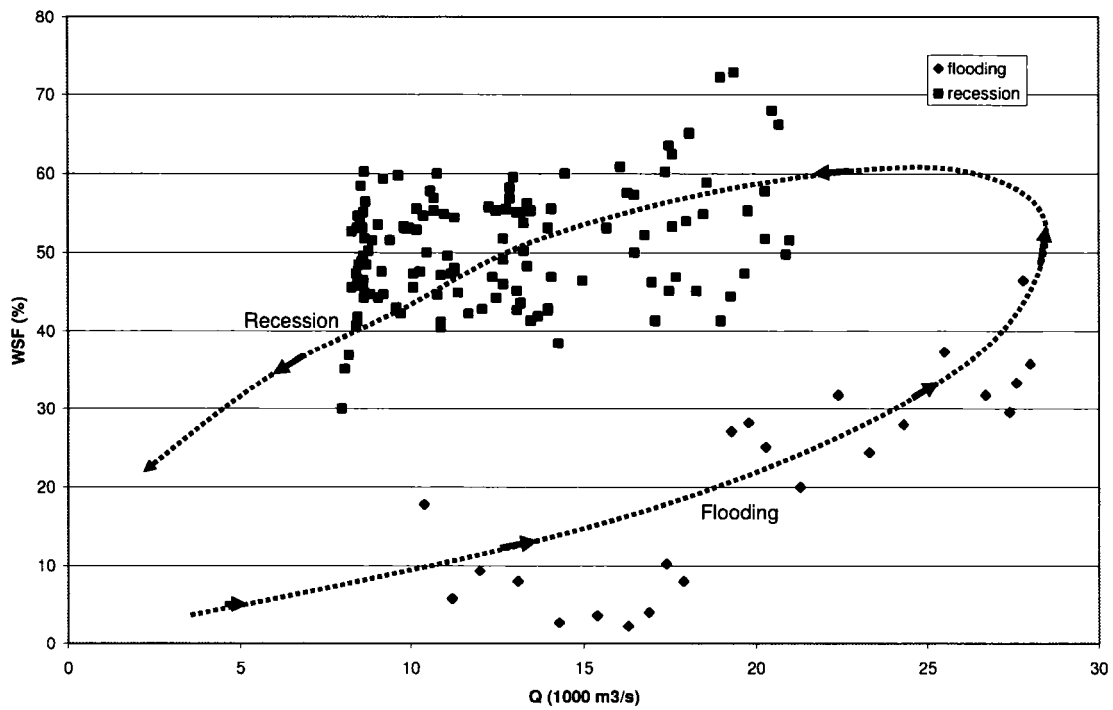


Figure 15 The relationship between measured flow and WSF estimated over the Mackenzie River Basin Outlet, during the summer of 1998

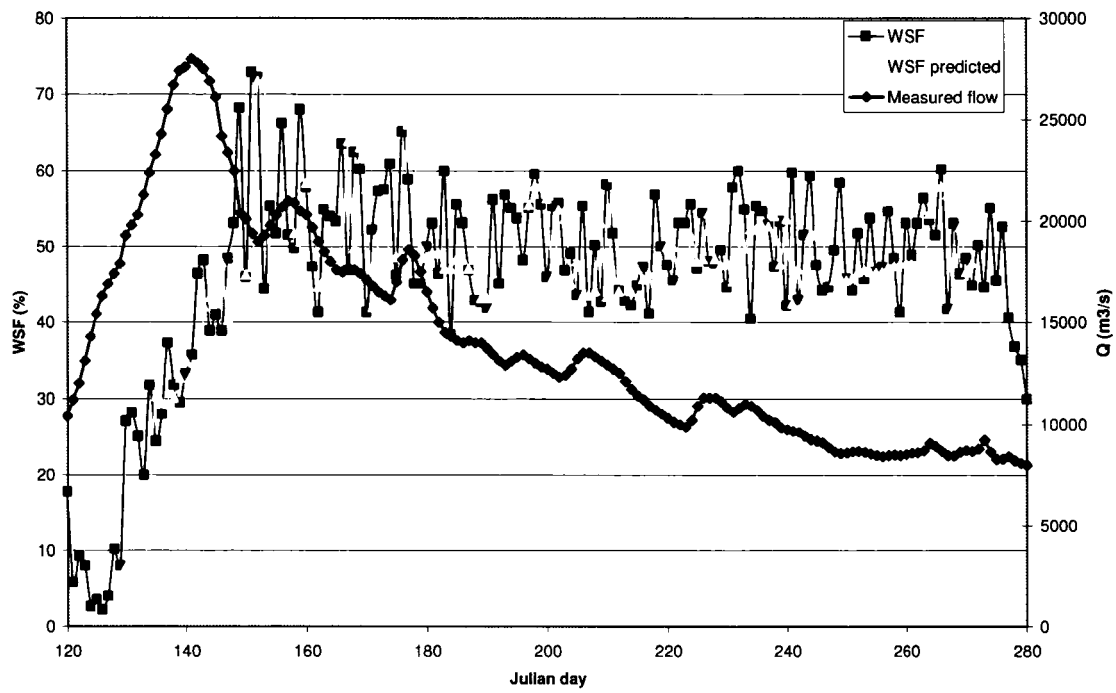


Figure 16 Predicted and estimated WSF compared to the Mackenzie River at Arctic Red River discharge, over the MRD, during the summer of 1998

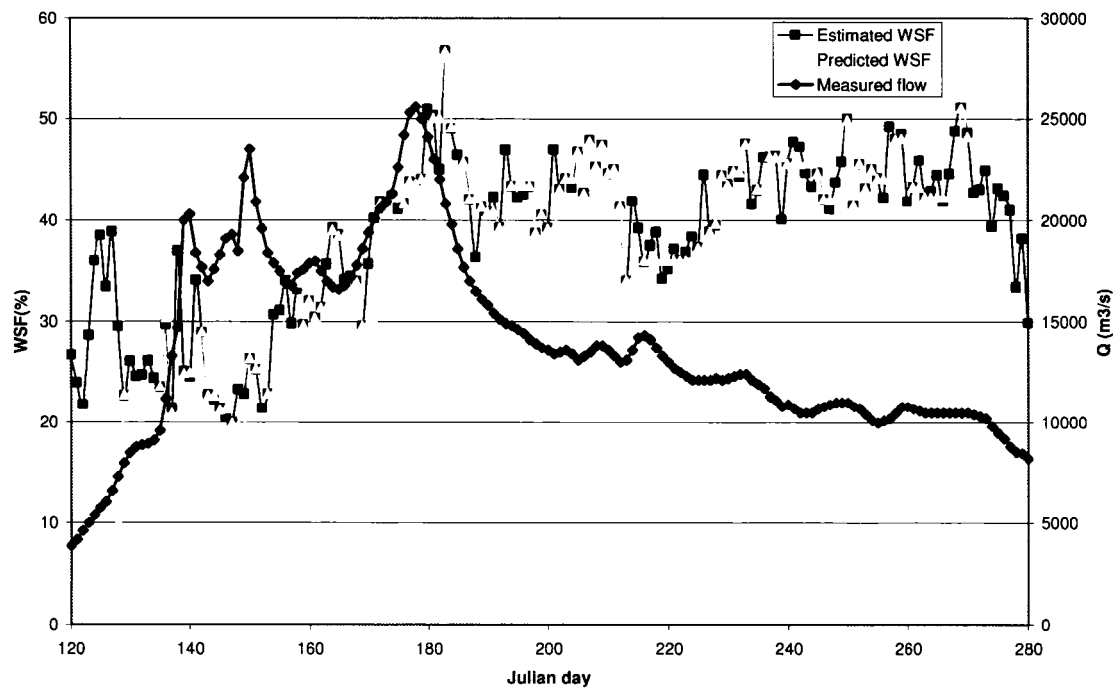


Figure 17 Predicted and estimated WSF compared to the Mackenzie River discharge, over the MRD, during the summer of 1999

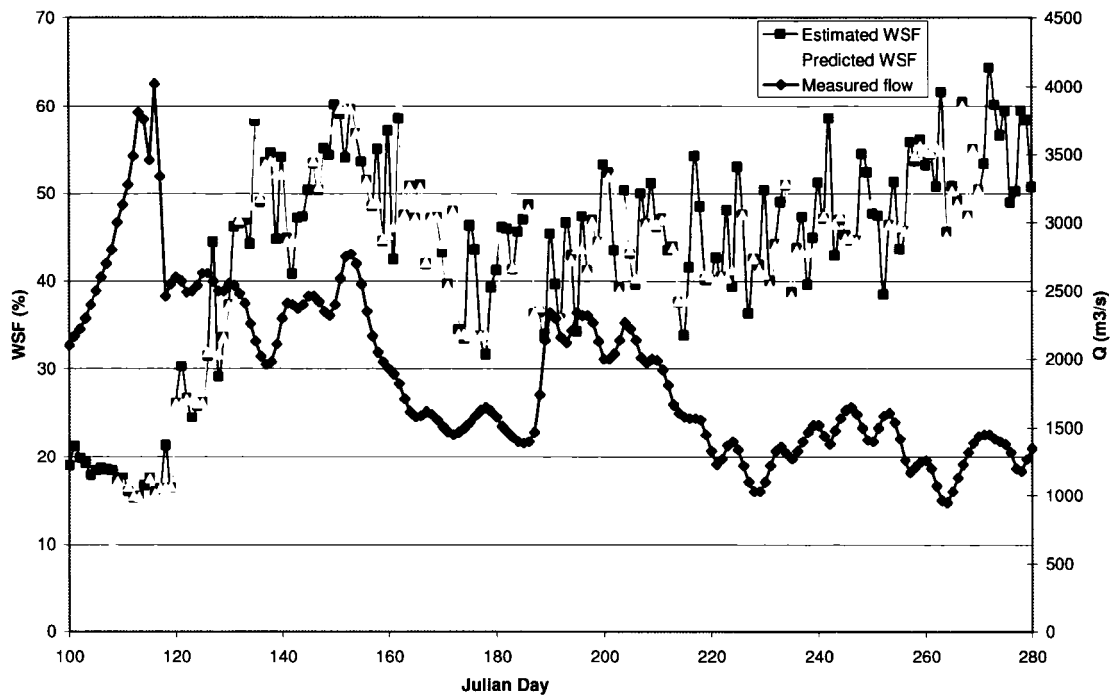


Figure 18 Predicted and estimated WSF compared to the Peace River discharge, over the PAD, during the summer of 1998

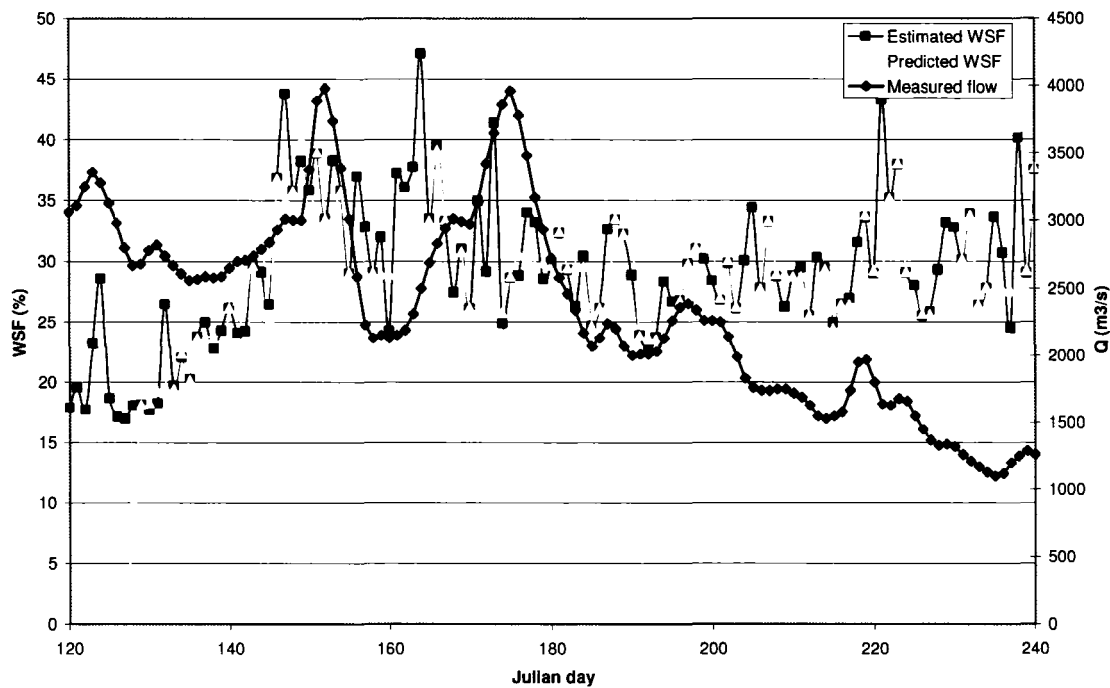


Figure 19 Predicted and estimated WSF compared to the Peace River discharge, over the PAD, during the summer of 1999

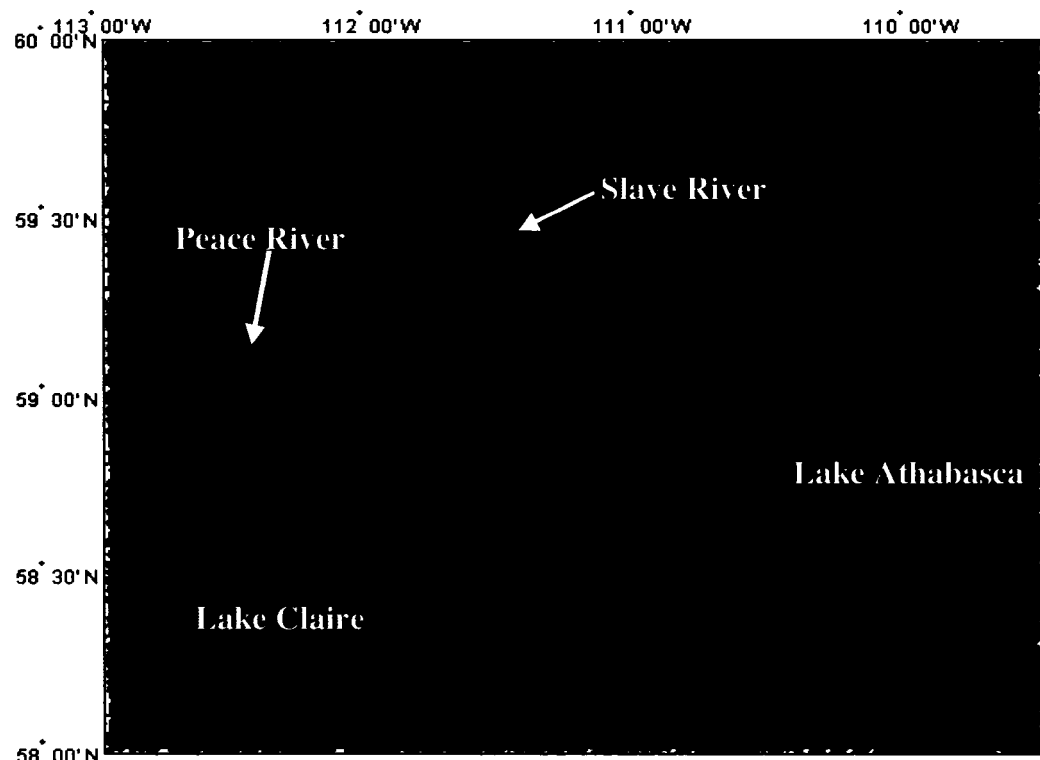


Figure 20 NOAA-AVHRR image of the PAD, August 24th, 1999

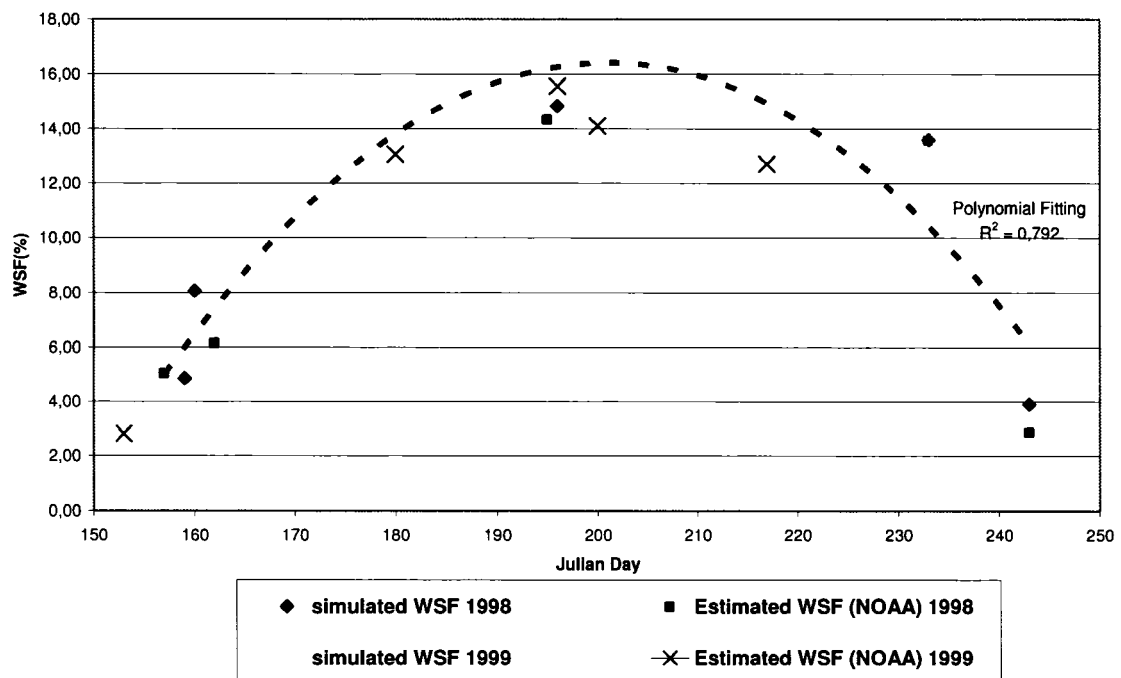


Figure 21 Predicted WSF compared to those estimated from NOAA-AVHRR images, over the PAD, during the summers of 1999 and 1998

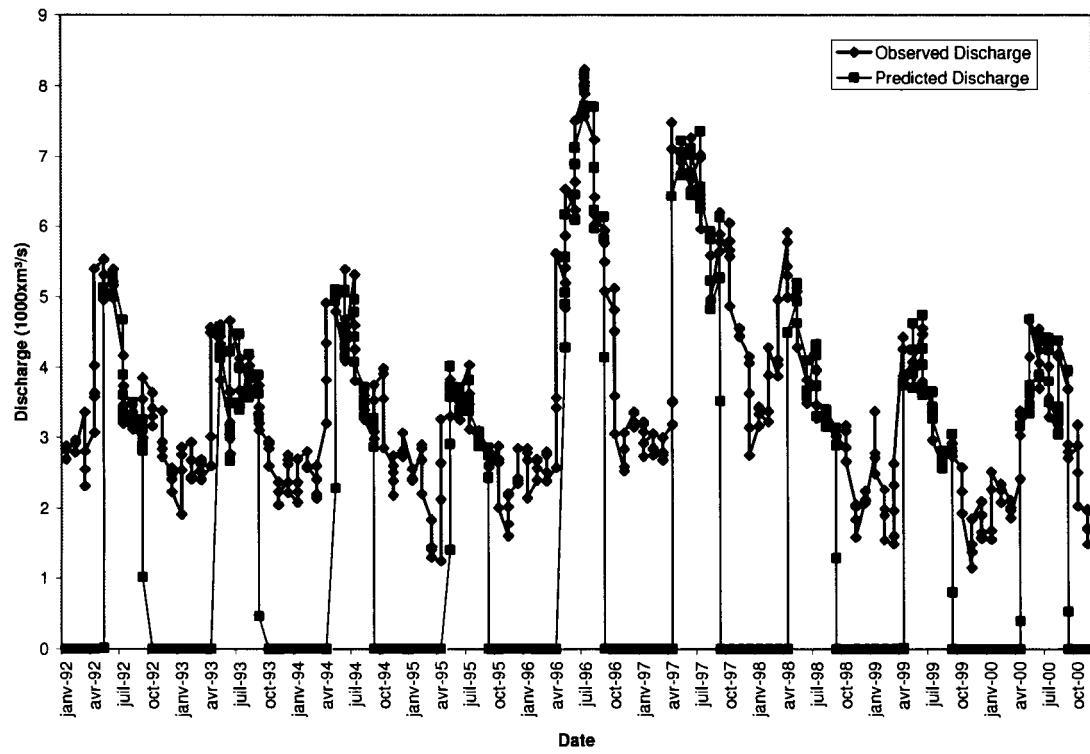


Figure 22 Predicted and observed discharge over the Slave River observing station from 1992 to 2000

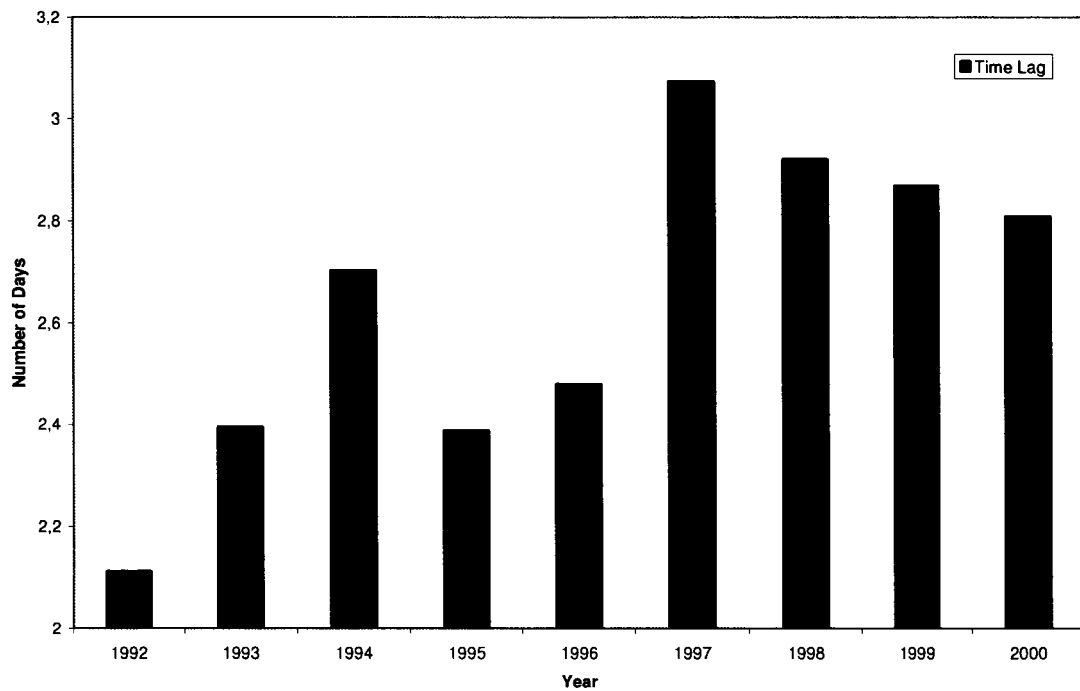


Figure 23 Variability of the Averaged Time Lag Parameter from 1992 to 2000 over the PAD area

CHAPITRE 5

FLOOD AND SOIL WETNESS MONITORING OVER THE MACKENZIE RIVER BASIN USING AMSR-E 37 GHZ BRIGHTNESS TEMPERATURE

Abstract

The proposed approach aims to estimate the flood extent and soil wetness using AMSR-E passive microwave data. The approach is applied over the Peace Athabasca Delta at the Mackenzie River Basin, which is situated in northwestern Canada. The methodology is based on the Polarization Ratio index (PR), which is computed using AMSR-E 37 GHz, vertically and horizontally polarized brightness temperature values. The Water Surface Fraction (WSF), which represents the fraction of flooded soil, was derived on a pixel-per-pixel basis. The fractional vegetation cover was added to the WSF calculation in order to take into account the temporal variation of the vegetation shading effect. The WSF derived from AMSR-E data, WSF(AMSR-E), was compared to those derived from the Moderate-resolution Imaging Spectroradiometer Terra instrument (MODIS-Terra) images (250 m), WSF(MODIS). A rating curve relationship was developed between the observed discharge and WSF(MODIS). It was noted that the WSF obtained from AMSR-E images systematically exceed those from MODIS, as they are formed from a combination of different contributions, including open water surface, flooded area and wetlands, which are abundant in the northern climates. Therefore, a wetness index was defined based on the difference between passive microwave and visible image responses. This index was able to qualitatively describe the temporal evolution of the wetness over a part of the Mackenzie River Basin. The availability of discharge observations and passive microwave data leads to the definition of a consistent wetness index and soil moisture monitoring over the region of the Mackenzie River Basin. The extrapolation of the developed algorithm to the entire Mackenzie River Basin should consider the dependency of the rating curve relationship on the site features. A

satisfactory agreement was noted between the wetness index, the precipitation, and the temperature values. The wetness index agrees well with the measured soil moisture.

Keywords: Flood; Soil moisture; Passive Microwave; Wetness index; Rating curve; Discharge observations.

5.1 Introduction

Passive microwave data present an interesting potential for flood monitoring and soil moisture estimation because of their ability to penetrate through clouds and provide a daily global coverage. Several studies have used the 37 GHz Polarization Difference ($PD = T_{bv} - T_{bh}$) to monitor flooded areas (Choudhury, 1989; Sippel et al., 1994; Tanaka et al., 2003b). The polarization difference at a 37 GHz frequency increases with increasing Water Surface Fraction (WSF) within a pixel (Choudhury, 1989; Choudhury, 1991). Choudhury (1989) developed an empirical relationship between the polarization difference and the fractional area of free water based on the polarization index. Sippel et al (1994) examined the potential of the polarization difference index in the determination of flooded areas over the Amazon River Floodplain. Sippel et al (1998) noted a significant correlation between the river stage and total flooded area. The methodology was also successfully applied by Hamilton et al. (2004). Prigent & Aires (2001) estimated the flooded areas by calculating the emissivity polarization difference, and taking into account the vegetation effect. They used ERS backscattering values to estimate the vegetation density and they assumed that for each vegetation density, the emissivity polarization difference varies linearly depending on the flooded area.

The sensitivity of the polarization difference to the amount of water over the soil surface is affected by vegetation and atmospheric conditions (Prigent & Aires, 2001). Temporal variations of vegetation and atmospheric effects are different. While the atmospheric

contribution is often rapid and instantaneous, the vegetation effect, on the other hand, follows a trend, and evolves depending on the vegetation growth. It is important to assess these effects in order to accurately retrieve the extent of the water bodies using passive microwave data.

Kerr and Njuko (1993) recommended the use of the Polarization Ratio ($PR = (Tb_v - Tb_h) / (Tb_v + Tb_h)$) as an alternative to the polarization difference because the former is less affected by atmospheric conditions and is not dependent on the effective soil temperature. The PR, which is computed in this study using AMSR-E 37 GHz passive microwave data, is a good indicator of the vegetation state, and simultaneously presents an interesting sensitivity to the amount of water over the soil surface (Owe et al., 2001). This index was used by Paloscia et al. (2001) to assess to vegetation effect and retrieve soil moisture using SSM/I passive microwave data.

Passive microwave data are sensitive to the amount of water at/near the soil surface. Therefore, the fractional water extent estimated using passive microwave is a combination of water body area, flooded area and soil moisture. However, the WSF derived from visible images does not include the effect of soil wetness, and exclusively provides an estimate of the water body extent. It is expected that critical information about the amount of water in the Mackenzie River Basin may be extracted from the difference between visible and passive microwave data.

This work aims at providing an estimate of the fractional water extent and the soil wetness using the PR index, which is derived from the AMSR-E 37 GHz brightness temperature. The vegetation effect will be taken into account in a mixing model, which combines the contributions of the different surface types to the observed polarization ratio over the entire pixel. The derived water surface extent will be compared to that

retrieved using MODIS images (250m). The difference between the water surface extent derived from the visible and passive microwave images will also be investigated.

This work is a part of the MAGS (the MAckenzie Gewex Study) project. Considering the size of the Mackenzie River Basin (1.8 million km²), and the relatively high spatial resolution of MODIS-terra images (250 m), the proposed methodology will only be applied over a smaller area of the Mackenzie River Basin. The Peace Athabasca Delta (PAD) was selected as a control area to apply the proposed approach (Figure 24). The PAD is one of the largest inland deltas in the world. It has an area of about 4000 km². It is located at the western end of Lake Athabasca, and was created by a confluence of the Peace, Athabasca and Birch rivers. The Peace River has the largest discharge, with a mean annual flow at the Peace Point of 2100 m³/s. It generally flows in a northerly direction. However, this direction can be reversed when the water level in the Peace River exceeds that of Lake Athabasca (Leconte et al., 2001). Several wetland basins surround the delta (Toyra et al., 2002), and its central part is composed mainly of large and shallow lakes, which are connected to the Lake Athabasca by several channels.

Passive microwave data of the selected area were obtained from the NASA EOS Data Gateway Web site. AMSR-E 37 GHz frequency vertically and horizontally polarized brightness temperatures were used in this study. The sensor footprint size at this frequency is 8x14 km, which is an improvement over that of the SSM/I sensors (18x37 km). The AMSR-E sensor, whose frequencies cover the 6-86 GHz range, provides a daily global coverage. The sensor has low frequencies of 6 and 10.7 GHz, which are more suitable for soil moisture estimation. However, the sensor footprint at these frequencies is around 50 km, which makes it difficult to validate the soil moisture results.

5.2 Methodology

The proposed methodology is based on three steps. Firstly, the 37 GHz passive microwave data will be used to estimate the WSF on a pixel-per-pixel basis. The WSF fraction will be estimated by applying a linear mixing model, and the mixing model will be written as a linear combination of polarization indices characterizing open water, flooded, and non-flooded areas. Polarization indices will be estimated over each surface class to take into account the difference between their surface conditions. The development of the canopy during the summer will be considered when applying the mixing model.

In a second step, MODIS images will be classified in order to estimate the open water extent. The spatial resolution of the MODIS sensor (250 m) enables us to obtain an accurate estimation of the water surface area. It is expected that the WSF derived from the passive microwave data exceed those obtained using MODIS visible images since passive microwave data are sensitive to the amount of water at/near the soil surface. However, MODIS images can only reflect the response of the open water extent over the surface. This suggests that information about the soil wetness can lie in the difference between the data of the two sensors. This difference can be defined as the wetness index of the basin. The improved spatial resolution of the MODIS and AMSR-E sensors offers the possibility of an accurate retrieval of this wetness index. Moreover, the selection of the PR as a suitable polarization index for the WSF fraction estimation can improve the accuracy of the algorithm. Furthermore, the consideration of the vegetation effect in the retrieval method can provide an accurate estimate of the proposed wetness index.

In the third and last step, a rating curve model will be developed based on an existing relationship between the WSF derived from the MODIS sensor and the discharge measurements. A similar relationship has been successfully tested in a previous study carried out over the PAD area (Temimi et al., 2005). A predictive relationship of the

basin wetness index can therefore be developed using passive microwave data and discharge measurements. The availability of these data will enable us to monitor the wetness over the Mackenzie River Basin during several summer periods. The accuracy of the developed rating curve depends on the number of images which were treated to estimate the fraction of flooded area. Unfortunately, the number of available images could be reduced significantly because of the cloud contamination (Frazier et al., 2003).

5.2.1 Definition of the Wetness Index

The classification of MODIS images allows the estimation of the fractional open water extent over the PAD, referred here as WSF(MODIS). However, these flooded areas fall into one of the flowing categories: 1) flooded bare soil, which could be sensed by the MODIS and 2) flooded vegetation area, which could not be “seen” using visible sensors because of the shading effect of the canopy. Therefore, the WSF derived from MODIS images includes permanent open water and flooded bare soil. Passive microwave data, on the other hand, include flooded area (vegetated and bare soils) and soil moisture effects. Hence, the difference between passive microwave and visible data will include both soil moisture and flooded vegetation contributions. The consideration of the vegetation growth in the mixing model by introducing the canopy density term enables us to accurately retrieve the soil moisture effect.

Figures 25 and 26 show the temporal variability of the weekly averaged WSF(AMSR-E) and WSF(MODIS) provided by the mixing model and the rating curve model, respectively. The developed rating curve model was applied to estimate the extent of open water bodies (permanent open water bodies and flooded bare soil) using discharge observations from the summers of 2002 and 2003, which were taken at Slave River site. Although there is no AMSR-E data for the months of May and June 2002, it is nevertheless possible to state that the WSF(MODIS) and the WSF(AMSR-E) maintain

the same trend during the two summer seasons, especially the small decrease at the end of the season. They increase at the beginning of the spring melt period to reach a maximum at the beginning of the summer season. The WSF(AMSR-E) starts a recession phase at the beginning of June. However, the WSF(MODIS) starts to decrease a few weeks later, after a flattening period with some fluctuation. Finally, both of these variables decrease at the end of the summer season. As was expected, the WSF(AMSR-E) were systematically higher than the WSF(MODIS). Moreover, the two Figures present a variable gap between the WSF(AMSR-E) and the WSF(MODIS).

The difference between the WSF estimated from the AMSR-E and MODIS data seems to vary in time. We believe that the variability of this difference is the result of the soil moisture variation, since passive microwave data include the effect of soil moisture, which is not sensed by visible sensors. Consequently, we propose to define a Wetness Index (WI) based on the difference between these two sensor responses. This WI is defined by the following relationship:

$$WI = \frac{WSF(AMSR) - WSF(MODIS)}{1 - WSF(MODIS)} \quad (5.1)$$

where, WSF(AMSR-E) is the Water Surface Fraction derived from AMSR-E data, WSF(MODIS) is the Water Surface Fraction derived from MODIS data, which presents the area of the open water bodies and flooded bare soil. This WI varies between 0 and 1. It presents the fraction of the wetlands within the non-flooded area. The WI is equal to zero when the non-flooded soil is completely dry. In this case, the WSF(AMSR-E) should be equal to the WSF(MODIS). On the other hand, if the non-flooded soil is completely wet, the WSF(AMSR-E) should be equal to 1, and consequently, the wetness index is at a maximum (WI=1).

However, the WSF(MODIS) can be written as a function of discharge observations using the rating curve relationship developed in the previous section. The availability of AMSR-E data and discharge observations enables the estimation of a daily value of the developed wetness index, which can be written as:

$$WI = \frac{WSF(AMSR) - a.Q^b(t)}{1 - a.Q^b(t)} \quad (5.2)$$

By substituting the WSF(MODIS) by the rating curve model, we overcome the step involving the WSF estimation using MODIS images. This step is not straightforward given the non-availability of daily MODIS images that are cloud-free and cover the PAD area. The proposed algorithm used for the wetness index estimation has been summarized in the flow-chart shown in Figure 27.

The proposed algorithm follows two steps. The first is a calibration step, which aims to provide an estimate of the mixing model and the rating curve parameters. It is an off-line step, carried out once for each studied area. MODIS and AMSR-E images are used to calibrate these parameters. The same data set can be used to calibrate the mixing model and compute the WI. In addition, this relationship can only be used for the PAD area over which the model parameters were calibrated.

The second step aims to provide an estimate of the WI using the calibrated model. The flooded area, the WSF(MODIS), is estimated using the rating curve model. The entire fraction of wetness, the WSF(AMSR-E), at and near the soil surface over the studied area, is estimated using AMSR-E data. This step is carried out upon the reception of

each new AMSR-E image and discharge observation. The defined WI is therefore computed using Equation (5.2). This equation is a predictive model that can be applied to several summer periods. Although, the parameters of the rating curve model can show a seasonal variability because of the changing surface conditions, they will be considered as constant in this study. The variability of the rating curve parameters is beyond the scope of this work.

5.2.2 The linear mixing model

A linear mixing model was used in previous studies to estimate the fraction of open water extent (Choudhury, 1991; Hamilton, 1999; Sippel et al., 1998). In these studies, the proposed mixing model was based on the polarization difference index. However, this index depends significantly on the vegetation and atmospheric conditions. On the other hand, the PR is less affected by these perturbations, and also presents an interesting sensitivity to soil wetness (Kerr & Njoku, 1993). Hence, the Polarization Ratio presents an interesting potential to applying the mixing model and accurately estimating the amount of water at/near the soil surface. The PR will be used in this study to develop the mixing model and estimate the WSF using passive microwave data.

The observed PR index is a combination of different responses generated by the permanent open water surface, flooded area, non-flooded area and soil moisture. The PR characterizing each surface type is weighted by its surface fraction. Therefore, the observed PR can be written, over each pixel, as a linear combination of the contributions of these different fractions:

$$PR_{obs} = w.PR_w + f.PR_f + nf.PR_{nf} + sm.PR_{sm} \quad (5.3)$$

nf: non-flooded soil fraction

f: flooded soil fraction

w: fraction of the permanent open water surface

sm: fraction of the soil moisture contribution to the observed PR

PR_w, PR_f, PR_{nf} and PR_{sm} are respectively the PR of the open water, flooded area, non-flooded area and wetlands. Open water fraction is that of permanent water surface such as lakes and rivers. The entire amount of water, WSF(AMSR-E), at/near the soil surface, which is sensed by the passive microwave sensor, is the sum of the open water, flooded area and soil moisture fractions (WSF(AMSR-E)=w + f + sm).

The vegetation shading effect is significant at higher frequencies. It is important to account for this effect when applying the mixing model, especially over flooded pixels, where the canopy density gradually hides the underlying layer contribution to the satellite signal. Over a mixed pixel, the brightness temperature is a combination of the canopy and bare soil contributions. The observed PR over a flooded pixel can be desegregated into bare soil and canopy areas using a fractional vegetation cover (V). Hence, the PR_f index can be written as:

$$PR_f = V \cdot PR_{f\text{veg}} + (1 - V) PR_{f\text{soil}} \quad (5.4)$$

where:

PR_{f_{veg}}: is the PR index of the flooded vegetated area

PR_{f_{soil}}: is the PR index of the flooded bare soil

V: is the fractional vegetation cover which is estimated using the following relationship proposed by (Eagleson, 1982):

$$V = 1 - \exp(-\mu \cdot LAI) \quad (5.5)$$

where:

LAI is the Leaf Area Index and μ is the extinction coefficient. The value of μ varies depending on the canopy density between 0.35 (low vegetation density) to 0.7 (high vegetation density). In this work, a value of 0.4, which was recommended for crops, was assumed suitable, as it reflects the vegetation characteristics of the PAD area.

Moreover, we suppose in this work that $PR_{f\text{soil}}$ and PR_w are equal as the open water and flooded bare soil present relatively similar responses in the AMSR-E images since the penetration depth at high frequencies is only around a few millimeters. The PR_{sm} could not be calibrated as it depends on the amount of water in the soil, which varies in time. The estimation of the weight of the soil moisture contribution is one of the aims of this study. This objective will be achieved by calculating the difference between the passive microwave and visible responses, which will be discussed later in this paper. With the exception of the PR_{sm} , all the polarization indexes will be calibrated. The soil moisture effect will not be considered in the mixing mode as it will be incorporated into the flooded fraction. Following these hypotheses, the linear mixing model can be written as:

$$PR_{obs} = [w + (1 - V)f]PR_w + f \cdot V \cdot PR_{f\text{veg}} + nf \cdot PR_{nf} \quad (5.6)$$

$$\text{and} \quad 1 = w + f + nf \quad (5.7)$$

To resolve this system, the PR index should be calibrated, and the “w” fraction estimated. Therefore, two unknowns, f and nf , will remain in Equations (5.6) and (5.7). The calibration of the PR index and the estimation of the “w” will be discussed in the next section.

5.2.3 Calibration of the mixing model parameters

Three PR indexes need to be calibrated; PR_w , PR_{nf} , PR_{fveg} , and the permanent open water extent estimated. To begin, the PR indexes will be calibrated using the AMSR-E brightness temperatures measured over the Mackenzie River Basin. The time series of the brightness temperatures will be analyzed over each surface type, and the average value will be considered.

The calibration of the PR_w is more straightforward as it can be derived by analyzing the brightness temperatures measured over one of the Great Lakes of the Mackenzie River Basin. In this work, the Athabasca Lake was chosen for estimating the PR_w . A value of $PR_w=0.35$ seems to be representative of the PR index over open water areas. This value was derived only using brightness temperatures measured during the summer after the ice-thawing period when the Athabasca Lake is free of ice.

The PR_{nf} and PR_{fveg} were calibrated over some selected pixels, which were chosen based on their flood potential. This parameter presents the flooding priority of each pixel. The pixel with the highest flood potential will be covered by water first, while that with the lowest will be the last to be inundated. The flood potential, which is similar to that proposed by (Galantowicz, 2002), was estimated *a priori* for each pixel depending on its altitude and its location from the nearest river channel. Hence, a flood potential map was computed for the study area using the flood potential relationship:

$$fp = \frac{1}{\left[\Delta_{alt} + \frac{d}{d_{max}} \right]} \quad (5.8)$$

where Δ_{alt} and d are respectively the altitude and distance differences between the pixel over which fp is calculated and the nearest stream channel. Besides, d_{max} is the maximum value of the distance among all pixels with the same Δ_{alt} . The flood potential was estimated over the PAD area using Digital Elevation Model (DEM) data and rivers and lakes boundaries, which were imported from the NOAA's National Geophysical Data Center (NGDC) (<http://www.ngdc.noaa.gov/ngdc.html>).

The PR_{nf} was calibrated using brightness temperatures measured over pixels with the lowest flood potentials. Because of their low flood potential values, these pixels could not be covered by water under normal conditions. The topography of the PAD area is generally flat. Hence, the characteristics of the selected pixels should not be exceptional compared to the general conditions in the delta. The average of the AMSR-E measurements over these selected pixels during the summers of 2002 and 2003 provides an estimate of the PR_{nf} index. Following this analysis, an obtained value of $PR_{nf}=0.007$ seems to be a good approximation of the PR_{nf} index.

The third index of the flooded vegetation, PR_{fveg} , was also derived by using AMSR-E measurements over selected pixels. In this case, pixel selection was based on three criteria: 1) a LAI index higher than 2; this threshold was set in this work in order to classify the pixel as vegetated. The LAI index was derived from MODIS images; 2) a significant flood potential value; 3) in the case of the PAD, the incoming flow should be higher than $4000 \text{ m}^3/\text{s}$, which is the minimum needed to produce a significant flooding of the area (Beltaos, 2003). This calibration procedure provided an approximate value for $PR_{fveg}=0.1$. It is worth mentioning that the vegetation in the PAD is not dense enough to completely cover the contribution of the underlying flooded soil to the passive microwave signal. An additional effect caused by the dew covering the canopy could be added to the sensed passive microwave signal.

Finally, the WSF was estimated for each pixel of the AMSR-E image using a water body extent vector imported from the USGS database. This vector provides an estimate of the area of the permanent open water bodies, which included mainly lakes and rivers. Over the PAD area, the fraction of the permanent open water bodies is about 30%. By calibrating the different end-members of the mixing model, it is possible to apply the proposed methodology using AMSR-E 37 GHz passive microwave data and retrieve a daily estimate of the fraction of the flooded area over the PAD.

5.2.4 Development of the Rating Curve Model

Images of the Moderate-resolution Imaging Spectroradiometer Terra instrument (MODIS-Terra) were used in this work in order to estimate the water body extent over the PAD area. The first two channels of the MODIS sensors were used (channel 1: 620-670 nm and channel 2: 841-876 nm). The MODIS-Terra instrument is in a sun-synchronous orbit, and its images have been available since February 2000. The spatial resolution of the MODIS images at these frequencies is 250 m. The MODIS-Terra, with a daily global coverage, presents a better potential for flood monitoring and water body mapping due to its spatial resolution, which is higher than that of the NOAA-AVHRR sensor (1 km).

MODIS images were obtained from the NASA EOS Data Gateway Web site, in Hierarchical Data Format (HDF). The selected dataset was the MODIS/Terra Surface Reflectance Daily L2G Global 250m SIN Grid (MOD09GQK). Upon downloading the MODIS images, the MODIS Reprojection Tool (MRT), available free of charge at the LP DAAC Web site, (<http://lpdaac.usgs.gov/landdaac/tools/modis/index.asp>) was used to subset and reproject the area of study. The MRT output is an HDF file storing dataset of the selected area only. Using the MRT software is important as it allows a considerable reduction of the size of the original image files.

The images used were taken during the summers of 2002 and 2003, with only those that were cloud-free considered. The obtained images of the PAD area were classified separately for each band. To be retained, a pixel must be classified as water in both of these images. Hence, only common water pixels were considered. The fraction of the open water surface in the PAD area was estimated by dividing the area of all the classified water pixels by the total area of the selected region, which is equal to 3865 km². The WSF derived from MODIS images was computed using the ratio: Water surface area/Total PAD area.

WSF(MODIS) values derived from MODIS images were compared to discharge measurements taken at the Slave River site (59°52' N, 111°35' W). A rating curve was defined based on the relationship between discharge and WSF (Figure 28). The correlation coefficient of this relationship is equal to 0.75. We will use the terminology of rating curve model to indicate the relationship between discharge and WSF. The rating curve model will be written as:

$$WSF(t) = a.Q^b(t) \quad (5.9)$$

where WSF is the Water Surface Fraction, Q is the measured discharge and, a and b are two empirical parameters. The availability of discharge measurements enables the estimation of daily WSF over the PAD. The Slave River observation site was selected as it drains the entire PAD area, which implies a better relationship between the observed discharge and the temporal variability of the WSF. The developed relationship between discharge and WSF cannot easily be extrapolated to other sites in the Mackenzie River Basin. This relationship is affected by the topography of the area, its land use (vegetation cover, soil texture...) and the river morphology.

5.3 Results and Discussion

Simulations have been carried out using AMSR-E and MODIS images taken during the summers of 2002 and 2003 over the PAD area. The mixing model provided maps of flooded and non-flooded areas. Furthermore, a map of open water body fractions was estimated off-line. Figure 29 shows an example of the obtained spatial distribution of flooded area. In order to show the performance of the mixing model, these maps were developed over a larger area that includes the PAD area. Lakes were filtered out from the flooded and non-flooded maps. The developed maps agree with the topography of the area as they present higher values of flooded fractions (f_f) over pixels surrounding the Athabasca Lake and/or with low elevations, such as the northeastern area. However, this parameter shows low values over pixels, which are far from lakes and/or with high elevation.

It is worth mentioning that the flooded area parameter provided by the mixing model includes both wetlands and flooded vegetation effects. Consequently, some pixels can be presented as flooded by the model whereas they are only wet, i.e., a completely wet pixel may be presented as 20% flooded if these two states reproduce the same effects on the passive microwave data. The segregation between the wetness and flooding effects is not possible by the sole use of passive microwave data. Therefore, MODIS images were used in this study to achieve this objective.

Discharge observations were considered as proxies for WSF(MODIS) variations. The daily availability of discharge and passive microwave observations enables the daily estimation of the WSF(MODIS) and WSF(AMSR-E), and consequently, the calculation of the wetness index using Equation (5.2). Figures 30 and 31 show the variation of WI during the 2002 and 2003 summer seasons. The WI values were averaged on a weekly

basis over the entire PAD area. Because of the non-availability of AMSR-E data at the beginning of the summer of 2002, the results obtained using 2003 data seem to be more reliable in showing the index variability during this period. During 2003, the WI started to increase at the beginning of May. In fact, during this period, the melting snow provides a significant amount of water at/near the soil surface. Hence, the WI continues to increase as long as the snow continues to melt. Then, the WI decreases to maintain a constant stage, shown by Figures 30 and 31, until the end of July. Following this first stage, the WI index increases again at the beginning of August. However, this index does not reach the values seen during the spring melt period. The WI maintains this second stage until the month of October. Some fluctuations can be observed during the first and the second stages, which could be caused by the precipitation. Finally, the WI declines at the end of the autumn to reach a third and final stage. Beyond this phase, the soil surface is covered with snow, and the calibrated mixing model is no longer reliable since it was calibrated using snow-free images. As they come to an end, the two summer seasons, 2002 and 2003, show similar variabilities.

To allow a better understanding of the WI variability, this index was compared to the precipitation and temperature values (Figures 30 and 31). Measurements were taken at the RICHARDSON LO site, which is located in the PAD area (Latitude: 57°55' N, Longitude: 110°58' O, Altitude: 304.80 m). Temperatures were averaged on a weekly basis; precipitations were summed up on a weekly basis. During the week of 18/05/2003, the temperature over the PAD starts to increase. This increase causes the melting of additional quantities of snow. Consequently, the WI increases during this week. However, temperatures maintain almost the same stage during the month of June and July, during which the WI is almost stable. During these months, the temperature is maximal and the WI is minimal. By the end of July, temperatures start to decline, which reduces the evaporation flux. Hence, the WI increases again. However, this increase caused by the temperature recession is less significant than the first, observed at the beginning of the summer season when the soil surface is covered by snow. Although,

the temperature continues to decline, the WI index decreases until it reaches a given threshold, which presents a minimum of wetness that remains at/near the soil surface. This trend was assessed by determining the correlation coefficient between the WI and temperature gradient which is equal to the temperature of the present week minus that of the precedent week. A temperature increase would cause WI decrease. Estimated correlation coefficients using data of 2003 and 2002 are respectively -0.73 and -0.5. These values indicate that there is an actual inverse relationship between WI and temperature. The lower value of 2002 is due to the lack of data.

On the other hand, the precipitation effect seems not to be instantaneous as that described for the temperature. At the beginning of the summer season, the precipitation effect is less significant than that for the snow melting process, because the latter provides more water to the soil surface than the former. During the summer, when temperatures are higher and snow melting is over, precipitation has a greater effect on the variability of the WI. This effect depends on the temperature trend just before and after the rainfall event as discussed above. The effect of the precipitation is more significant when the temperature is decreasing. For example, rainfall events observed on 01/06 and 13/07/2003 present two different responses although they have similar total depths. The first occurs when the temperature is decreasing. Hence, the WI maintains almost the same value as the precipitation wetness remains at/near the soil surface. However, the second event occurs when the temperature is rising. The WI consequently shows an abrupt decrease. The index continues to decrease as long as the temperature is increasing, until the maximum is attained on 27/07, which is followed by a steady temperature decrease and WI increase.

It is important to compare the estimated WI index to the soil moisture measurements over the PAD area. However, soil moisture measurements are not available for the summers of 2002 and 2003. Therefore, the WI was compared to the measured soil

moisture at the McMillan site (Latitude: $63^{\circ} 14' N$; Longitude: $132^{\circ} 02' W$) during the summers of 1998, 1999 and 2000. Figure 32 shows that the measured soil moisture and the estimated WI present similar trends during a given summer. Correlation coefficients were calculated to assess the relationship between WI and measured soil moisture using values of 1998, 1999 and 2000. Obtained correlation coefficients are respectively equal to 0.62, 0.66 and 73. In fact, WI and soil moisture both increase at the beginning of the snowmelt period. Then, they decrease during the hottest period of June and July. Soil moisture increases again as does the WI at the beginning of August as a response to the temperature decrease and precipitation supply. The observed time lag between the soil moisture and WI maximum is probably due to the northern location of the site of the soil moisture observations. The wetness maximum occurs first at the PAD area because of the northward progress of the snowmelt effect. This implies that the developed WI can be considered as a surrogate of the soil moisture as it provides a qualitative estimate of this variable. Moreover, the availability of soil moisture measurements at the same location and period of the AMSR-E observation will enable the development of a predictive soil moisture model based on a regression relationship between the WI and the observed soil moisture. This will be covered in a future work.

5.4 Conclusion

The aim of this work was to provide an estimate of wetlands and flooded area fractions over a selected area of the Mackenzie River Basin. The fraction of the flooded area was derived using a calibrated mixing model, which was applied using AMSR-E passive microwave data. The vegetation shading effect was taken into account when applying the mixing model. The canopy density was estimated on a pixel-per-pixel basis using the LAI index provided by MODIS.

A rating curve model was developed to estimate the flooded area using observed discharge data. The rating curve model is based on an existing correlation between the flooded area and discharge observations. The flooded area used to develop the rating curve model was derived from MODIS images as this sensor is only sensitive to the amount of water over the soil surface (lakes, rivers and flooded bare soil). A wetness index was defined based on the difference of the wetness effect on the passive microwave and visible data.

This study has successfully demonstrated the ability of a combination of visible and passive microwave data to segregate wetness and flooded area effects. A satisfactory agreement was observed between the defined wetness index, precipitation, and temperature values. Between these two measurements, it is the temperature that has a dominant effect on the wetness index variation as it causes an instantaneous variation of the index. The non-significant dependence on the precipitation could be caused by the use of local precipitation measurements instead of spatial distributed data. In addition, the eventual difference between the satellite overpass and the rainfall occurrence can contribute to reduce the relationship between the computed WI and the precipitation measurements. In fact, the AMSR-E 37 GHz brightness temperatures are only sensitive to a few millimeters at the top of the soil surface, which can be rapidly drained after the rainfall event. The consideration of a perfect synchronism in the rating curve development and the constancy of model parameters can also affect the accuracy of the algorithm. However, the precipitation effect on the wetness index is more significant during the hottest periods, when the basin is the driest. Similar precipitation events have different effects on the WI, if they occur at different temperatures. In order to appreciate the performances of the proposed wetness index, the results obtained were compared to soil moisture measurements taken during different summer seasons. The wetness index trend was similar to that of the soil moisture measurements. This implies that the developed wetness index has successfully described the temporal variability of the soil moisture over the studied area.

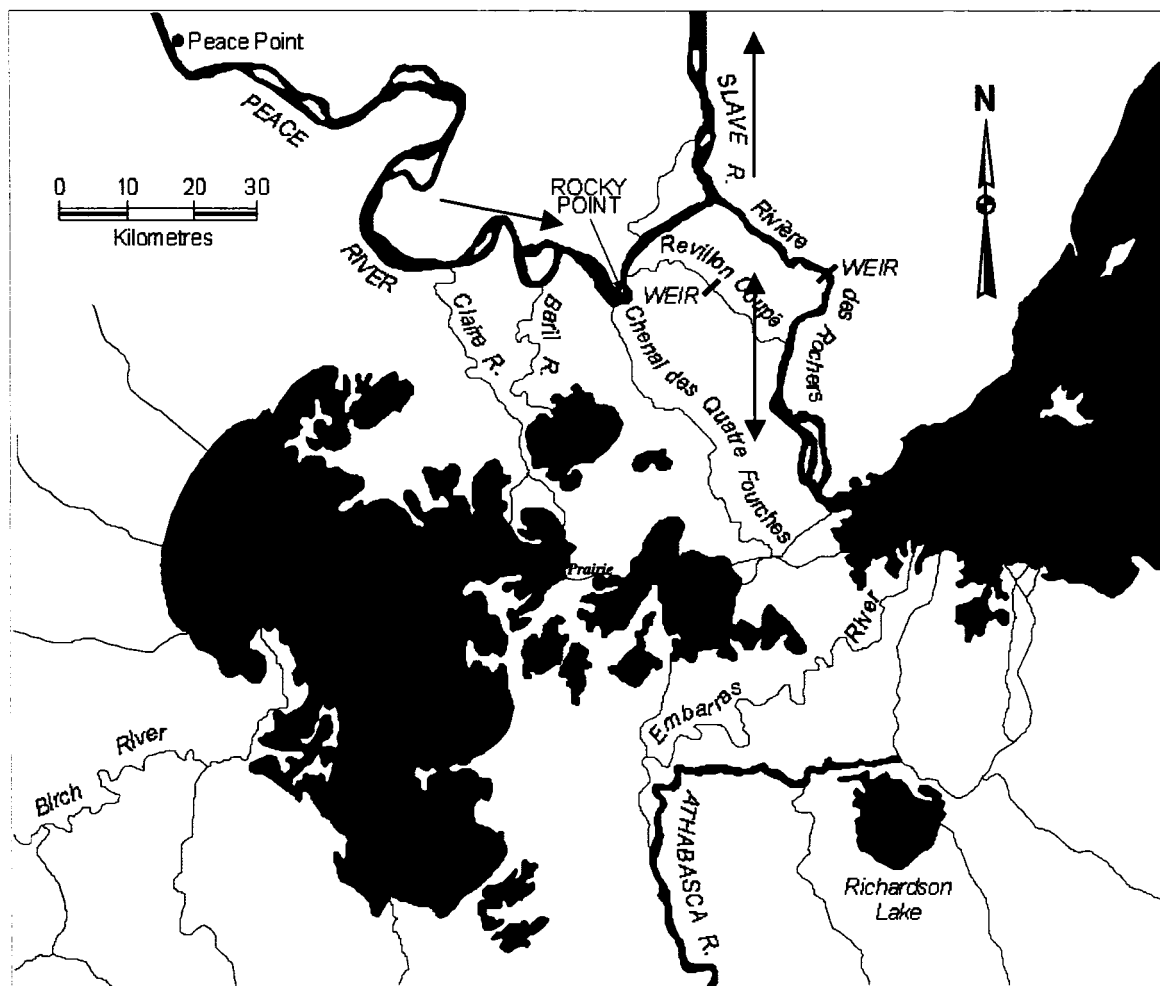


Figure 24 The Peace-Athabasca Delta, PAD

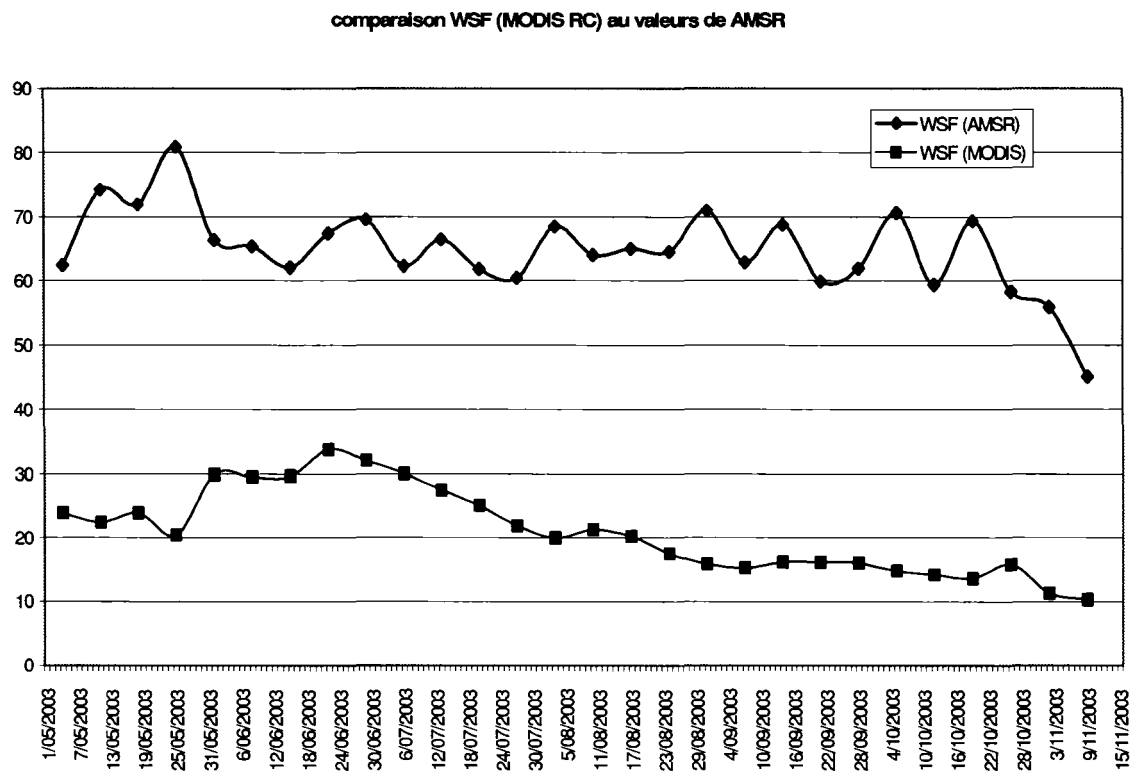


Figure 25 WSF(AMSR-E) and WSF(MODIS) temporal variability during the summer of 2003, over the PAD area

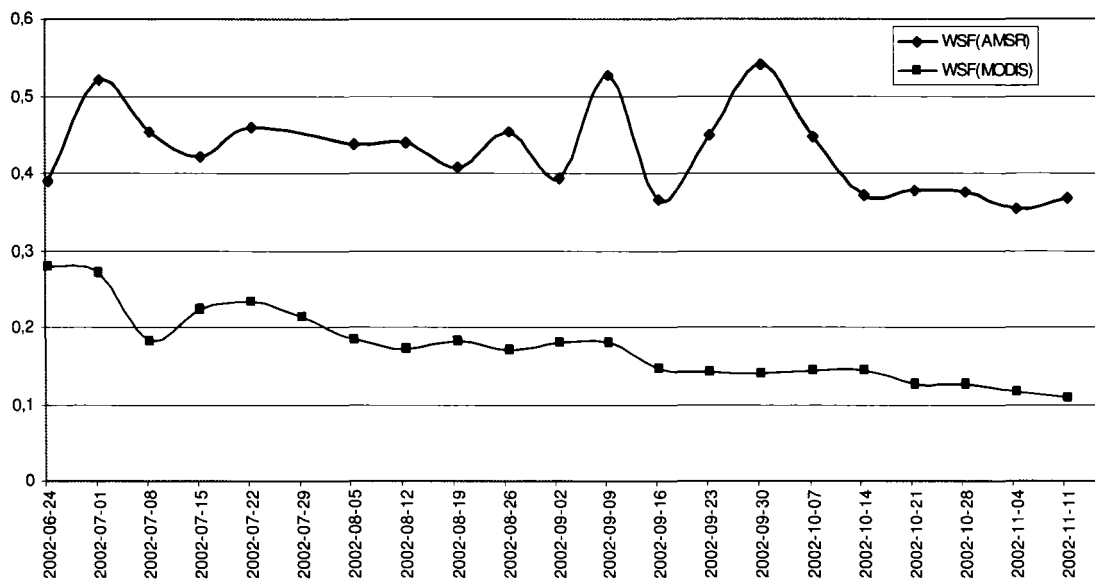


Figure 26 WSF(AMSR-E) and WSF(MODIS) temporal variability during the summer of 2002, over the PAD area

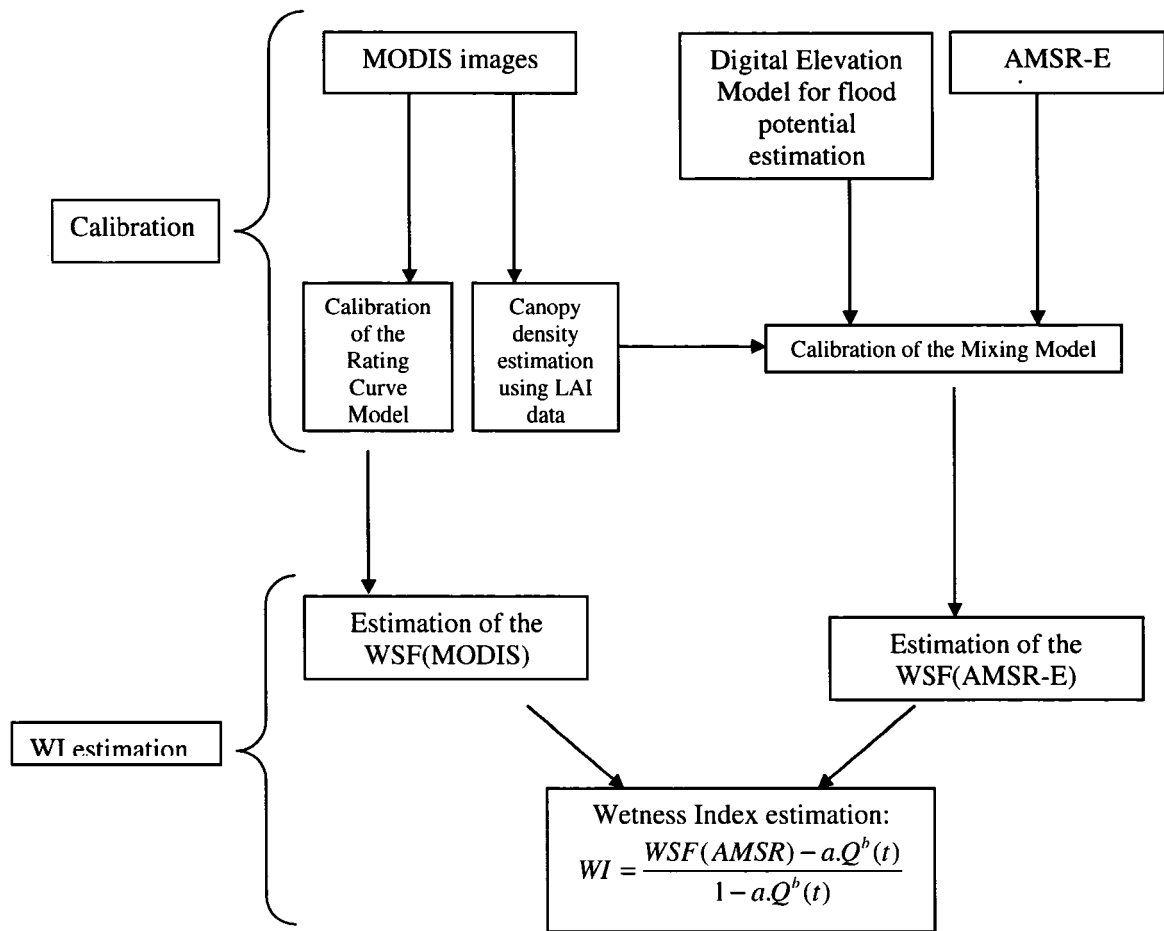


Figure 27 Flow-chart of the proposed algorithm

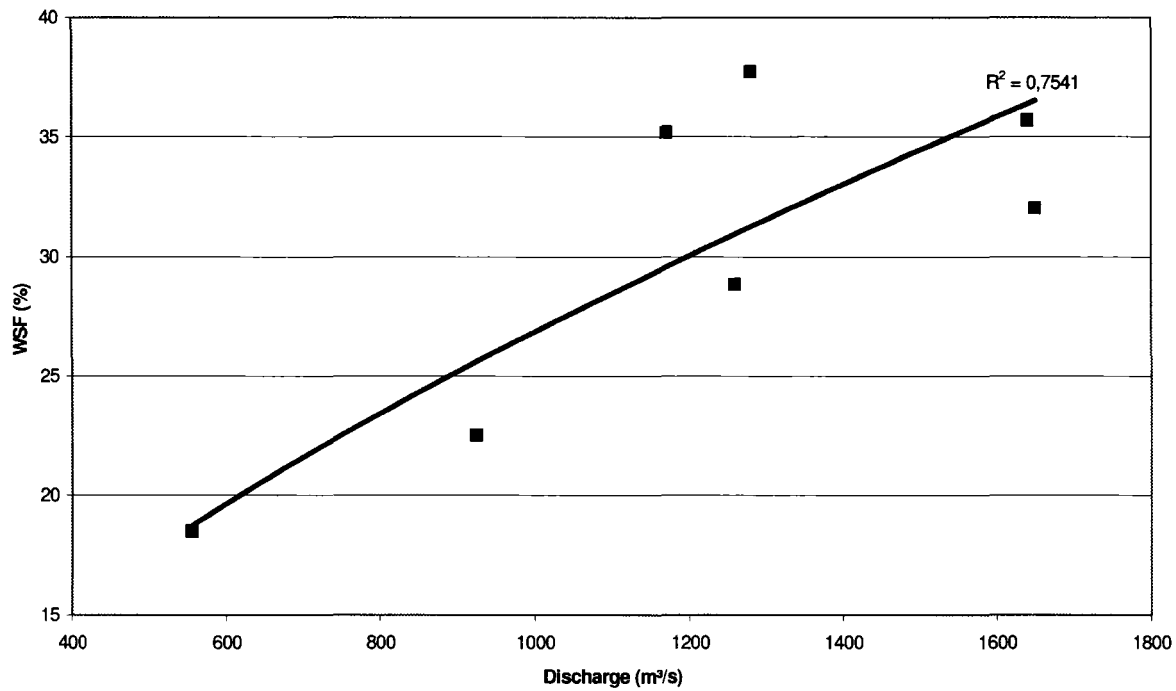


Figure 28 Rating Curve developed for the region of the PAD using 2002 and 2003 summer season MODIS images and discharge data

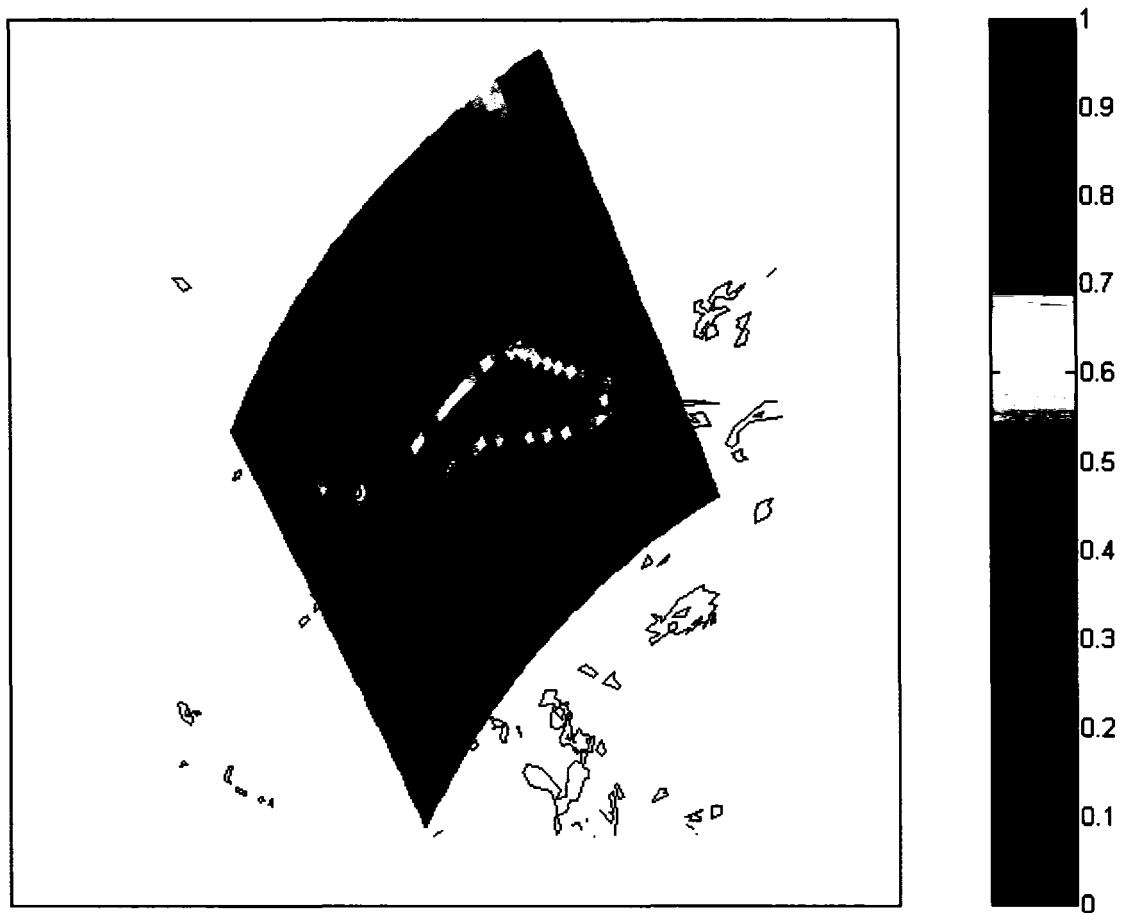


Figure 29 An example of flooded fraction map estimated over the PAD area on August 31, 2003

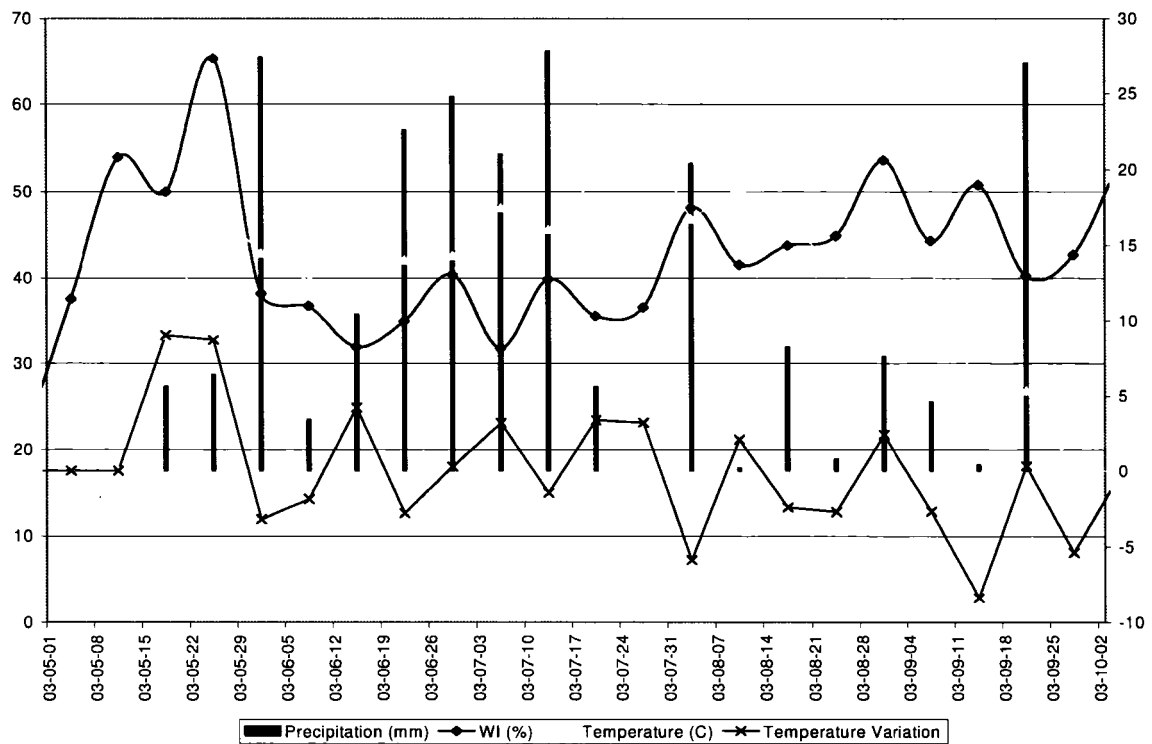


Figure 30 Temporal variability of the WI compared to the precipitation and temperature values observed during the summer of 2003

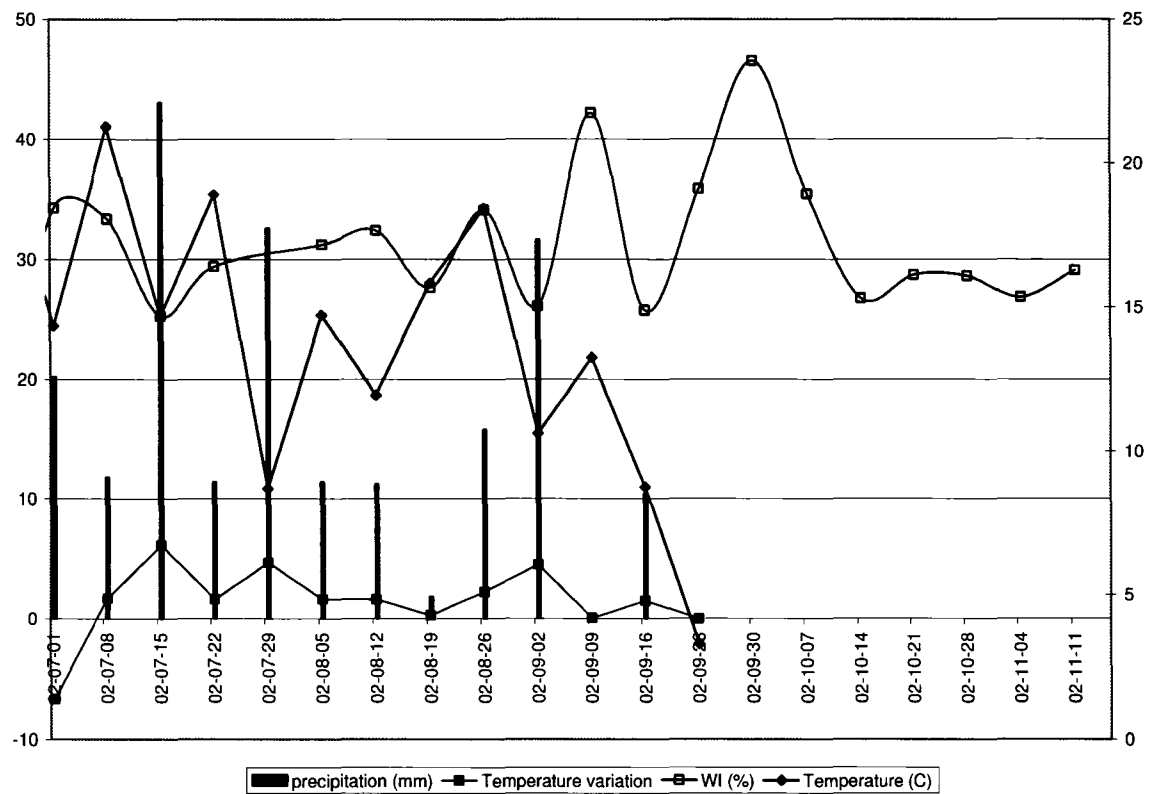


Figure 31 Temporal variability of the WI compared to the precipitation and temperature values observed during the summer of 2002

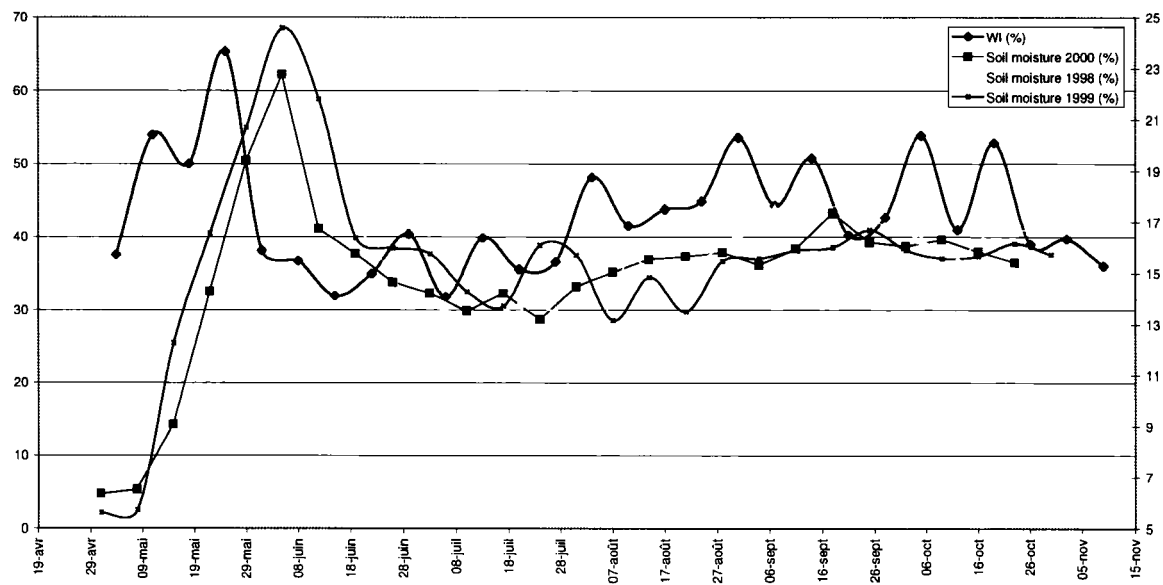


Figure 32 Temporal variability of the WI over the PAD compared to the measured soil moisture during the summer of 1998, 1999 and 2000.

CHAPITRE 6

A COMBINATION OF REMOTE SENSING DATA AND TOPOGRAPHIC ATTRIBUTES FOR THE SPATIAL AND TEMPORAL CONTROL OF THE SOIL WETNESS OVER THE MACKENZIE RIVER BASIN

Abstract

This work presents a methodology for the daily mapping of soil wetness over the Mackenzie River Basin. The approach is based on the use of a combination of passive microwave data from AMSR-E images and topographic attributes from a Digital Elevation Model. Classic wetness indices, which are defined exclusively using topographic attributes, are static and unable to catch the temporal variability of soil moisture. Other parameters, such as vegetation cover, have a significant effect on the spatial distribution of the soil water content over a basin. In this work, we propose to overcome the static behaviour of classic wetness indices by assessing the temporal variability of the soil water content using passive microwave data and by introducing the vegetation effect into a wetness index. The vegetation effect will be taken into account using a mosaic approach to segregate between bare and vegetated soils. AMSR-E 37 GHz will be used to assess the wetness of the entire basin. The proposed approach is an improvement in a dynamic sense of the classic topographic indices. The new dynamic wetness index will downscale the assessed wetness derived from passive microwave data and take into account the variability of the surface conditions in the basin. The basin is virtually wetted up or dried down depending on the values of the dynamic wetness index. The results obtained were compared to those derived from the classic index to assess the reliability of the dynamic index. The proposed index has provided a better estimation of the wetness over the basin. This implies that a combination of passive microwave data and topographic attributes has an interesting potential to improve the water balance closure over northern basins.

Keywords: Soil moisture; Topography; Passive microwave; Visible images; Downscaling.

6.1 Introduction

Soil moisture is a key parameter of the hydrological cycle. It controls the partitioning of rainfall into infiltration and runoff. However, this parameter exhibits significant variability in both space and time. Several approaches have been proposed in the literature to monitor the spatial and temporal variability of soil moisture. These approaches fall into one of the three following categories. First, remote sensing has been used because of the high sensitivity of the microwave frequencies to the amount of water at the soil surface (Jackson, 1993; Lakshmi, 1996; Njoku et al., 2003; Wigneron et al., 2003). Brightness temperatures measured at low frequencies (L band), were recommended for soil moisture retrieval since they minimize atmospheric and vegetation effects. The spatial and temporal coverage of the passive microwave sensors presents a significant advantage of this approach for frequently monitoring large basins. However, there are no satellite sensors operating at L band. Moreover, the low spatial resolution of the retrieved soil moisture maps makes the validation of the obtained results difficult.

Secondly, spatially distributed hydrological models have been used for modeling spatial and temporal variability of soil moisture (MacKay et al., 1998; Radeva & Ritchie, 2001). This approach provides an estimate of the amount of water near the soil surface. However, the use of this approach over large watersheds is not straightforward, as it needs a lot of data to calibrate and validate the hydrological model.

Finally, the third category is based on the use of Terrain-based Wetness Indices. Several indices have been proposed in the literature (Beven & Kirkby, 1979; Chaplot & Walter, 2003; Crave & Gascuel-Odoux, 1997; Gomez-Plaza et al., 2000; Romano & Palladino, 2002; Wilson et al., 2005). These indices provide a systematic spatial distribution of the soil wetness over a watershed. The change in soil moisture is controlled by two main factors 1/ the spatial variability of soil properties such as field capacity and hydraulic conductivity, which are related to soil texture. 2/ the topographic attributes such as the slope, the aspect, the distance to the stream bank, the elevation above the stream bank, etc. However, topographic attributes present a more significant effect on the spatial distribution of soil moisture. Chaplot and Walter (2003) stated that soil moisture at several depths is significantly correlated to the topographic attributes. They developed a non-linear predictive relationship based on the existing correlation between soil moisture and topographic attributes. A similar relationship based on the elevation difference between the data point and the flow pathway has been developed by Crave and Gascuel-Odoux (1997). The vegetation cover, the spatial distribution of the precipitation and the time since last rainfall can also influence the spatial pattern of the soil moisture over a watershed. The effect of each of these factors varies depending on the watershed features.

However, classic topography based wetness indices are static and will never capture the temporal variability of the soil water content. Most of the proposed indices in the literature do not explain more than 50% of the spatial distribution of the soil moisture (Western et al., 1999). These classic indices were developed according to the steady state assumption. This assumption is not realistic especially during a wet/dry transition period. This is one reason, among others, that explains the low ability of the wetness indices to predict the spatial distribution of soil moisture.

Moreover, these indices are generally based on the topographic attributes. However, several studies have demonstrated the major influence of the vegetation cover on the soil moisture spatial distribution (Gomez-Plaza et al., 2000; Gomez-Plaza et al., 2001; Qiu et al., 2001; Western et al., 2002). Hence, it is important that topographical indices take into account the vegetation cover in order to improve their prediction of the spatial distribution of the water content in catchments. This requires assessing the vegetation cover development. Ancillary data such as MODIS images can be used for a daily assessment of the vegetation cover.

The temporal and spatial coverage of satellite passive microwave sensors allows for daily soil moisture mapping. However, their low spatial resolution presents their main limitation. On the other hand, terrain-based wetness indices are derived from a digital elevation model which has a higher resolution compared to that of the passive microwave images. However, as mentioned above, these indices are static and cannot capture the temporal variability of soil moisture. Hence, the combination of remote sensing data and topographic attributes presents an interesting potential to monitor the spatial and temporal variation of the soil wetness over a watershed. It is expected that this combination will improve the low resolution of the passive microwave map and overcome the static behaviour of the developed wetness indices.

The objective of this work is to combine remote sensing data and topographic attributes to control spatial and temporal evolution of the wetness over the basin. This aim will be achieved through the use of Basin Wetness Index, BWI, derived from passive microwave data and a wetness index, WI, derived from topographical data. The availability of the passive microwave data enables a daily prediction of the spatial distribution of the soil water content.

6.2 Methodology

6.2.1 Area of study

The study case is the PAD area of the Mackenzie River Basin, of north-western Canada. The Peace Athabasca Delta (PAD) was selected as a control area to apply the proposed approach (Figure 33). The PAD is one of the largest inland deltas in the world. It has an area of about 4000 km². It is located at the western end of Lake Athabasca, and was created by the confluence of the Peace, Athabasca and Birch rivers. The Peace River has the largest discharge, with a mean annual flow at the Peace Point of 2100 m³/s. It generally flows in a northerly direction. However, this direction can be reversed when the water level in the Peace River exceeds that of Lake Athabasca (Leconte et al., 2001). Several wetland basins surround the delta (Toyra et al., 2002), and its central part is composed mainly of large and shallow lakes, which are connected to Lake Athabasca by several channels.

Over this northern area (the PAD) the climate is humid and precipitation generally exceeds evaporation except during a few weeks of the summer season (Strong et al., 2002). Therefore, the basin is generally considered as moisture sink. Over the Mackenzie River Basin, the difference between precipitation and evapotranspiration varies within a summer season. These humid conditions promote the dominance of the topographic attributes in the control of the basin wetness (Cosh et al., 2004; Kim & Barros, 2002; O'Loughlin, 1986)

6.2.2 The wetness index

The classic wetness index proposed by Beven and Kirkby (1979) was based on two parameters and is written as: $WI = \ln(a/\tan\beta)$, where a is the contributing area and $\tan\beta$ is the local slope of the terrain. Similar indices were proposed in the literature based on the use of topographic attributes other than a and $\tan\beta$ such as the elevation above the stream bank, the downslope gradient and the terrain curvature (Barling et al., 1994; Crave & Gascuel-Odoux, 1997; Wilson et al., 2005). Several topographic attributes have been considered because they influence the spatial distribution of the soil wetness over a basin differently. Their effect depends on the basin features. However, the classic WI proposed by Beven and Kirkby (1979) is the mostly used in the literature as it merely represents the wetness state as a function of the ratio of the drained area divided by the local slope.

The state of the basin, wet or dry, is very important to determine which factors dominate the spatial pattern of soil water content. The difference between precipitation and evaporation states whether the basin is wet or dry. Grayson et al. (1997) have identified two different sets of factors that influence the spatial pattern of soil water content. The first set of factors, such as slope, aspect and soil profile dominates under dry conditions and was denoted as local control. The second set of factors, such as the contributing area, prevails during wet conditions and was denoted as non-local control. Consequently, depending on the basin state, we are able to select the appropriate dominant parameters.

The classic wetness index does not take into account the effect of the surface heterogeneity within a pixel, on the spatial distribution of the wetness over a watershed. Qiu et al. (2001) concluded that the differences in vegetation resulting from different land use types can dominate the spatial distribution of the soil moisture. In addition, the

authors noted that, under certain conditions, the vegetation cover altered the distribution of the soil moisture at deeper layers more than at the soil surface. The vegetation transpiration of the soil water content depends on the root zone depth and on the vegetation type. Moreover, the shading effect of the vegetation reduces the evaporation effect at soil surface and fosters wet conditions. Hence, upper soil layers, which affect the passive microwave signal, seem to be wetter under dense vegetation. Bare soil areas are expected to be more exposed to solar radiation and therefore to have lower amounts of water in the upper soil layer. This effect is more present over south and west facing slopes where the solar radiation effect is maximal (Moore et al., 1988; Western et al., 1999). Moreover, Gomez-Plaza et al (2001) stated that the topographic attributes effect on the wetness state depends largely on the vegetation cover. In a vegetated area, factors such as soil depth and contributing area control the spatial distribution of the wetness. However, in the case of bare soil, other factors such as the slope have a more significant effect. The aspect which could be considered as a surrogate for evaporation has a similar effect for vegetated or bare soil conditions.

Gomez-Plaza et al. (2001) stated that several factors control the soil wetness of a vegetated area. The identified factors were classified by Grayson et al. (1997) as non-local control factors which prevail under wet conditions. A second set of factors that prevail in the case of bare soil was identified also by Gomez-Plaza et al. (2001). These factors were considered by Grayson et al. (1997) as local control factors which prevail under dry conditions. Consequently, factors which prevail under wet/dry conditions coincide with those controlling the soil water content in vegetated/bare area. These results are in accordance with the study of Qiu et al. (2001), mentioned above. Conclusions were similar in spite of the difference of climate for the studied watersheds which facilitates their extrapolation to the case of the Mackenzie River Basin. This accordance can be explained by the vegetation shading effect which reduces the evaporation of soil water content in the upper soil layers and fosters wet conditions and vice versa.

Therefore, we suggest modifying the static index by weighting its components using the vegetation canopy density to account for the variable effect of the vegetation which largely influence the spatial distribution of the soil moisture. According to the mosaic approach the pixel will be segregated in two different parts: a bare soil and a vegetated soil. The shading effect of the canopy tends to reduce solar radiation and therefore to decrease evaporation. Hence, a vegetated area is expected to be wetter than a bare ground. Under wet conditions, non-local control dominates. However, in the case of dry soil, the control is local. Consequently, the classic wetness index can be written as a combination of two parts based on the vegetation canopy density. These two parts, vegetated and bare soil, will affect the soil moisture distribution differently. The modified index will be written as a linear combination of topographic attributes:

$$WI = V \cdot \ln(a) + (1-V) \cdot \ln(1/\tan\beta) \quad (6.1)$$

V is the fractional vegetation cover which is estimated using the following relationship proposed by Eagleson (1982):

$$V = 1 - \exp(-\mu \cdot LAI) \quad (6.2)$$

where:

LAI is the Leaf Area Index and μ is the extinction coefficient. The value of μ varies depending on the canopy density between 0.35 (low vegetation density) to 0.7 (high vegetation density). In this work, a value of 0.4, which was recommended for crops, was assumed suitable as it reflects the vegetation characteristics of the PAD area.

The proposed index presents two components reflecting topographical attributes which are weighted by the vegetated and bare soil fractions within a pixel and reflects the

proportion of the local or non-local controls on the soil moisture distribution. The weight of the wetness index will be assessed on a pixel per pixel basis. This weight is the fraction of bare soil for the local control attributes and the fraction of vegetation cover for the non-local control attributes. The fraction V increases during the spring and summer to reflect the vegetation growth. This weighting approach allows taking into account the temporal variation of the land use and its influence on the soil moisture control.

The proposed approach is in accordance with the recommendation of Western et al. (1999) to use a combination of different wetness indices instead of using one terrain based index. We believe that such a combination should reflect the basin heterogeneity. In addition, this combination with variable weighting allows introducing a variable component in the index formula. By substituting the fractional vegetation cover in Equation 6.1 by Equation 6.2, we obtain the following formula of the wetness index:

$$WI = \ln(a) - \ln(a * \tan(\beta)) * e^{-\mu * LAI} \quad (6.3)$$

According to equation 6.3, the proposed WI is no longer static as the LAI values are variable with time. In addition, its formula accounts for the vegetation effect on the spatial distribution of soil moisture. The changing value of V which mirrors the vegetation development over the basin leads to variable WI maps and therefore to time varying estimates of the spatial distribution of the soil water content. This contributes to overcome the static behaviour of the classic wetness index. In addition, the temporal variability of the soil water content will also be taken into account by the variable Basin Wetness Index which will be used to (virtually) wet up or dry down the basin as will be seen next section. It is expected that the variation with time of the WI maps and BWI values will improve the prediction of the spatial distribution of the soil water content and

the spatial resolution of the soil moisture maps. Simulations will be carried out using the classic and modified formulas of the wetness index in order to assess the performance of the proposed wetness index.

6.2.3 Estimation of the basin wetness index, BWI, using passive microwave data

Passive microwave data are sensitive to the amount of water at/near soil surface. Several studies have been carried out to estimate the open water extent using passive microwave data (Basist et al., 2001; Fily et al., 2003; Tanaka et al., 2002). The fractional water extent estimated using passive microwave is a combination of water body area, flooded area and soil moisture. However, water surface fraction derived from visible images does not include the effect of soil wetness and provides exclusively an estimate of the extent of water bodies. Hence, critical information about the amount of water in the Mackenzie River Basin may be extracted from the difference between visible and passive microwave data.

The proposed methodology is based on three steps. Firstly, the 37 GHz passive microwave data will be used to estimate the Water Surface Fraction (WSF) on a pixel per pixel basis. The WSF will be estimated by applying a linear mixing model. The mixing model will be written as a linear combination of polarization indices characterizing open water, flooded and non-flooded areas. The mixing model is written as:

$$PR_{obs} = ow \cdot PR_{ow} + f \cdot PR_f + nf \cdot PR_{nf} + sm \cdot PR_{sm} \quad (6.4)$$

nf: non-flooded soil fraction

f: flooded soil fraction

ow: fraction of the permanent open water surface

sm: fraction of the soil moisture contribution to the observed PR

PRow, PRf, PRnf and PRsm are respectively the polarisation ratio, which is defined as ($PR = (T_{bv} - T_{bh}) / (T_{bv} + T_{bh})$), of the open water, flooded area, non-flooded area and wetlands. The entire amount of water, WSF(AMSR-E), at/near soil surface, which is sensed by the passive microwave sensor is the sum of the open water, flooded area and soil moisture fractions ($WSF(AMSR-E) = ow + f + sm$). Polarization indices will be estimated over each surface class to take into account the difference between their surface conditions. Three PR indices and the permanent open water extent were calibrated a priori. Time series of brightness temperatures were analyzed over each surface type and the average value was considered. The PRsm could not be calibrated as it depends on the amount of water in the soil layers, which varies in time. The soil moisture effect will not be considered in the mixing mode as it will be incorporated in the flooded fraction. However, the estimation of the weight of the soil moisture contribution is one of the aims of this study. This objective will be achieved by calculating the difference between the passive microwave and visible responses, which will be discussed later in this paper.

In a second step, open water extent will be estimated using a rating curve based on an existing relationship between discharge observations and flooded areas. Discharge measurements were taken at the salve river site ($59^{\circ}52' N$, $111^{\circ}35' W$). MODIS images were classified in order to estimate the open water extent. The spatial resolution of the MODIS sensor (250 m) has enabled us to obtain an accurate estimation of the water surface area. A rating curve model was developed based over the PAD area (Figure 34). The relationship was written as:

$$WSF(t) = a \cdot Q(t)^b \quad (6.5)$$

The WSF derived from the passive microwave data should overestimate the ones obtained using MODIS visible images since passive microwave data are sensitive to the amount of water at/near soil surface. However, MODIS images can only reflect the response of the open water extent over the surface. This suggests that information about the soil wetness can lie in the difference between the two sensors data. This difference can be defined as a Basin Wetness Index which can be computed as a third step according to the following relationship:

$$BWI = \frac{WSF(AMSR) - WSF(MODIS)}{1 - WSF(MODIS)} \quad (6.6)$$

where, $WSF(AMSR-E)$ is the Water Surface Fraction derived from AMSR-E data, $WSF(MODIS)$ is the Water Surface Fraction derived from MODIS data which presents the area of the open water bodies and flooded bare soil. This basin wetness index varies between 0 and 1. It presents the fraction of the wetlands within the non-flooded area. The basin wetness index is equal to zero when the non-flooded soil is completely dry. In this case, the $WSF(AMSR-E)$ should be equal to $WSF(MODIS)$. On the other hand, if the non-flooded soil is completely wet, the $WSF(AMSR-E)$ should be equal to 1 and consequently the wetness index is maximum ($BWI=1$).

However, the $WSF(MODIS)$ can be written as a function of discharge observations using the rating curve relationship developed in the previous section. The availability of AMSR-E data and discharge observations enables the estimation of a daily value of the developed basin wetness index, which otherwise could not be possible because cloud

free MODIS images are not available on a daily basis. Hence, the BWI can be written as:

$$BWI = \frac{WSF(AMSR) - a.Q^b(t)}{1 - a.Q^b(t)} \quad (6.7)$$

By substituting the WSF(MODIS) with the rating curve model we overcome the step of the WSF estimation using MODIS images. This step is not straightforward because of the unavailability of daily MODIS images free of clouds and covering the PAD area. The improved spatial resolution of the MODIS and AMSR-E sensors offers the possibility of an accurate retrieval of this wetness index. Moreover, the selection of the PR as a suitable polarization index for the WSF fraction estimation can improve the accuracy of the algorithm. A predictive relationship for the basin wetness index can therefore be developed using passive microwave data and discharge measurements. The availability of these data will enable us to monitor the wetness over the Mackenzie River Basin during several summer seasons.

The BWI reflects the fraction of saturated soils within the entire non-flooded area. On the other hand, the WI provides a map as a prediction of a systematic spatial organisation of soil moisture over the same non-flooded area. The idea is to downscale the BWI values estimated over the entire basin according the WI maps. According to the proposed approach the basin is wetted up by saturating (virtually) the pixel with the highest wetness index and vice versa. This approach leads to the development of a soil moisture map on the scale of the digital elevation model used to estimate the WI which is generally better than the spatial resolution of the passive microwave images. It is worth noting that the BWI derived from passive microwave data and MODIS images retrieves only the water content of the upper soil layers (only few millimetres). Hence,

the combination between the BWI and the WI will reflect only the spatial distribution of the soil water content in the upper layer.

6.3 Results and discussion

Simulations in this work are carried out in three steps. In the first step, the classic WI index and dynamic WI maps are estimated based on the topographical attributes and fractional vegetation cover. Since the dynamic WI depends on the vegetation cover, different WI maps will be developed. In the second step, the BWI which is based on the use of discharge observations and passive microwave data is tested and estimated. Finally, the dynamic WI is combined to the BWI in order to predict the spatial distribution of the soil water content.

6.3.1 Development of the WI maps

The digital elevation model of the PAD area has been imported from the USGS database. The DEM horizontal resolution is 1km. This resolution is compatible with PAD extent which is about 4000 km². In addition, the low resolution of the DEM do not affect the accuracy of the derived slope (Zhou & Liu, 2004). However, the contributing areas can be overestimated (Chaplot & Walter, 2003). Because of the non-availability of a DEM with a higher horizontal resolution covering the PAD area, it was assumed that the imported DEM is appropriate for preserving topographic features of the PAD. It is expected that this assumption will affect the accuracy of the results.

The topographical attributes (a: contributing area and $\tan(\beta)$: slope), used to calibrate the dynamic and classic WIs, were estimated using the terrain analysis model of the PCI

GEOMATICA software. The contributing area map is a matrix where each cell is assigned a value equal to the number of cells that flow into it. The slope angle (β) is in radians. The classic wetness index map was developed using the obtained topographical features. Figure 35 shows the resulting map. The WI values ranges between 4 and 16. Lakes were assigned a maximum value. The central part of the PAD, surrounding Mamawi Lake, presents a concentration of pixels with a relatively high value of the wetness index. The WI of pixels surrounding the Mamawi Lake decreases as the distance from the lake increases.

However, as mentioned above, the classic wetness is static and cannot capture the dynamic features of wetness pattern and/or the vegetation cover. Therefore, we suggested developing a dynamic WI map by taking into account the changing vegetation cover. The temporal variation of the vegetation cover affects the wetness control process and therefore the influence of the topographic attributes. This variability is explained by the varying weights of the proposed index of Equation 6.1. The vegetation cover fraction is the weight to be considered to segregate between the local and non-local control proportions. This weight will be estimated according to Equation 6.2 which is based on the LAI value. The LAI maps were derived from MODIS-Terra images. The variation of the LAI over the PAD area is significant during a summer season. Its values range from 1 to 3.6. According to the 2002 and 2003 MODIS images, the LAI shows a seasonal variability over the PAD. An average trend of the LAI over the PAD was derived based on the MODIS values and polynomial relationships were developed, on a pixel basis, to describe the variation of the LAI with time during the summer season. These relationships were used to develop daily maps of the vegetation coverage. Figure 36 presents an example of three maps of the vegetation fraction over each pixel developed for the first of June, July and August respectively. These maps show the rapid evolution of the vegetation density particularly at the beginning of the summer season, during the month of June. From July to August, the PAD presents a sustained high vegetation density since the LAI area reaches its maximum during this period of the year.

The variability of the vegetation cover was used to compute the dynamic wetness index. The daily values of the Weight V were derived from the developed maps in conjunction with the static topographic attributes. Hence, it is possible to develop WI maps on a daily basis. However, these maps were developed on the basis of a 7-day interval. As an example of the developed maps, Figure 37 presents the spatial distribution of the WI estimated for the first of June, July and August. The main conclusions that can be drawn from these maps are that the WI shows a significant seasonal variability when we consider the vegetation growth in its formula. Secondly, the wetness index decreases as the vegetation cover increases during the summer seasons. The WI decreases rapidly at the beginning of the summer season when the vegetation growth is fastest. Thirdly, the area surrounding Mamawi Lake presents a concentration of pixels with a relatively high WI as it was stated in the case of classic wetness index. At the beginning of the summer season, pixels with the highest values of WI are located between the Mamawi and Athabasca Lakes. The spatial distribution of WI changes during the summer season. At the end of the season, the spatial distributions of dynamic and classic wetness indices are similar. Hence, the consideration of the dynamic relationship is crucial at the beginning of the summer season to generate a realistic soil moisture map which takes into account the vegetation effect.

6.3.2 Estimation of the BWI

Simulations were carried out to estimate the BWI using AMSR-E and MODIS images taken during 2002 and 2003 summer seasons, over the PAD area. The mixing model provided maps of flooded and non-flooded areas. Furthermore, a map of the fraction of open water bodies was estimated off-line. Note that the flooded area parameter in the mixing model includes both wetlands and flooded vegetation effects. Consequently, some pixels can be identified as flooded by the model whereas they are only wet, i.e., a completely wet pixel may also correspond to 20% flooded if these two states reproduce

the same effects on the passive microwave data. The segregation between the wetness and flooding effects is not possible by the sole use of passive microwave data. MODIS images were used in this study to separate the two effects.

To allow for a better understanding of the causes behind the BWI variability, the index was compared to the precipitation and temperature measurements taken at a meteorological stations located in the PAD area (Latitude: 57°55' N, Longitude: 110°58' O, Altitude: 304.80 m) (Figures 38 and 39). Temperatures were averaged on a weekly basis; precipitations were summed up on a weekly basis.

As air temperature in the PAD starts to increase, snow melt is accelerated, which results in a significant rise of the BWI. This is followed by levelling of air temperature during the months of June and July, during which the WI is approximately stable. During these months, air temperature is maximal and BWI is minimal. By the end of July, temperatures start to decline reducing evaporation. This is accompanied by another increase of the BWI, which is, however, less significant than the one observed at the beginning of the summer season when snow melting occurs. With a further decline of air temperature, the BWI starts to decrease until it reaches a threshold corresponding to a minimum of wetness that remains at/near the soil surface.

On the other hand, the precipitation effect is not as obvious as that described for the temperature. At the beginning of the summer season, the precipitation effect is less significant than that for the snow melting effect, because the latter provides more water to the soil surface than the former. During the summer, when temperatures are higher and snow melting is over, precipitation has a greater effect on the variability of the BWI. The BWI response following a rainfall event is more significant when air temperature is decreasing. A rising air temperature attenuates the WI increase after rainfall.

It was not possible to directly compare the estimated BWI to soil moisture measurements in the PAD area, as no measurements were available at the site. In an attempt to unravel possible linkages between BWI and soil moisture, the BWI was therefore compared to measured soil moisture at a site located away from the PAD, at the following coordinates to the north (Latitude: $63^{\circ} 14' N$; Longitude: $132^{\circ} 02' W$). As measurements were available for the summers of 1998, 1999 and 2000 and not 2002 and 2003, the comparison in Figure 40 is merely qualitative. Despite limitation, it is observed that the measured soil moisture and the estimated BWI present similar trends during the summer season. They both increase at the beginning of the snowmelt period. They decrease during the hottest period of June and July. Soil moisture and BWI increase again at the beginning of August as a response to air temperature decrease and precipitation increase. The observed time lag between the soil moisture and BWI maximum is perhaps due to the northern location of the site of the soil moisture observations. It is hypothesized that the maximum of wetness occurs first in the PAD area because snowmelt effect is delayed northward. This implies that the developed BWI may be considered as a surrogate to soil moisture as it provides a qualitative estimate of this variable. Therefore, the availability of soil moisture measurements at the same location and period of the AMSR-E observation should allow for the development of a predictive soil moisture model based on a regression relationship between the WI and the observed soil moisture. This will be covered in a future work.

6.3.3 Combination of the WI and the BWI

Soil wetness estimation is possible using a combination of the BWI and the dynamic WI. The WI will provide information about the spatial organisation of the soil wetness, whereas BWI will determine the temporal variability of soil wetness. Hence, the basin is wetted or dried according to the variations with time of the area averaged BWI. Pixels

with the highest WI are wetted up/dried down first. Hence, the high spatial resolution of the soil wetness can be predicted for each low spatial resolution of BWI. The proposed approach allows, therefore, for a downscaling of the daily value of the BWI based on the WI map which indicates the priority of each pixel to either be wetted up or dried down depending on the BWI fluctuations. For example, if the BWI is equal to 50%, half of the pixels in the non-flooded area which have the highest values of WI are considered humid. In addition, if two pixels present an equal WI, priority will be given to the one with the highest/lowest elevation when wetting up/drying down the basin.

The result will be considered as a prediction of the spatial distribution of soil water content over the studied area. It is worth mentioning that the temporal variation of the surface condition is not solely explained by the BWI. The vegetation growth is also taken into account by the changing weighting of the modified WI. Therefore, the developed wetness maps will vary through the summer season with respect to basin wetness and vegetation density and its spatial distribution. For example, if the PAD area is 40% wet (i.e. BWI=40%) at the beginning and at the end of the summer season, the developed maps showing the spatial distribution of soil moisture in the basin will present some differences as the WI maps are different. It is more realistic to observe a difference between the developed maps as the surface conditions change in time. Consequently, the changing surface conditions will mirror the variability of the spatial distribution of soil moisture. This is an improvement in a dynamic sense of the classic wetness indices which are static and provide similar maps over various landuse conditions.

Ladson & Moore (1992) used passive microwave data and topographic attributes. The authors compared the spatial pattern of the emissivity, derived from passive microwave data to the predicted spatial distribution of soil moisture using digital elevation model. Our study is an improvement of Ladson & Moore's (1992) work as it combines both passive microwave and topographic attributes to predict the spatial distribution of soil

water content. Moreover, vegetation growth and its influence on the soil water content were taken into account in the proposed approach. In addition, the proposed methodology provides a daily estimate of soil wetness based on the use of a simple algorithm and available discharge observations and passive microwave images which are needed to calculate the BWI. Soil wetness can therefore be estimated using the simple BWI as a surrogate of soil moisture, instead of using a radiative transfer model, which needs to be calibrated, as it was done by (Pellenq et al., 2003).

The results obtained from the downscaling of the BWI were compared to the observed precipitation at the Prairie River and Fort Chipewyan A stations of the PAD area which are located at (Latitude: 58° 37' N; Longitude: 111° 40' W) and (Latitude: 58° 46' N; Longitude: 111° 7' W) respectively (Figure 33). The basin was wetted up/dried down according to the described approach and only the pixel that corresponds to the Prairie River station was considered to analyse the correlation with precipitation observations. Two possible values can be assigned to a given pixel: 1 if the pixel is considered as wet or 0 if it is dry. In order to take into account the geo-location error, the WI values were averaged over 9 pixels (a window of 3x3 pixels) surrounding the station. Correlation coefficients were determined between the observed meteorological parameter and the average of wetness values of pixels within the selected window. The results are presented in Table II.

Precipitations observed during summers of 2002 and 2003 were used to analyse the correlation with the wetness values. Analysis was carried out by considering either a synchronous time series (time lag =0) or 1 week (time lag = 1 week) lagged observations. At the Prairie River site, when a 1 week time lag was considered between precipitation and wetness values, the correlation coefficients were more significant compared to those obtained with non-lagged observations. The time lag effect was observed with the modified as well as with the classic wetness indices during both

summer periods of 2002 and 2003. However, at the Fort Chipewyan A station, the correlation was more significant with a time lag equal to zero. This result was expected regarding the WI values over the Prairie River and Fort Chipewyan A stations. A lower WI value over the Fort Chipewyan station leads to a quick drainage and therefore a low correlation between estimated wetness and 1 week lagged precipitation observations. On the other hand, the Prairie River station presents a higher WI which implies a higher wetness potential. Consequently, the Prairie River will drain surrounding pixels, if we consider a 1 week time lag, which increases its wetness and its correlation with the precipitation variability.

Furthermore, satisfactory results were obtained with the modified WI compared to that provided by the classic WI. Over the Prairie River station, the mean correlation coefficient of wetness values provided by the modified WI is 0.54 which exceeds that of 0.32 obtained using the classic WI. Over Fort Chipewyan A station, the modified WI also provided a better agreement between observed precipitation and estimated soil wetness. Hence, the modified WI is a better surrogate for soil moisture as it provides a better correlation with precipitation values. It is expected that the correlation between the estimated wetness and soil moisture measurements will be better than that of the precipitation observations as the developed approach is based on the steady state assumption which is not compatible with the temporal variability of the precipitation. The developed wetness maps should fulfill the steady state condition and not necessarily reflect the spatial distribution of the precipitation. The results of this study are, therefore, an improvement of the static indices reliability as most of the proposed indices in the literature do not explain more than 50% of the spatial distribution of the soil moisture (Western et al., 1999).

The proposed approach can be generalized over the entire Mackenzie River Basin. Similar rating curve relationships should be calibrated over different locations of the

MRB to allow the monitoring of surface water extent over the entire basin. The BWI would therefore be estimated over the entire MRB. On the other hand, an improvement of the DEM horizontal resolution will certainly increase the accuracy of the proposed approach as it will provide a more accurate estimate of the topographical attributes of the PAD area (contributing area and local slope).

Satisfactory results were obtained using the available DEM of 1 km as spatial resolution. However, it would be worthwhile to test the potential of this approach using a DEM that presents a higher spatial resolution. In addition, the reliability of the downscaling approach was assessed using precipitation and temperature observations because of the unavailability of soil moisture measurements over this area. The lack of soil moisture measurements can possibly be overcome by using simulated values derived from a hydrological model. The use of high definition DEM to improve the spatial resolution and of a hydrological model to generate spatially distributed soil moisture values will be the aim of future work.

6.4 Conclusion

The aim of this study was to provide an estimate of soil wetness using satellite data and topographic attributes. The approach was tested over the Peace Athabasca Delta (PAD) located within the Mackenzie River Basin. Passive microwave AMSR-E 37 GHz data and MODIS images were used to determine a basin wetness index (BWI). Passive microwave data are sensitive to the amount of water at/near soil surface. However, visible MODIS images can only detect the open flooded areas and permanent water bodies such as lakes and rivers. The BWI was based on the difference between passive microwave and visible responses. This index presented a satisfactory agreement with observed precipitations and temperatures. However, it can only reflect a spatially

averaged soil wetness value over the entire studied area. Therefore, topographic attributes were used to downscale the BWI values. A Digital Elevation Model was used to determine a wetness index (WI) over the studied area on a pixel per pixel basis. The developed WI takes into account the vegetation development and its effect on the spatial distribution of soil moisture. The PAD area was virtually wetted up and dried down according to the BWI with respect to the WI values derived from the DEM data. Pixel with the highest wetness index will saturate first. This approach allows a daily mapping of soil wetness over the PAD. Because the soil moisture measurements are scarce to non-existent over the Mackenzie River Basin, the reliability of the approach was assessed by comparing the estimated wetness values to the observed precipitation. The use of soil moisture maps generated by a hydrological model can also be explored to assess the reliability of the proposed approach. The estimated soil wetness using the modified WI showed a satisfactory agreement with the observed precipitations over two stations of the PAD. A better agreement was observed when the WI value of the station site was higher. Correlations between precipitation and wetness were more significant when a 1 week time lag was considered over the station displaying high WI values. This implies that the proposed approach allows a qualitative monitoring of the soil moisture over the PAD area. The improvement of the spatial resolution of the DEM should increase the accuracy of the proposed approach.

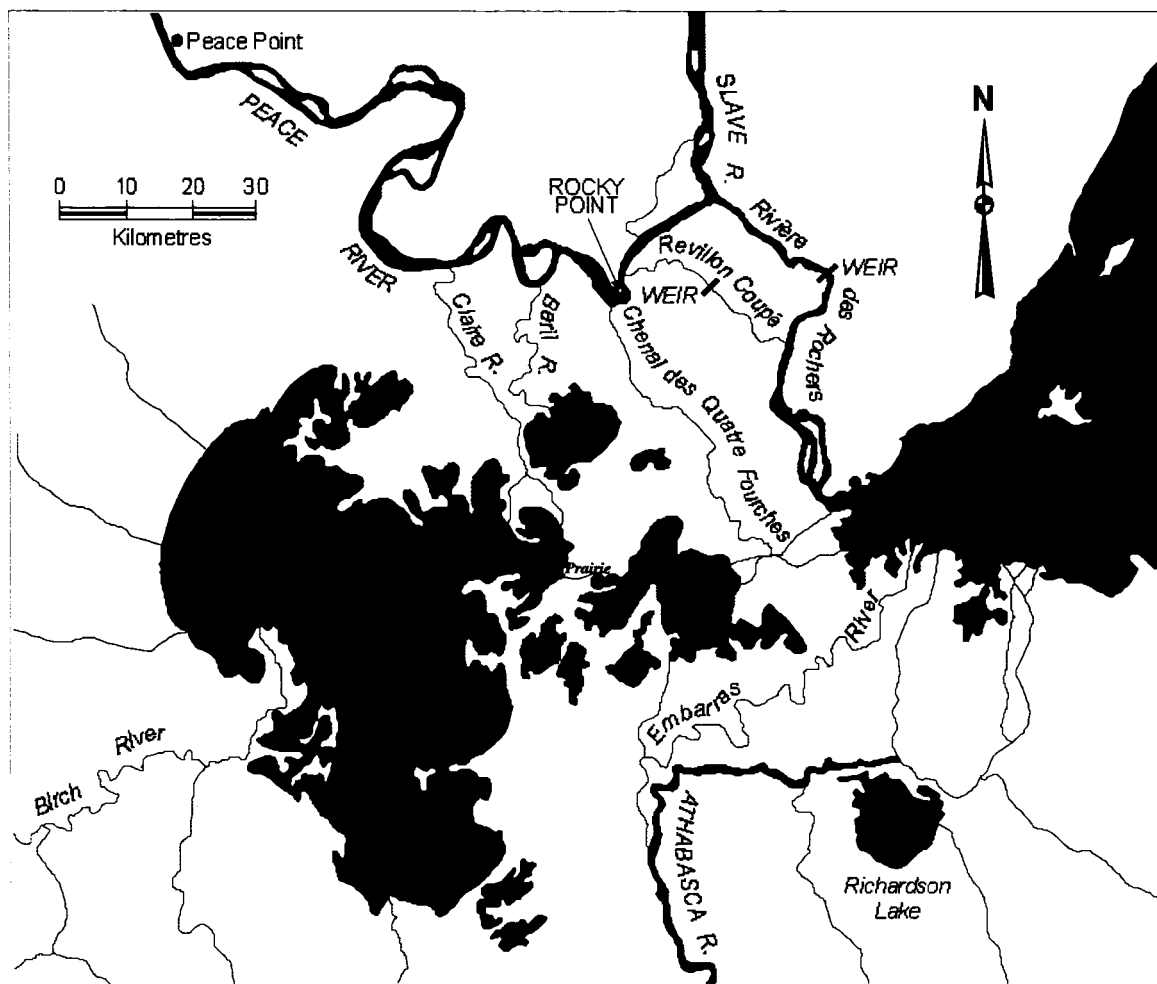


Figure 33 The PAD area (Leconte et al., 2001)

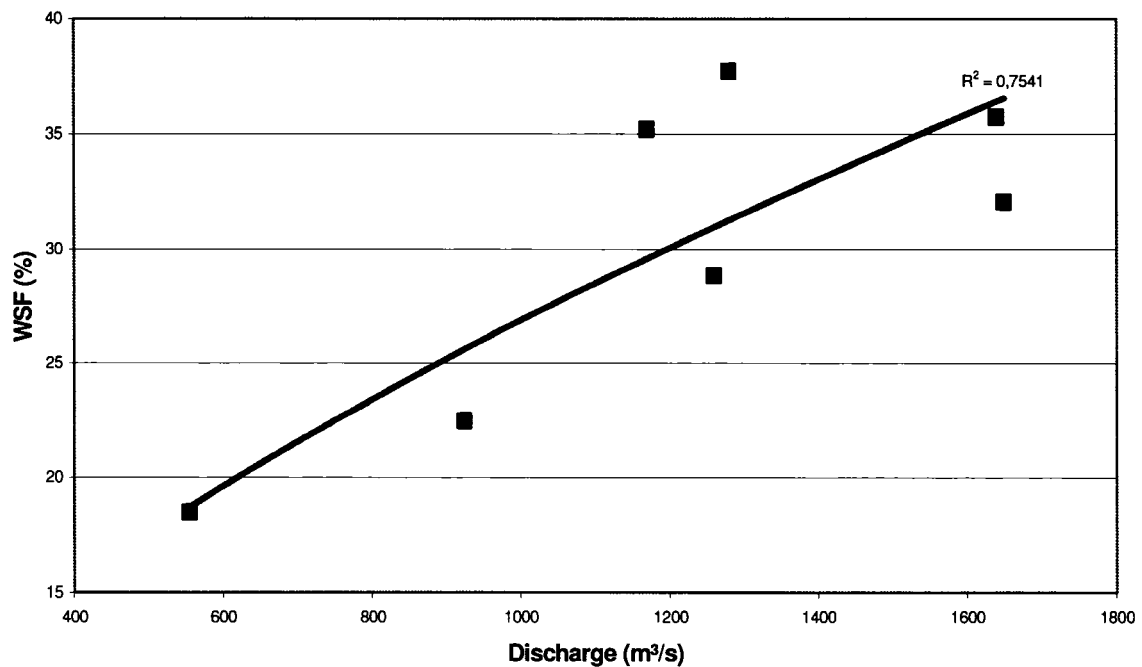


Figure 34 Rating Curve developed for the region of the PAD using 2002 and 2003 summer season MODIS images and discharge data

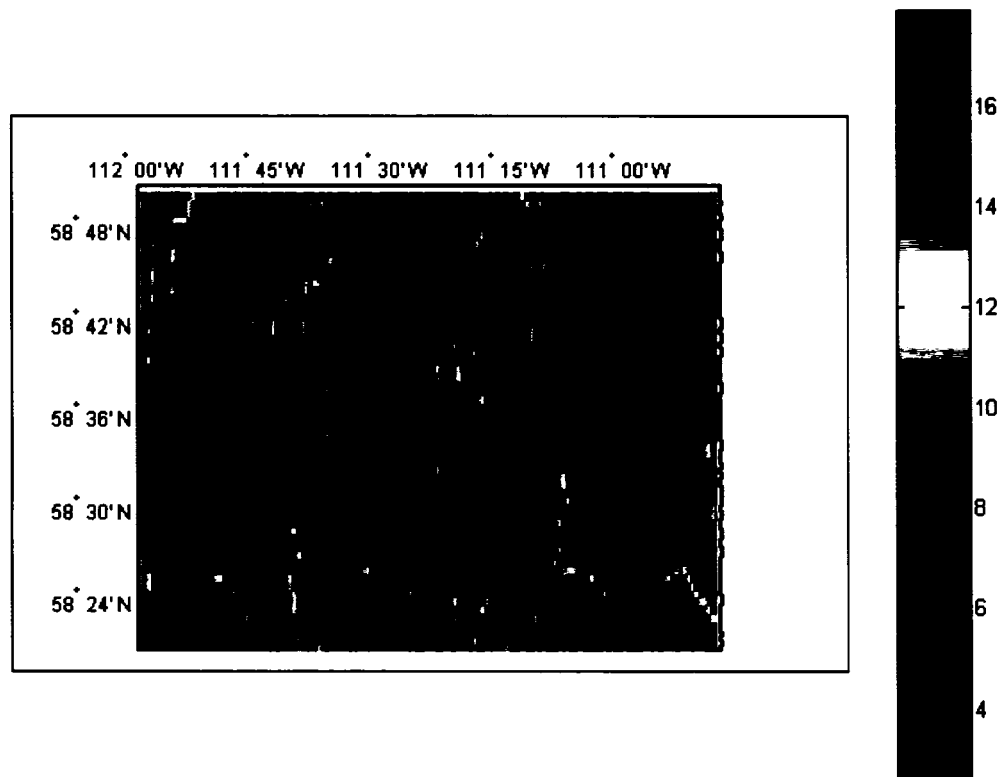
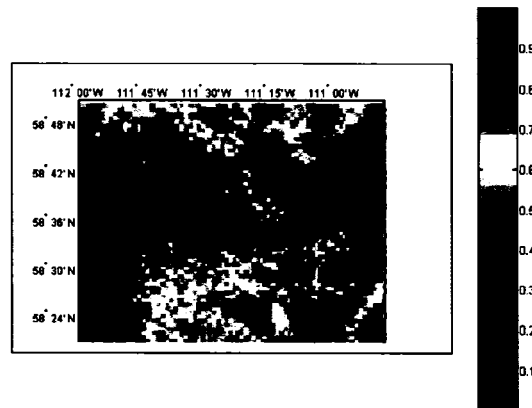
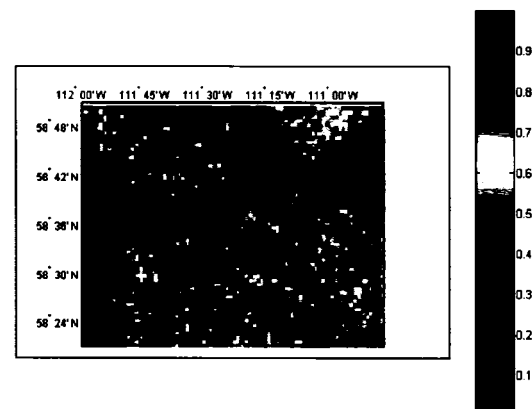


Figure 35 The spatial distribution of the classic WI

01/06



01/07



01/08

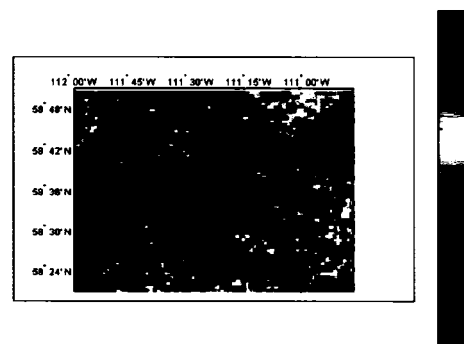


Figure 36

An example of variation of the vegetal cover fraction (V) over the PAD area during a summer season

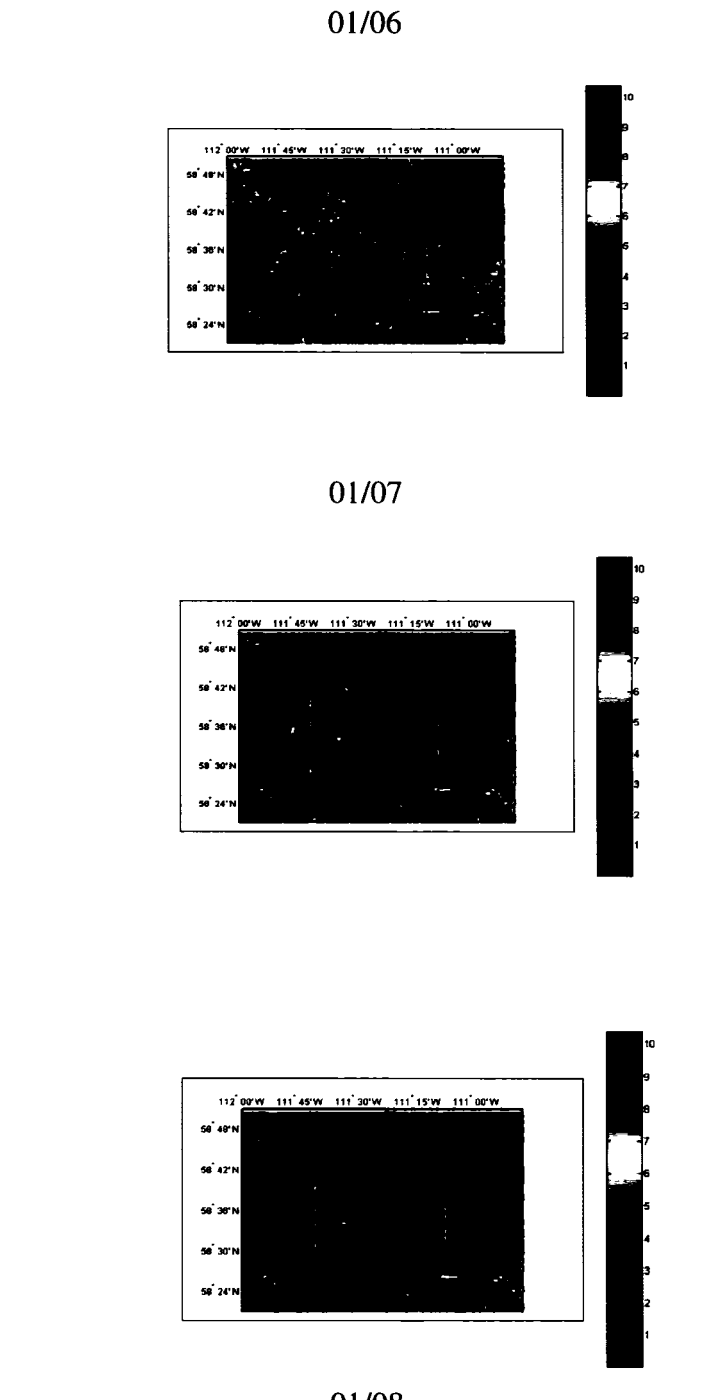


Figure 37 Seasonal variability of the dynamic WI

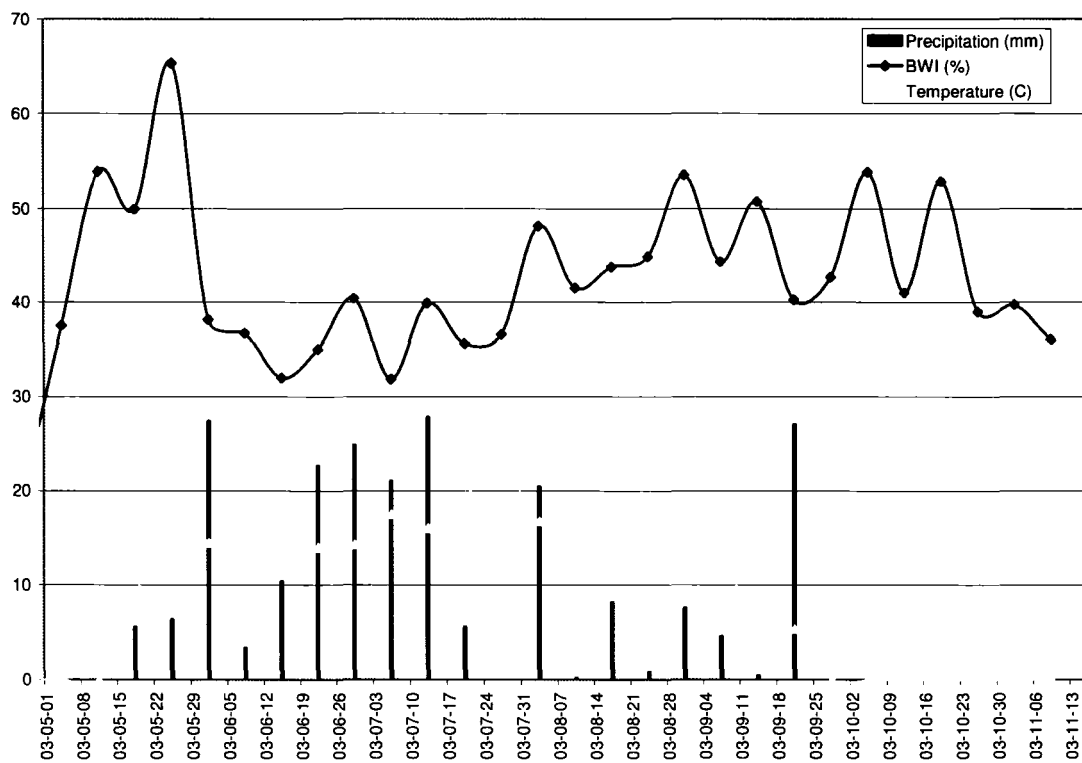


Figure 38 Temporal variability of the BWI compared to the precipitation and temperature values observed during the summer of 2003

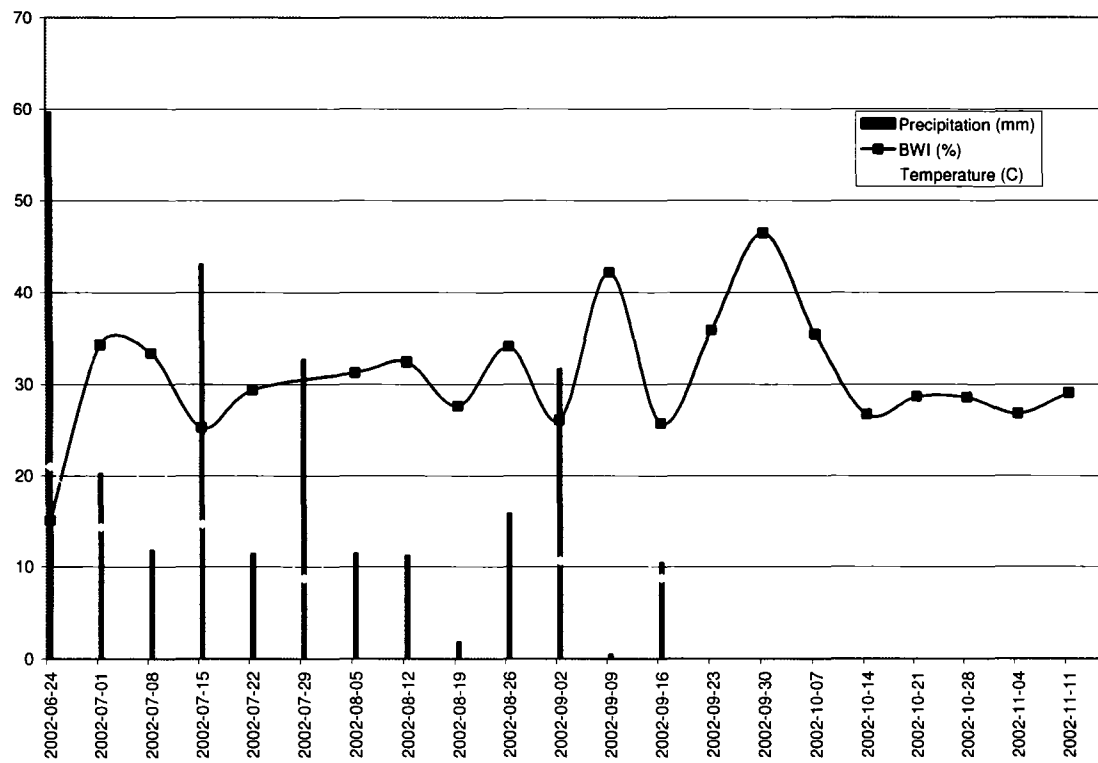


Figure 39 Temporal variability of the BWI compared to the precipitation and temperature values observed during the summer of 2002

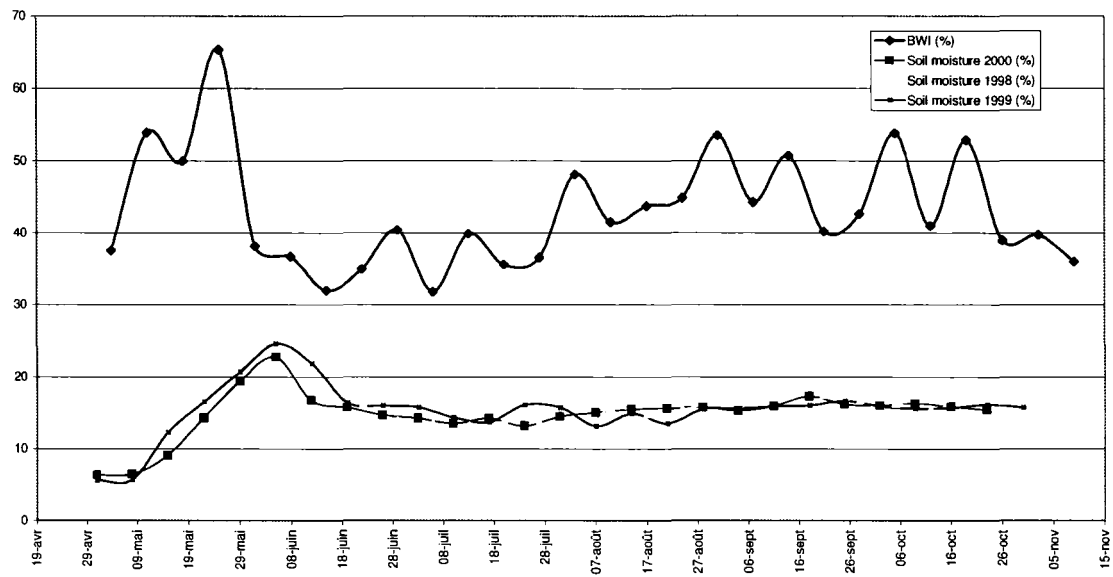


Figure 40 Temporal variability of the WI over the PAD compared to the measured soil moisture during the summer of 1998, 1999 and 2000.

Table II

Average of the correlation coefficients between precipitation observations and estimated soil wetness during the summer of 2002 and 2003

	FORT CHIPEWYAN A		PRAIRIE RIVER	
	0 lag	1 week lag	0 lag	1 week lag
Dynamic WI	0.49651386	0.25543928	0.15030912	0.54143954
Classic WI	0.37035134	0.13579415	0.1432659	0.32238724

CHAPITRE 7

ANALYSE ET DISCUSSION

7.1 Contribution de la thèse

La considération de l'évolution spatio-temporelle des conditions à la surface du bassin dans l'estimation de l'humidité du sol est au cœur de la contribution de cette recherche. L'ajustement des paramètres caractérisant la surface du sol a été recommandé pour une meilleure estimation de l'humidité du sol. Compte tenu de la large étendue du bassin du Mackenzie, un intérêt plus particulier a été réservé au cours de cette thèse aux approches globales. Ces approches, tel que discuté dans le deuxième chapitre, se basent sur la corrélation qui existe entre l'humidité du sol et un indice d'humidité qui est généralement une combinaison linéaire des températures de brillance mesurées à différentes fréquences et polarisations. Le caractère global de ces approches découle premièrement de la résolution spatiale des images utilisées dans le calcul des paramètres d'humidité (BWI, WSF, WI ..etc.) et deuxièmement de la considération non détaillée du processus de transfert radiatif qui n'exige pas de modéliser les effets du couvert végétal, de la rugosité et de l'atmosphère. Selon la première hypothèse de ce travail, l'effet de l'humidité et des plans d'eau demeure dominant malgré la présence d'un bruit causé par les facteurs cités. Ces approches globales expriment donc cette dominance à travers des équations simples qui font la définition des indices d'humidité.

L'application présentée dans le troisième chapitre s'inscrit dans le cadre de cette catégorie d'approches globales. L'indice d'humidité considéré dans cette application a été proposé par Basist et al. (1998). Le 'Basin Wetness Index' (BWI) selon sa formulation classique proposée par (Basist et al., 1998) fait appel à des paramètres constants dans le temps et dans l'espace. Dans la première partie du travail, les

paramètres du BWI ont été réajustés à la réception de chaque nouvelle image et d'un pixel à l'autre dans la même image. Cette démarche a permis de déceler une répétitivité saisonnière de la tendance des paramètres de l'indice. Cette répétitivité reflète l'effet des conditions des surfaces, notamment celui de la végétation qui présente un développement cyclique d'une saison à l'autre. Des fluctuations des paramètres empiriques de l'indice ont été également observées. Ces fluctuations peuvent être expliquées par l'effet de l'atmosphère sur les températures de brillance mesurées. Deux effets sont donc à distinguer en examinant la variabilité temporelle des paramètres empiriques, à savoir, l'effet de la végétation qui suit une tendance saisonnière et celui de l'atmosphère qui est plutôt instantané. Il faut distinguer à ce niveau entre l'effet de ces facteurs sur les paramètres empiriques d'une part et sur le BWI d'autre part. En fait, le second représente plus la réponse à la variation des conditions d'humidité suite à une pluie par exemple. Malgré que ces deux facteurs affectent implicitement le BWI, la contribution de l'humidité du sol et des plans d'eau dans le pixel observé aux variations de ce dernier demeure prépondérante. Cette hypothèse a été validée par la corrélation significative qui a été trouvée entre les fraction des plans d'eau (communément appelée dans les articles de ce travail : FWS) estimées à partir des températures de brillance mesurées et les variables hydrologiques et météorologiques observées. Cette corrélation a été exploitée dans le deuxième travail (Chapitre 4) pour développer une approche pour le suivi de l'évolution des plans d'eau à partir des mesures en micro-ondes passives.

La méthodologie présentée dans le chapitre 4 s'est basée sur la corrélation entre l'évolution des plans d'eau et le débit observé. La méthodologie a été appliquée aux deltas du fleuve Mackenzie (MRD) et des rivières de la Paix et de l'Athabasca (PAD). En fait, la fonte de la neige qui s'accumule au cours de l'hiver engendre annuellement des inondations dans ses deltas dont la magnitude varie d'une saison à l'autre. Des accumulations exceptionnelles de la neige devraient causer des inondations importantes notamment si la fonte de la neige s'accompagne par des précipitations significatives. Les volumes d'eau disponibles dans les régions deltaïques se drainent par la rivière des

Esclaves vers le grand lac des Esclaves dans le cas du PAD et vers la mer de Beaufort dans le cas du delta de Mackenzie. Par ailleurs, l'eau disponible dans le delta provient également des apports externes. Dans le cas du PAD, les apports sont principalement ceux de la rivière de la Paix et la rivière Athabasca. Ces derniers ramènent les eaux de fonte de la neige des régions qui sont plus au sud du bassin versant du Mackenzie. Ainsi, les deltas servent comme zones tampons dans lesquelles l'eau est retenue temporairement, avant qu'elle soit drainée par la rivière des Esclaves. L'étendue des plans d'eau dans les deltas est d'autant plus importante que l'apport est significatif. Cependant, si le débit est observé à l'aval de la zone deltaïque, ses valeurs sont d'autant plus élevées que les inondations dans les deltas sont importantes.

Un temps de réponse qui est défini comme le déphasage (en valeur absolue) entre le maximum des débits mesurés et les superficies des plans d'eau estimées à partir des températures de brillance a été observé. Ce temps dépend des caractéristiques de la région, la texture du sol, la topographie et de la morphologie des rivières. Il a été prouvé dans le travail présenté au chapitre 4 que ce déphasage n'est pas sujet à des variabilités interannuelles. Ce paramètre est donc une caractéristique du site étudié dont la valeur varie au cours de la saison mais sa moyenne demeure presque constante entre une saison et une autre.

L'indice d'humidité BWI, présenté au troisième chapitre, est une combinaison linéaire des températures de brillance mesurées, pondérées par deux paramètres empiriques. Un autre indice qui est la fraction des zones inondées par pixel, FWS, a été dérivé à partir des valeurs de BWI. Ce nouvel indice donne le pourcentage de la fraction inondée par pixel. L'analyse de la variabilité interannuelle de cet indice a reflété une sensibilité aux effets du changement des conditions climatiques.

Le deuxième travail de cette thèse qui a fait l'objet du chapitre 4 a présenté une comparaison entre les FWS dérivées à partir des images captées en micro-ondes passives et des images NOAA-AVHRR captées dans le domaine du visible et de l'infrarouge. Cette comparaison a mis en lumière la différence de sensibilité entre ces deux sources d'informations. En fait, les micro-ondes passives sont sensibles aux plans d'eaux et l'humidité du sol. Cependant, les images captées dans le visible ne sont pas en mesure de "voir" l'humidité du sol. Ces images reflètent donc seulement l'étendue des plans d'eau. Il a été supposé donc qu'une information concernant l'humidité du sol réside dans la différence de sensibilités de ces deux types d'images. Cette réflexion a fait l'objet du troisième travail de cette recherche qui est présenté au chapitre 5.

Dans le chapitre 5, les images captées en micro-ondes passives et visibles sont fournies respectivement par les capteurs AMSR-E et MODIS. Ces deux nouveaux capteurs présentent une amélioration de la résolution spatiale par rapport aux capteurs SSM/I et NOAA utilisés dans les deux premiers travaux de cette thèse. L'approche a été appliquée à la région du PAD. Une courbe de tarage a été calibrée en se basant sur les mesures de débits et les estimations des fractions des plans d'eau par pixel, dérivées à partir des données micro-ondes passives. Cette courbe de tarage se substitue aux estimations de l'étendue des plans d'eau dérivées à partir des images captées dans le domaine du visible. Ceci présente une alternative intéressante compte tenu de l'impossibilité d'extraire l'information des images captées dans ce domaine vu la présence des nuages. La courbe de tarage a permis donc de surmonter ce problème. Donc, il a été possible d'estimer quotidiennement la variation de l'étendue des plans d'eau dans la région du PAD à partir des mesures de débits. Par ailleurs, le capteur AMSR-E assure une couverture quotidienne de la totalité de la région étudiée. Des fractions des plans d'eau par pixel (FWS) ont été estimées à partir des images captées dans le domaine des micro-ondes passives. La fraction des plans dans la région du PAD est la somme des fractions des plans d'eau estimées pour chaque pixel. Cette approche offre donc deux estimations quotidiennes de l'étendue des plans d'eau dérivées respectivement des données micro-

ondes passives et des mesures de débits, en utilisant la courbe de tarage. Ainsi, un indice d'humidité a été défini, au chapitre 5, en se basant sur la différence de ces deux fractions. L'application d'un tel indice d'humidité à des bassins à l'échelle du Mackenzie n'a pas été abordée dans la littérature auparavant. L'indice proposé a montré une sensibilité aux variables météorologiques observées de température de l'air et de précipitation. Cet indice reflète ainsi l'état d'humidité d'un bassin. L'avantage principal de cette approche réside dans sa capacité de fournir des estimations de l'état d'humidité d'un bassin de large étendue et ce en se basant sur des mesures disponibles quotidiennement.

Cependant, l'indice proposé dans le chapitre 5 reflète l'état 'global' d'humidité dans le bassin étudié, à une échelle spatiale de l'ordre de quelques dizaines de km (ex : 25 km avec l'emploi de données SSM/I). Pour estimer 'localement' l'humidité du sol à une échelle plus fine, une mise en échelle de cet indice est nécessaire. Ceci a fait l'objet du chapitre 6. La méthodologie de mise en échelle préconisée dans ce chapitre se base sur des données topographiques fournies par un modèle d'élévation de terrain. À partir des attributs topographiques dérivés de DEM, un indice d'humidité topographique similaire à celui proposé par Beven et Kirkby (1979) a été calculé. L'indice topographique proposé dans cette thèse tient compte de l'effet de la végétation. En se basant sur l'approche de mosaïque, le pixel a été subdivisé en une première fraction couverte de végétation et une deuxième fraction de sol nu. Il a été prouvé que l'effet des attributs topographiques sur la distribution spatiale de l'humidité du sol dépend de la densité de la végétation. L'indice topographique classique proposé par Beven et Kirkby (1979) a été donc reformulé pour tenir compte de l'effet de la végétation. Le nouvel indice topographique proposé a donc servi pour la mise en échelle de l'indice d'humidité présenté dans le chapitre 5. Cette combinaison des données topographiques avec les données micro-ondes passives a été rarement abordée dans la littérature. L'avantage principal de cette approche est de distribuer dans l'espace l'indice d'humidité et le ramener à une échelle 'locale' (1 km, dans cette étude). Ces estimations locales de

l'humidité du sol ont présenté une meilleure concordance avec les mesures de précipitations et de températures.

7.2 Recommandations et travaux futurs

Deux catégories d'approches ont été identifiées suite à la synthèse bibliographique présentée au début de ce travail. La première catégorie regroupe les approches qui se basent sur des modèles de transfert radiatif pour l'estimation de l'humidité du sol. Ces approches utilisent généralement des mesures de températures de brillance effectuées dans les bandes C et/ou X. Cependant, la bande L (1,4 GHz) est de loin préférable pour l'inversion des modèles de transfert radiatif. Actuellement, il n'existe pas de capteurs satellitaires équipés pour mesurer des températures de brillance à cette fréquence. L'inconvénient majeur des données captées dans les micro-ondes passives réside dans la faiblesse de leur résolution spatiale. À titre indicatif, les données fournies par AMSR-E à la bande C ont une résolution spatiale de 50 km. Il est difficile de valider par des mesures locales des humidités du sol dérivées à partir de ces températures de brillances.

De l'autre coté, la deuxième catégorie propose des approches globales qui se basent sur la notion de l'indice d'humidité et ne nécessitent pas l'inversion d'un modèle de transfert radiatif. Cet indice offre une estimation qualitative de l'humidité du sol. Dans cette thèse, cette piste a été approfondie. Ce choix semble être imposé par l'état actuel des technologies spatiales. En fait, l'absence des mesures effectuées à la bande L et la faible résolution spatiale des celles réalisées aux bandes X et C suggère la sélection de cette deuxième catégorie d'approche. En outre, le vaste étendue du bassin du Mackenzie, objet de cette étude, et son hétérogénéité, motivent encore plus cette option.

Il a été démontré dans ce travail que ces approches globales présentent un potentiel intéressant pour l'estimation de l'humidité du sol notamment dans le cas des bassins

hétérogènes et de large étendue, tel que le Mackenzie. Le potentiel de la première catégorie d'approches qui font appel à des modèles de transfert radiatif devrait s'améliorer suite à l'évolution des techniques des mesures satellitaires. Ces améliorations sont planifiées dans le cadre de la mission SMOS de l'ESA (European Space Agency). Les données de SMOS devraient être disponibles en 2007. Compte tenu de l'état actuel des technologies de mesures de températures de brillance, il est judicieux d'explorer le potentiel des approches globales.

Le présent travail de recherche propose une amélioration par rapport aux indices d'humidité proposés dans la littérature. L'indice d'humidité proposé dans le chapitre 6 de cette thèse, présente une combinaison de plusieurs sources d'informations. En fait, les températures de brillances mesurées ont été combinées aux débits observés qui substituent les images captées dans le domaine du visible, aux indices de surface foliaire (ISF) qui caractérisent l'état du couvert végétal et aux données topographiques. La considération des ces sources d'information supplémentaires a nettement amélioré le potentiel de l'indice proposé.

En outre, cet indice se base, entre autres, sur la courbe de tarage ('rating curve') qui exprime la corrélation entre les débits observés et les fractions des plans d'eau estimées. Les paramètres de cette courbe de tarage dépendent du site étudié. Ces paramètres ne peuvent pas être extrapolés d'un site à l'autre. Ce point devrait être approfondi dans le cadre des travaux futurs dans le but d'établir une méthodologie pour déceler le lien entre ces paramètres et les caractéristiques du site étudié. Une telle approche permettra d'estimer ces paramètres connaissant les caractéristiques du site (topographie, morphologie de la rivière, végétation, texture du sol, etc.). Dans la même optique, il est recommandable d'inclure le paramètre de déphasage dans le modèle de la courbe de tarage. Ce paramètre est proportionnel à la distance qui sépare le site étudié du point de mesure de débits. Le modèle de la courbe de tarage a montré un potentiel intéressant

dans le suivi des inondations. Cependant il n'a été testé que sur deux sites du bassin du Mackenzie. L'application de cette approche à d'autres sites permettrait de tracer, en extrapolant entre ces différents sites, une cartographie globale de l'étendue des plans d'eau dans le bassin du Mackenzie.

Les résultats obtenus au troisième et quatrième chapitres ont permis d'apprécier le potentiel des indices d'humidité en tant qu'indicateur de la variation des conditions climatiques. Ce potentiel devrait être exploré dans des études futures pour établir le lien entre les changements des conditions climatiques et les variations de ces indices. Ceci pourrait être possible par l'analyse des séries temporelles plus longues. Pour cette fin, des données SSM/I pourraient être utilisées puisqu'elles couvrent une période d'approximativement 20 ans.

Par ailleurs, il a été expliqué au sixième chapitre que la topographie joue un rôle prépondérant dans le contrôle de la distribution spatiale du contenu en eau du sol. Le modèle d'élévation de terrain utilisé dans le cadre de cette thèse a une résolution spatiale de 1 km. L'apport d'un DEM plus précis devrait être évalué, surtout lorsque le site à l'étude possède une topographie peu accentuée.

Par ailleurs, des variables météorologiques, telles que la température et la précipitation, ont été utilisées dans cette thèse pour valider les résultats obtenus. Des mesures locales d'humidité de sol ont servi dans le chapitre 5 pour valider la tendance de l'indice d'humidité proposé. Actuellement, des travaux sont en cours pour calibrer le logiciel WATCLASS, sous sa nouvelle version, WATFLOW. La disponibilité de ces résultats générera une redondance d'information intéressante qui permettra de corroborer les résultats obtenus en appliquant les approches proposées dans cette thèse. Ce point devrait être considéré dans le cadre des travaux futurs.

CONCLUSION

Cette thèse s'inscrit dans le cadre de la deuxième phase du projet MAGS. Sa contribution ultime réside dans le développement d'une approche pour le suivi de l'évolution de la composante surfacique de la réserve hydrique dans le bassin du Mackenzie. Le cœur de ce travail a fait l'objet des quatre travaux, présentés par les chapitres, 3, 4, 5 et 6. Au terme de ces travaux, il ressort que :

- 1- Les micro-ondes passives présentent un potentiel intéressant pour le suivi de la composante surfacique de la réserve hydrique. Cette composante inclut l'humidité du sol en surface/près de la surface, ainsi que les plans d'eau permanents (rivières et lacs) et les zones inondées occasionnellement. La couverture spatiale des capteurs opérants dans ce domaine du spectre offre une couverture quotidienne des bassins de large étendue, tel que le Mackenzie. La fréquence d'acquisition qui peut atteindre deux images par jour est compatible avec la dynamique des phénomènes hydrologiques et est très fiable pour le suivi des inondations.

- 2- Dans le cas des bassins hétérogènes et de large étendue, il est recommandable d'opter pour des approches globales qui se basent sur des indices d'humidité pour estimer le potentiel hydrique de ces bassins. Ces approches sont une alternative intéressante par rapport aux approches physiques et détaillées qui se basent sur des modèles de transfert radiatifs. L'application des modèles de transfert radiatifs exige une connaissance détaillée des conditions à la surface et dans l'atmosphère et ce notamment si des fréquences élevées (supérieures à 18 GHz) sont utilisées. Les indices d'humidité issus de ces approches globales offre une description qualitative de l'évolution de la réserve hydrique dans un bassin.

Les indices développés dans les chapitres 5 et 6, concordent assez bien avec les variables météorologiques observées de précipitation et de température de l'air.

- 3- Une corrélation a été notée entre la superficie des plans d'eau et le débit observé à des stations situées à l'amont ou à l'aval du bassin étudié. Une courbe de tarage a été développée en se basant sur cette corrélation. Les paramètres empiriques de la courbe de tarage dépendent du site étudié et de la morphologie des cours d'eau. Un déphasage a également été observé entre les maximums des plans d'eau et les maximums des surfaces inondées. Ce déphasage est proportionnel à la distance qui sépare la station d'observation de débit du site étudié. Ce déphasage a été introduit à la formulation classique de la courbe de tarage. La relation proposée a été exploitée avec succès pour simuler un suivi en temps réel des inondations printanières au Mackenzie.
- 4- L'évolution du couvert végétal au cours de la saison doit être prise en compte. La comparaison des résultats obtenus avec des indices qui tiennent compte de cet effet et des indices qui n'en tiennent pas compte a permis d'appréciation l'apport de cette considération. L'ISF pourrait être utilisé pour le suivi de l'évolution de la densité du couvert végétal.
- 5- Les micro-ondes passives reflètent l'effet des plans d'eau et de l'humidité du sol en surface et près de la surface. Cependant, les images captées dans le domaine du visible reflètent seulement l'étendue des plans d'eau. Un indice d'humidité a été défini en se basant sur la différence de sensibilité des deux sources de mesure. La tendance saisonnière de cet indice concorde avec celle de l'humidité du sol observée.

- 6- La topographie contrôle la distribution spatiale de l'humidité du sol. L'indice d'humidité 'global' a été mis en échelle en utilisant un indice topographique qui reflète le potentiel d'humidité du chaque pixel. La végétation influence le rôle joué par la topographie dans le contrôle de la distribution latérale du contenu en eau du sol. L'effet des attributs topographiques, tels que la pente du terrain, l'élévation et l'aire de drainage, dépend de la densité du couvert végétal. Ceci a été tenu en compte dans la formulation de l'indice topographique utilisé pour la mise en échelle de l'humidité du sol. Cette prise en compte a amélioré les résultats obtenus avec la formulation classique de l'indice topographique.

Suite à ces conclusions, il ressort que l'objectif de la thèse a été atteint. Des études futures sont néanmoins nécessaires pour corroborer les résultats obtenus et continuer le travail de l'estimation de l'humidité du sol, selon les recommandations formulées.

BIBLIOGRAPHIE

- Armstrong, R., Knowles, K., Brodzik, M., & Hardman, M. (1994). DMSP SSM/I Pathfinder daily EASE-Grid brightness temperatures,". *National Snow and Ice Data Center, Boulder, CO.*
- Barling, R. D., Moore, I. D., & Grayson, R. B. (1994). A Quasi-Dynamic Wetness Index for Characterizing the Spatial-Distribution of Zones of Surface Saturation and Soil-Water Content. *Water Resources Research, 30*(4), 1029-1044.
- Basist, A., Grody, N. C., Peterson, T. C., & Williams, C. N. (1998). Using the special sensor microwave/imager to monitor land surface temperatures, wetness, and snow cover. *Journal of Applied Meteorology, 37*(9), 888-911.
- Basist, A., Williams, C., Grody, N., Ross, T. F., Shen, S., Chang, A. T. C., Ferraro, R., & Menne, M. J. (2001). Using the special sensor microwave imager to monitor surface wetness. *Journal of Hydrometeorology, 2*(3), 297-308.
- Beltaos, S. (2003). Numerical modelling of ice-jam flooding on the Peace-Athabasca delta. *Hydrological Processes, 17*(18), 3685-3702.
- Beven, K. J., & Kirkby, M. J. (1979). A physically based, variable contributing area model of basin hydrology. *Hydrological Sciences Bulletin, 24*(1), 43-69.
- Bindlish, R., Jackson, T. J., Wood, E., Gao, H. L., Starks, P., Bosch, D., & Lakshmi, V. (2003). Soil moisture estimates from TRMM Microwave Imager observations over the Southern United States. *Remote Sensing of Environment, 85*(4), 507-515.
- Burke, E. J., Bastidas, L. A., & Shuttleworth, W. J. (2002). Exploring the potential for multipatch soil-moisture retrievals using multiparameter optimization techniques. *Ieee Transactions on Geoscience and Remote Sensing, 40*(5), 1114-1120.
- Burn, C. R. (1995). Hydrologic regime of Mackenzie River and connection of 'no-closure' lakes to distributary channels in the Mackenzie Delta, Northwest Territories. *Canadian Journal of Earth Sciences, 32*(7), 926-937.
- Chaplot, V., & Walter, C. (2003). Subsurface topography to enhance the prediction of the spatial distribution of soil wetness. *Hydrological Processes, 17*(13), 2567-2580.
- Choudhury, B. J. (1989). Monitoring global land surface using Nimbus-7 37 GHz data. Theory and examples. *International Journal of Remote Sensing, 10*(10), 1579-1605.

- Choudhury, B. J. (1991). Passive microwave remote sensing contribution to hydrological variables. *Surveys in Geophysics*, 12, 63-84.
- Choudhury, B. J. (1993). Reflectivities of selected Land Surface Types at 19 and 37 GHz from SSM/I Observations. *Remote Sensing of Environment*, 46, 1-17.
- Choudhury, B. J., Schmugge, T., Chang, A. T. C., & Newton, R. W. (1979). Effect of soil roughness on th emicrowave emission from soils. *J. Geophys. Res.*, 84, 5699-5706.
- Choudhury, B. J., Wang, J. R., Hsu, A. Y., & Y.L., C. (1990). Simulated and observed 37 Ghz emission over Africa. *International Journal of Remote Sensing*, 11(10), 1837-1868.
- Cohen, S. J. (1997). *Mackenzie basin imapct study : final report and summary of results*. Ontario: Atmospheric Environment Service, Environement Canada.
- Cosh, M. H., Stedinger, J. R., & Brutsaert, W. (2004). Variability of surface soil moisture at the watershed scale. *Water Resources Research*, 40(12), 1-9.
- Coté, J., Gravel, S., Méthot, A., Patoine, A., Roch, M., & Staniforth, A. (1998). The operational CMC-MRB gobal environmental multiscale (GEM) model. Part I: Design considerations and formulation. *Mon. Wea. Rev.*, 126, 1397-1418.
- Crave, A., & Gascuel-Odoux, C. (1997). Influence of topography on time and space distribution of soil surface water content. *Hydrological Processes*, 11(2), 203-210.
- Du, Y., Ulaby, F. T., & Dobson, M. C. (2000). Sensitivity to soil moisture by active and passive microwave sensors. *Ieee Transactions on Geoscience and Remote Sensing*, 38(1), 105-114.
- Eaglson, P. S. (1982). Ecological Optimality in Water-Limited Natural Soil-Vegetation Systems 1. Theory and Hypothesis. *Water Resources Research*, 18(2), 325-340.
- Fily, M., Royer, A., Goita, K., & Prigent, C. (2003). A simple retrieval method for land surface temperature and fraction of water surface determination from satellite microwave brightness temperatures in sub-arctic areas. *Remote Sensing of Environment*, 85(3), 328-338.
- Frazier, P., Page, K., Louis, J., Briggs, S., & Robertson, A. I. (2003). Relating wetland inundation to river flow using Landsat TM data. *International Journal of Remote Sensing*, 24(19), 3755-3770.

- Galantowicz, J. F. (2002). *High-resolution flood mapping from low-resolution passive microwave data*. Paper presented at the 2002 IEEE International Geoscience and Remote Sensing Symposium (IGARSS 2002), Jun 24-28 2002, Toronto, Ont., Canada.
- Gloersen, P., & Barath, F. T. (1977). A scanning multichannel microwave radiometer for Nimbus-G and Seasat-A. *IEEE J. oceanic Eng., OE-2*, 172-178.
- Gomez-Plaza, A., Alvarez-Rogel, J., Albaladejo, J., & Castillo, V. M. (2000). Spatial patterns and temporal stability of soil moisture across a range of scales in a semi-arid environment. *Hydrological Processes, 14*(7), 1261-1277.
- Gomez-Plaza, A., Martinez-Mena, M., Albaladejo, J., & Castillo, V. M. (2001). Factors regulating spatial distribution of soil water content in small semiarid catchments. *Journal of Hydrology, 253*(1-4), 211-226.
- Grayson, R. B., Western, A. W., & Chiew, F. H. S. (1997). Preferred states in spatial soil moisture patterns: Local and nonlocal controls. *Water Resources Management, 33*(12), 2897-2908.
- Hamilton, S. K. (1999). Potential effects of a major navigation project (Paraguay-Parana Hidrovia) on inundation in the Pantanal floodplains. *Regulated Rivers: Research and Management, 15*, 289-299.
- Hamilton, S. K., Sippel, S. J., & Melack, J. M. (2004). Seasonal inundation patterns in two large savanna floodplains of South America: The Llanos de Moxos (Bolivia) and the Llanos del Orinoco (Venezuela and Colombia). *Hydrological Processes, 18*(11), 2103-2116.
- Hollinger, J. P., Pierce, J. L., & Poe, G. A. (1990). SSM/I instrument evaluation. *IEEE Transactions on Geoscience and Remote Sensing, 28*, 781-790.
- Jackson, T. J. (1993). measuring surface soil moisture using passive microwave remote sensing. *Hydrological Processes, 7*(139-152.).
- Jackson, T. J., Gasiewski, A. J., Oldak, A., Klein, M., Njoku, E. G., Yevgrafov, A., Christiani, S., & Bindlish, R. (2002). Soil moisture retrieval using the C-band polarimetric scanning radiometer during the Southern Great Plains 1999 Experiment. *Ieee Transactions on Geoscience and Remote Sensing, 40*(10), 2151-2161.
- Jackson, T. J., & Le Vine, D. M. (1996). Mapping surface soil moisture using an aircraft-based passive microwave instrument : algorithm and example. *Journal of Hydrology, 184*, 85-99.

- Jackson, T. J., Le Vine, D. M., Swift, C. T., Schmugge, T., & schiebe, R. F. (1995). Large area mapping ao soil moisture using the ESTAR passive microwave radiometer in Washita 92. *Remote Sensing of Environment*, 53, 27-37.
- Jackson, T. J., & Schmugge, T. (1991). Vegetation effects on the microwave emission from soil. *Remote Sensing of Environment*, 36, 203-212.
- Jin, Y.-Q. (1999). Flooding index and its regional threshold value for monitoring floods in China from SSM/I data. *International Journal of Remote Sensing*, 20(5), 1025-1030.
- Kerr, Y. H., & Njoku, E. G. (1993). On the use of passive microwaves at 37 GHz in remote sensing of vegetation. *International Journal of Remote Sensing*, 14(10), 1931-1943.
- Kim, G., & Barros, A. P. (2002). Space-time characterization of soil moisture from passive microwave remotely sensed imagery and ancillary data. *Remote Sensing of Environment*, 81(2-3), 393-403.
- Kochtubajda, B., Stewart, R. E., Gyakum, J. R., & Flannigan, M. D. (2000, 15-17 November). *Convection, lightning and fire disturbances in the Mackenzie River Basin*. Paper presented at the 6th Scientific Workshop for MAGS.
- Kruus, J., Deutsch, M., Hansen, P. L., & Ferguson, H. L. (1981). *Flood application of satellite imagery*. Paper presented at the Fifth Annual William T. Pecora Memorial Symposium on Remote Sensing, 1979.
- Ladson, A. R., & Moore, I. D. (1992). Soil water prediction on the Konza Prairie by microwave remote sensing and topographic attributes. *Journal of Hydrology*, 138(3-4), 385-407.
- Lakshmi, V. (1996). *Use of Special Sensor Microwave Imager Data for Soil Moisture Estimation*. Princeton University.
- Lakshmi, V., & Wood, E. F. (1997). Evaluation of Special Sensor Microwave/Imager Satellite Data for regional Soil Moisture Estimation over the Red River Basin. *Journal of Applied Meteorology*, 36, 1309-1328.
- Leconte, R., Pietroniro, A., Peters, D. L., & Prowse, T. D. (2001). Effects of flow regulation on hydrologic patterns of a large, inland delta. *Regulated Rivers-Research & Management*, 17(1), 51-65.

- Liou, Y. A., & England, A. W. (1998). A land surface process radiobrightness model with coupled heat and moisture transport in soil. *IEEE Transactions on Geoscience and Remote Sensing*, 36(1), 273-286.
- Louie, P. Y. T., Hogg, W. D., MacKay, M. D., Zhang, X., & Hopkinson, R. F. (2002). The water balance climatology of the Mackenzie basin with reference to the 1994/95 water year. *Atmosphere-Ocean*, 40(2), 159-180.
- MacKay, M. D., Seglenieks, F., Verseghe, D., Soulis, E. D., Snelgrove, K. R., Walker, A., & Szeto, K. (2003). Modeling Mackenzie basin surface water balance during CAGES with the Canadian regional climate model. *Journal of Hydrometeorology*, 4(4), 748-767.
- MacKay, M. D., Stewart, R. E., & Bergeron, G. (1998). Downscaling the hydrological cycle in the Mackenzie Basin with the Canadian Regional Climate Model. *Atmosphere-Ocean*, 36(3), 179-211.
- Marsh, P., & Hey, M. (1989). The flooding hydrology of Mackenzie Delta Lakes near Inuvik, N.W.T., Canada. *Arctic*, 42, 41-49.
- Mattikalli, N. M., Engman, E. T., Ahuja, L. R., & Jackson, T. J. (1998). Microwave remote sensing of soil moisture for estimation of profile soil property. *International Journal of Remote Sensing*, 19(9), 1751-1767.
- Mo, T., & Schmugge, T. (1987). A parameterization of the effect of surface roughness on microwave emission. *IEEE Transactions on Geoscience and Remote Sensing*, GE-25(Julyt), 481-486.
- Moore, I. D., Burch, G. J., & Mackenzie, D. H. (1988). Topographic effects on the distribution of surface soil water and the location of ephemeral gullies. *Transactions of the American Society of Agricultural Engineers*, 31, 1098-1107.
- Mosley, M. P. (1983). Response of braided rivers to changing discharge. *Journal of Hydrology*, 22(1), 18-67.
- Njoku, E. G., Jackson, T. J., Lakshmi, V., Chan, T. K., & Nghiem, S. V. (2003). Soil moisture retrieval from AMSR-E. *Ieee Transactions on Geoscience and Remote Sensing*, 41(2), 215-229.
- Njoku, E. G., & Li, L. (1999). Retrieval of land surface parameters using passive microwave measurements at 6-18 GHz. *Ieee Transactions on Geoscience and Remote Sensing*, 37(1), 79-93.

- Njoku, G. E., & Entekhabi, D. (1996). Passive microwave remote sensing of soil moisture. *Journal of Hydrology*, 184, 101-129.
- Njoku, G. E., & Kong, J. A. (1977). theory for passive microwave remote sensing of near surface soil moisture. *J. Geophys. Res.*, 82, 3108-3118.
- O'Loughlin, E. M. (1986). Prediction of Surface Saturation zones in Natural Catchments by Topographic analysis. *Water Resources Research*, 22(5), 794-804.
- Owe, M., De Jeu, R., & Walker, J. (2001). A methodology for surface soil moisture and vegetation optical depth retrieval using the microwave polarization difference index. *IEEE Transactions on Geoscience and Remote Sensing*, 39(8), 1643-1654.
- Paloscia, S., Macelloni, G., Santi, E., & Koike, T. (2001). A multifrequency algorithm for the retrieval of soil moisture on a large scale using microwave data from SMMR and SSM/I satellites. *IEEE Transactions on Geoscience and Remote Sensing*, 39(8), 1655-1661.
- Pellenq, J., Kalma, J., Boulet, G., Saulnier, G.-M., Wooldridge, S., Kerr, Y., & Chehbouni, A. (2003). A disaggregation scheme for soil moisture based on topography and soil depth. *Journal of Hydrology*, 276(1-4), 112-127.
- Prigent, C. (1997). Microwave land surface emissivities estimated from SSM/I observations. *Journal of Geophysical Research*, 102(D18), 21867-21890.
- Prigent, C., & Aires, F. (2001). Joint characterization of vegetation by satellite observations from visible to microwave wavelenghts: A sensitivity analysis. *Journal of Geophysical Research*, 106(D18), 20665-20685.
- Proctor, B. A., Strong, G. S., Smith, C. D., Wang, M., & Soulis, E. D. (2000). Atmospheric moisture budgets for the Mackenzie GEWEX project water years 1994-1995 through 1998-1999., 164-177.
- Qiu, Y., Fu, B. J., Wang, J., & Chen, L. D. (2001). Soil moisture variation in relation to topography and land use in a hillslope catchment of the Loess Plateau, China. *Journal of Hydrology*, 240(3-4), 243-263.
- Radeva, E., & Ritchie, H. (2001). Impact of the Canadian land surface scheme on monthly ensemble predictions of water and energy budgets over the Mackenzie river basin. *Atmosphere-Ocean*, 39(2), 71-88.
- Romano, N., & Palladino, M. (2002). Prediction of soil water retention using soil physical data and terrain attributes. *Journal of Hydrology*, 265(1-4), 56-75.

- Rouse, W. R. (2000). Progress in hydrological research in the Mackenzie GEWEX study. *Hydrological Processes*, 14(9), 1667-1685.
- Schmugge, T. (1998). Applications of passive microwave observations of surface soil moisture. *Journal of Hydrology*, 213(1-4), 188-197.
- Schultz, G. A., & Engman, E. T. (2000). *Remote sensing in Hydrology and Water Management*. New York.
- Shabbar, A., Bonsal, B., & Khandekar, M. (1997). Canadian precipitation patterns associated with the southern oscillation. *Journal of Climate*, 10(12), 3016-3027.
- Sippel, S. J., Hamilton, S. K., Melack, J. M., & Choudhury, B. J. (1992). Inundation area and morphometry of lakes on the Amazon River floodplain, Brasil. *Arch. Hydrobiol.*, 123, 385-400.
- Sippel, S. J., Hamilton, S. K., Melack, J. M., & Choudhury, B. J. (1994). Determination of inundation area in the Amazon river floodplain using the SMMR 37 GHz polarization difference. *Remote Sensing of Environment*, 48(1), 70-76.
- Sippel, S. J., Hamilton, S. K., Melack, J. M., & Novo, E. M. M. (1998). Passive microwave observations of inundation area and the area/stage relation in the Amazon River floodplain. *International Journal of Remote Sensing*, 19(16), 3055-3074.
- Smith, L. C., Isacks, B. L., & Bloom, A. L. (1996). Estimation of discharge from three braided rivers using synthetic aperture radar satellite imagery: Potential application to ungaged basins. *Water Resources Research*, 32(7), 2021-2034.
- Smith, L. C., Isacks, B. L., Forster, R. R., Bloom, A. L., & Preuss, I. (1995). Estimation of discharge from braided glacial rivers using ERS 1 synthetic aperture radar: first results. *Water Resources Research*, 31(5), 1325-1329.
- Soulis, E. D., Snelgrove, K. R., Kouwen, N., Seglenieks, F., & Verseghy, D. L. (2000). Towards closing the vertical water balance in Canadian atmospheric models: Coupling of the Land Surface Scheme CLASS with the distributed hydrological model WATFLOOD. *Atmosphere-Ocean*, 38(1), 251-269.
- Stewart, R. E., Leighton, H. G., Marsh, P., Moore, G. W. K., Ritchie, H., Rouse, W. R., Soulis, E. D., Strong, G. S., Crawford, R. W., & Kochtubajda, B. (1998). The Mackenzie GEWEX Study: The water and energy cycles of a major North American river basin. *Bulletin of the American Meteorological Society*, 79(12), 2665-2683.

- Strong, G. S., Proctor, B., Wang, M., Soulis, E. D., Smith, C. D., Seglenieks, F., & Snelgrove, K. (2002). Closing the Mackenzie Basin water budget, water years 1994/95 to 1996/97. *Atmosphere-Ocean*, 40(2), 113-124.
- Tanaka, M., Adjadeh, T. A., Tanaka, S., & Sugimura, T. (2002). Water surface area measurement of Lake Volta using SSM/I 37-GHz polarization difference in rainy season. *Advances in Space Research*, 30(11), 2501-2504.
- Tanaka, M., Sugimura, T., & Tanaka, S. (2000). Monitoring water surface ratio in the Chinese floods of summer 1998 by DMSP-SSM/I. *International Journal of Remote Sensing*, 21(8), 1561-1569.
- Tanaka, M., Sugimura, T., Tanaka, S., & Tamai, N. (2003a). Flood-drought cycle of Tonle Sap and Mekong Delta area observed by DMSP-SSM/I. *International Journal of Remote Sensing*, 24(7), 1487-1504.
- Tanaka, M., Sugimura, T., Tanaka, S., & Tamai, N. (2003b). Flood-drought cycle of Tonle Sap and Mekong Delta area observed by DMSP-SSM/I. *International Journal of Remote Sensing*, 24(7), 1487-1504.
- Temimi, M., Leconte, R., Brissette, F., & Chaouch, N. (2005). Flood monitoring over the Mackenzie River Basin using passive microwave data. *Remote Sensing of Environment*, v 98(n 2-3), 344-355.
- Toyra, J., Pietroniro, A., Martz, L. W., & Prowse, T. D. (2002). A multi-sensor approach to wetland flood monitoring. *Hydrological Processes*, 16(8), 1569-1581.
- Ulaby, F. T., Moore, R. K., & Fung, A. K. (1982). *Microwave remote sensing : active and passive*. (Vol. 2): Addison-wesley, Reading, MA.
- Ulaby, F. T., Moore, R. K., & Fung, A. K. (1986). *Microwave remote sensing : active and passive*. (Vol. 3): Artech House, Reading, MA.
- Verseghy, D. L. (2000). The Canadian Land Surface Scheme (CLASS): Its history and future. *Atmosphere-Ocean*, 38(1), 1-13.
- Vorosmarty, C. J., Willmott, C. J., Choudhury, B. J., Schloss, A. L., Steams, T. K., Robeson, S. M., & Dorman, T. J. (1996). Analyzing the discharge regime of a large tropical river through remote sensing, ground-based climatic data, and modeling (Paper 96WR01333). *Water Resources Research*, 32(10), 3137-3150.
- Wang, J. R., & Choudhury, B. J. (1981). Remote sensing of soil moisture content over bare fiel at 1.4 GHz frequency. *J. Geophys. Res.*, 86, 5277-5282.

- Western, A. W., Grayson, R. B., & Bloschl, G. (2002). Scaling of soil moisture: A hydrologic perspective. *Annual Review of Earth and Planetary Sciences*, 30, 149-180.
- Western, A. W., Grayson, R. B., Bloschl, G., Willgoose, G. R., & McMahon, T. A. (1999). Observed spatial organization of soil moisture and its relation to terrain indices. *Water Resources Research*, 35(3), 797-810.
- Wigneron, J. P., Calvet, J. C., Pellarin, T., Van de Griend, A. A., Berger, M., & Ferrazzoli, P. (2003). Retrieving near-surface soil moisture from microwave radiometric observations: current status and future plans. *Remote Sensing of Environment*, 85(4), 489-506.
- Williams, C. N., Basist, A., Peterson, T. C., & Grody, N. (2000). Calibration and Verification of Land Surface Temperature Anomalies Derived from the SSM/I. *Bulletin of the American Meteorological Society*, 81(9), 2141–2156.
- Wilson, D. J., Western, A. W., & Grayson, R. B. (2005). A terrain and data-based method for generating the spatial distribution of soil moisture. *Advances in Water Resources*, 28(1), 43-54.
- Zhou, Q., & Liu, X. (2004). Analysis of errors of derived slope and aspect related to DEM data properties. *Computers and Geosciences*, 30(4), 369-378.